Analysing Fly-Ash Erosion in Coal-Fired Boilers using Computational Fluid Dynamics

BY

JOHANNES CHRISTIAAN KLOPPERS

Submitted in partial fulfilment of the requirements for the degree of Master of Engineering (Mechanical Engineering)

in the

Faculty of Engineering

University of Pretoria

Pretoria

November 1999

Summary

Analysing Fly-Ash Erosion in Coal-Fired Boilers using Computational Fluid Dynamics

Johannes Christiaan Kloppers

Study leader: Prof. K.J. Craig
Department: Department of Aeronautical and Mechanical Engineering, University of Pretoria
Degree: Master of Engineering

Boiler tube failure due to fly-ash erosion is a major cause of forced outages of boiler plants worldwide. This problem is exacerbated in Southern Africa because of the high quartz (SiO_2) content in the coal. Specifically, Babcock boilers at Sasol in Secunda suffer from fly-ash erosion, especially in the convection pass where the ash temperatures are below 1100K and the ash no longer has the propensity for the formation of adhesive deposits.

The first part of this study is an extensive literature survey on boiler operation, tube failures caused by erosion and erosion-oxidation, and remedial measures for boiler tube failures. Flow in tube banks as well as CFD modelling of erosion and boiler flow are included in the literature survey.

The second part of this study concentrates on the simplification of the CFD modelling of the boiler. STAR-CD is used as the CFD solver in this study. As combustion is not modelled, the burner geometry is simplified and the burners are 'replaced' with hot air, seeded with fly-ash particles. In this simplification, the effect of the location of the burner/boiler inlets on the global flow patterns in the boiler is investigated. Methods to simplify boiler internals such as the boiler bank and airheaters are also investigated. Porous sections, of which the porosity is obtained by a detailed CFD hydraulic model of these elements, replace the boiler bank and airheaters.

In the third part of this study, remedial measures for boiler tube erosion in the Babcock boilers are investigated. The areas where erosion occur is at the superheater tubes near the top of the boiler, and in areas where there are larger than usual tube spacings. The remedial measures used in this dissertation are flow-modifying approaches through the use of baffles and tube fins. The remedial measures are applied with success to reduce peak velocities and high fly-ash particle concentration in regions of high erosive wear.

This study is successful because all the requirements of remedial measures for boiler tube failures were met. Boiler CFD models were successfully simplified by using a uniform boiler inlet geometry and 2D models. The effect

of boiler internals such as the tube bank can be omitted in boiler CFD models for erosion studies in the upper boiler. This leads to simple inexpensive CFD models that significantly reduces solution time.

Key words:
Computational Fluid Dynamics
Boiler Tube Failures
Erosion
Remedial Measures
Flow-Modifying Devices
Superheater Tubes
Bullnose
Two-Phase Flow
In-Line Tube Bank
Porosity
Model Simplification

Samevatting

Analysing Fly-Ash Erosion in Coal-Fired Boilers using Computational Fluid Dynamics

Johannes Christiaan Kloppers

Studieleier: Prof. K.J. Craig
Departement: Departement van Lugvaartkundige en Meganiese Ingenieurswese, University of Pretoria
Graad: Magister in Ingenieurswese

Stoomketelbuisfalings as gevolg van vliegas is een van die hoofoorsake van onbeplande afsluitings van ketelaanlegte wêreldwyd. In Suidelike Afrika word die probleem vererger deur die hoë kwartsiet (SiO_2) inhoud van die steenkool. Meer spesifiek, die Babcock ketels by Sasol Secunda ondervind vliegas erosie, veral in die konveksie gedeelte waar die astemperature onder 1100K daal en die as nie meer 'n geneigtheid het om klewerige nedersettings te vorm nie.

Die eerste gedeelte van hierdie studie is 'n uitgebruide literatuurstudie van ketelwerking, buisfalings veroorsaak deur erosie en erosie-oksidasie, en metodes om buisfalings te verminder. Vloei in die konveksie buisbank en Berekeningsvloeidinamika (BVD) modellering van erosie en ketelvloei is ingesluit in die literatuurstudie.

Die tweede deel van hierdie studie konsentreer op die vereenvoudiging van BVD ketel modellering. STAR-CD word gebruik as die BVD oplosser in hierdie studie. Omdat verbranding nie gemodeleer word nie, word die verbranders 'vervang' deur warm lug waarin vliegas partikels vrygestel word. In hierdie vereenvoudiging word die effek van die posisie van die verbrander/ketel inlaat ondersoek op die globale vloeiveld in die ketel. Metodes om die interne buise in die ketel te vereenvouding word ook ondersoek. Poreuse gedeeltes, waarvan die porositeit verkry word deur deur 'n gedetaileerde hidrouliese model, vervang interne buise van die ketel.

In die derde gedeelte van hierdie studie word metodes ondersoek om ketelbuisfalings te voorkom. Die gebiede waar erosie in die ketel voorkom is by die oorverhitte stoombuise naby die bopunt van die ketel, en in die gebiede waar daar groter as gewoonlik gapings tussen die buise is. Die metode wat gebruik word om die falings te verhoed is die vloeimodifiserings benadering deur gebruik te maak van keerplate en buisvinne. Hierdie metode word met sukses toegepas om hoë pieksnelhede en hoë partikel konsentrasies te verminder om sodoende erosie te verminder.

Hierdie studie is suksesvol afgehandel omdat metodes gevind is om ketelbuis erosie hok te slaan. Ketel BVD modelle is suksesvol vereenvoudig deur gebruik te maak van uniforme inlaat geometrieë en 2D. Die effek van die interne buise in die ketel kan uitgelaat word waar ketel BVD modelle vir erosie studies in die boonste gedeeltes van die ketel gebruik word. Al die vereenvoudigings lei tot eenvoudige, goedkoop BVD modelle wat relatief vinnig oplossings verskaf.

Sleutelterme:
Berekeningsvloeidinamika
Ketel Buisfalings
Erosie
Remediërende maatstawwe
Vloei Modifiseringstoestel
Oorverhitte Buise
Bulneus
Tweefase vloei
Inlyn Buisbank
Porositeit.
Model Vereenvoudiging

Acknowledgements

I would like to thank the following people and organisations for their support and contribution to this dissertation.

Sasol, for their Researcher's Sponsorship;
Prof. Ken Craig, my study leader;
Hein Botes, my mentor at Sastech;
Lynette, my wife, and her parents;
My mother and grandfather.

Table of Contents

List of Symbols

English Symbols

D	Diameter of tube
E	Internal energy
f	Friction factor
g	Acceleration of gravity
h	Enthalpy
J	Jacobian of transformation
k	Thermal conductivity; Turbulence kinetic energy
L	Characteristic length
N_L	Number of tube rows in tube bank
p	Pressure
P	Control parameter, Eq. (2-5)
P_L	Relative longitudinal pitch; S_L/D
P_T	Relative transverse pitch; S_T/D
Q	Control parameter, Eq. (2-5)
S_L	Longitudinal pitch of bank of tubes
S_T	Transverse pitch of bank of tubes
t	Time
T	Temperature
u,v,w	Cartesian velocity components
u',v'	Turbulent velocity fluctuations
V	Velocity
x,y,z	Cartesian coordinates

Greek Symbols

α	Metric coefficient, Eq. (2-5)
β	Metric coefficient, Eq. (2-5); Angle of incidence, Eq. (4-1) and (4-2)
χ	Correction factor
ε	Erosion rate [$mg.g^{-1}$]; Turbulent dissipation
λ	Second viscosity coefficient; Metric coefficient, Eq. (2-5)
η	Computational domain coordinate, Eq. (2-5)
μ	Dynamic viscosity
ρ	Density
τ_{ij}	Stress tensor
τ	Boundary layer shear stress
ξ	Computational domain coordinate, Eq. (2-5)

Dimensionless Groups

Eu	Euler number; $\Delta p/\rho u_0$
Re	Reynolds number; $\rho VL/\mu$

Subscripts

0	Conditions of main flow
L	Longitudinal
N	Normal
t	Turbulent
T	Tangential, transverse

Superscripts

n	Velocity exponent of erosion (Section 3.3.3.1.1)

1 Introduction

1.1 Motivation

Boiler tube failures are a major cause of forced outages world-wide. These failures are also the cause of forced outages of the Babcock boilers at Sasol in Secunda. In addition, many boiler tubes have to be replaced at each major scheduled boiler shutdown due to surface degradation. It is believed that erosion due to fly-ash impingement is the main cause of boiler tube surface degradation. Tube failures have occurred more frequently during the last few years. This problem has led to Sasol's sponsorship of this research project to investigate boiler tube surface degradation and boiler tube failures.

Tube surface degradation occurs at locations throughout the whole boiler. The first location of tube degradation due to fly-ash erosion is at the sidewalls at the edge of the bullnose. The superheater tubes at the top of the boiler also suffer from surface degradation. The biggest problem, however, is tube surface degradation that occurs in the tube bank. Surface degradation occurs adjacent to sections with larger than usual tube spacing. Finally, tubes fail at the inlet of the airheater in the boiler back pass.

1.2 Objectives of this Dissertation

The two main objectives of this dissertation are:

- To study the phenomenon of erosion in detail as well as to investigate remedial measures proposed by other researchers for boiler tube failures due to erosion. The following sub-objectives are identified:
    - Computational Fluid Dynamics (CFD) boiler models used by other researchers are investigated to become familiar with boiler flows. The assumptions on which their models are based on are investigated and how these models compare to experimental observations.
    - The simplification of boiler CFD models is investigated due to the complexity of boiler environments. These simplifications include neglecting heat transfer, simplified inlet geometry, and the usage of 2D boiler models for comparative studies.

- Investigation of the unique boiler tube failures in the Babcock boilers at Sasol using CFD, and the proposal of remedial measures to combat these failures. To achieve this objective the following sub-objectives must be met:
    - Erosion must be reduced at the superheater tubes and tube bank tubes in the top of the boiler.
    - Erosion that occurs in the tube bank adjacent to the larger than usual gaps in the tube bank must be reduced.
    - Airheater erosion in the boiler back pass must also be reduced.

Research has been performed on boiler tube failures due to fly-ash erosion and flows in tube banks. No research was found that deals specifically with flows in tube banks with irregular gaps. It is believed that the effect of the larger than usual gaps in the tube banks is the main contributor to fly-ash erosion. The effect of gaps in tube banks on flow and fly-ash erosion will therefore be investigated in this study. The purpose of this study therefore is to make suggestions as to why erosion occurs in all the regions discussed above, and to suggest methods as to how to minimise and hopefully prevent boiler tube erosion.

1.3 Layout of this Dissertation

CFD is used in this study to model the boiler and to investigate ways to minimise boiler tube erosion. The commercially available CFD solver, STAR-CD, is used. A brief background on CFD is given in Chapter 2, after which a literature survey on boiler tube failures follows in Chapter 3. Boiler tube failures due to erosion are investigated in detail. Remedial measures proposed by other researchers for fly-ash erosion in boilers are also discussed. Literature pertaining to the CFD modelling of boilers is discussed in Chapter 4. This chapter also describes a parametric study performed by the author using CFD. In this parametric study, factors like inlet configuration and fly-ash particle size and distribution are investigated. Porosity coefficients are also obtained for the boiler bank tubes and airheaters using a CFD hydraulic model. In Chapter 5 ways to combat boiler tube erosion are investigated. The remedial measures used are methods described in the literature as well as other new methods suggested by the author. Chapter 6 contains conclusions drawn from this study and suggestions for future work.

2 Background on Computational Fluid Dynamics

2.1 Introduction

Computational Fluid Dynamics (CFD) is, in part, the art of replacing the governing partial differential equations of fluid flow with numbers, and advancing these numbers in space and/or time to obtain a final numerical description of the complete flow field of interest [**1**].

The governing equations for flows of practical interest are usually so complicated that an exact solution is unavailable and it is necessary to seek a computational solution. Computational techniques replace the governing non-linear partial differential equations with systems of algebraic equations, so that a computer can be used to obtain the solution [**2**].

CFD provides four major advantages compared to experimental fluid dynamics [**2**]:

- Lead-time in design and development is significantly reduced.
- CFD can simulate flow conditions not reproducible in experimental model tests.
- CFD provides more detailed and comprehensive information.
- CFD is more cost-effective than wind tunnel or scale-model testing.

To obtain a well-posed problem, three conditions must be met: the solution must exist, the solution must be unique, and the solution must depend continuously on the initial and boundary conditions [**2**].

The commercial CFD solver STAR-CD is used in this study to solve the Reynolds-Averaged Navier-Stokes equations [**3**]. STAR-CD can handle complex phenomena in the flow field such as chemical reactions, combustion, dispersed multiphase flow, thermal radiation and distributed resistances.

2.2 The Basic Equations

There are three basic non-linear partial differential equations of conservation for physical fluid systems:

- Conservation of mass (Equation of continuity)
- Conservation of momentum (Navier-Stokes equations)
- Conservation of energy

In these equations there are three unknown variables, i.e. velocity, V, thermodynamic pressure, p, and absolute temperature, T. Variables like ρ, h, μ and k can be uniquely determined from the independent variables p and T. Refer to the List of Symbols for the definition of these variables.

When diffusion and chemical reactions are involved in the flow, there are at least two extra basic equations that must be considered:

- Conservation of species
- Conservation of chemical reaction

The first three equations above are now stated mathematically.

2.2.1 Equation of Continuity

$$\frac{D\rho}{Dt} + \rho div\bar{V} = 0 \tag{2-1}$$

2.2.2 The Navier-Stokes Equations

$$\begin{aligned}
\rho\frac{Du}{Dt} &= \rho g_x - \frac{\partial p}{\partial x} + \frac{\partial}{\partial x}\left(2\mu\frac{\partial u}{\partial x} + \lambda div\bar{V}\right) + \frac{\partial}{\partial y}\left[\mu\left(\frac{\partial u}{\partial y} + \frac{\partial v}{\partial x}\right)\right] + \frac{\partial}{\partial z}\left[\mu\left(\frac{\partial w}{\partial x} + \frac{\partial u}{\partial z}\right)\right] \\
\rho\frac{Dv}{Dt} &= \rho g_y - \frac{\partial p}{\partial y} + \frac{\partial}{\partial x}\left[\mu\left(\frac{\partial v}{\partial x} + \frac{\partial u}{\partial y}\right)\right] + \frac{\partial}{\partial y}\left(2\mu\frac{\partial v}{\partial y} + \lambda div\bar{V}\right) + \frac{\partial}{\partial z}\left[\mu\left(\frac{\partial v}{\partial z} + \frac{\partial w}{\partial y}\right)\right] \\
\rho\frac{Dw}{Dt} &= \rho g_z - \frac{\partial p}{\partial z} + \frac{\partial}{\partial x}\left[\mu\left(\frac{\partial w}{\partial x} + \frac{\partial u}{\partial z}\right)\right] + \frac{\partial}{\partial y}\left[\mu\left(\frac{\partial v}{\partial z} + \frac{\partial w}{\partial y}\right)\right] + \frac{\partial}{\partial z}\left(2\mu\frac{\partial w}{\partial z} + \lambda div\bar{V}\right)
\end{aligned} \tag{2-2}$$

2.2.3 The Energy Equation

$$\rho\frac{D}{Dt}\left(e + \frac{p}{\rho}\right) = \frac{Dp}{Dt} + div\left(k\nabla T\right) + \tau_{ij}'\frac{\partial u_i}{\partial x_j} \tag{2-3}$$

2.3 Modelling of Turbulence

As far as we know, the Navier-Stokes equations do apply to turbulent flow [**4**]. Direct numerical simulation is a technique to solve turbulent flow directly with the Navier-Stokes equations. The solution grid used must be infinitesimally small because the smallest eddy size is about 0.04mm. Presently, the computational power does not exist to implement direct numerical simulation for practical applications, because literally millions of mesh points would be needed to solve a small domain of a few cubic centimeters.

To implement turbulence practically, there exist a few empirical modelling ideas for certain mean statistical properties of turbulent shear flows. These can be classified as zero-equation, one-equation, two-equation and Reynolds stress models.

Reynolds averaging of the Navier-Stokes equations leads to extra stress terms called Reynolds stresses. These stresses can be modelled as 'viscous' stresses with an eddy viscosity in the same way as laminar shear stresses, e.g.

$$\tau_t = -\rho\overline{u'v'} = \mu_t\frac{\partial\bar{u}}{\partial y} \tag{2-4}$$

The eddy viscosity, μ_t, varies with flow conditions and geometry and is not a fluid property although it has the same dimensions as fluid viscosity. In the class of eddy-viscosity turbulence models, the models are constructed to find a description of the eddy viscosity μ_t, i.e. an 'equivalent' viscosity due to turbulence.

2.3.1 Zero-Equation Models

The mixing-length theory of Prandtl proposes that each turbulent fluctuation can be related to a length scale and a velocity gradient. Iteration is required to find the edge of the boundary layer. Different zero-equation models exist, e.g. Cebeci-Smith[**5**], and van Driest[**6**]. Most of these models require a specification of the outer edge of the boundary layer. A model that circumvents this problem is the Baldwin-Lomax[**7**] model.

2.3.2 One-Equation Models

These are usually models that describe the transport of turbulent kinetic energy. The turbulent kinetic energy equation can be described as follows [**4**]:

The rate of chance of turbulent energy =
convective diffusion + *production* +
work done by turbulent viscous stresses +
turbulent viscous dissipation.

The terms in this relation are so complex that they cannot be computed from first principles, therefore the one-equation model combines features of eddy-viscosity modelling with that of Reynolds stress models.

2.3.3 Two-Equation Models

If a second equation modelling rate of change is coupled with the turbulent energy equation described above, better results are usually obtained because the convection of turbulence is accounted for. The second rate of change can be that of turbulence dissipation, turbulent length scale, or vorticity, but dissipation is more commonly used. From there the k-ε model, where k is the turbulent kinetic energy and ε the turbulence dissipation.

2.3.4 Reynolds Stress Models

Turbulence can also be modelled using Reynolds stresses (like the one shown in Equation (2-4)), with additional partial differential equations describing the stresses. The modelling of Reynolds stresses is more complex than the previous models and is called a second-order closure. The stresses are computed directly and therefore the usage of the eddy viscosity and velocity gradient approaches are discarded.

2.4 Boundary Conditions

Any CFD model is as good as the assumptions it is based on. One can have a sufficiently converged solution, but if the boundary conditions do not resemble reality, the solution is useless. Thus, it is very important to apply the correct boundary conditions. The following are some of the boundary conditions that

can be applied to a CFD model. As STAR-CD is used in this study, the boundary conditions implemented in STAR-CD are described below.

2.4.1 Prescribed Flow or Inlet

This can be used for an inlet where the fluid properties and mass flux properties are known.

2.4.2 Outlet

The mass flow rate at this exit boundary is fixed from continuity considerations and all the variables' gradients are taken to be zero in the direction of the local flow direction at the exit boundary.

2.4.3 Prescribed Pressure

The static pressure at this boundary is specified and, unlike the outlet boundary condition, the direction and magnitude of the flow must be determined to describe the near-wall region [**4**].

2.4.4 Impermeable Wall and Baffle Surfaces

The no-slip condition next to the wall is applied and 'wall functions' are applied with certain turbulence models.

2.4.5 Symmetry Plane

When the flow domain is symmetrical relative to a plane, great simplifications can be made to the CFD model regarding grid size. At the symmetry plane the normal velocity and the normal gradients of all other variables are zero.

2.5 Computational Grids

A grid is generated in the domain where the fluid flow equations are solved through computational techniques. To obtain good results the grid must meet certain requirements:

- The grid points must be clustered near solid boundaries to provide high resolution of the viscous boundary layer.
- The grid resolution must be the highest in expected areas of high gradients of the flow variables.
- Excessive skewness of the grid must be avoided.

Body-fitted grids are generated in this study using either an algebraic method or a scheme based on elliptical partial differential equations.

2.5.1 Algebraic Grid Generation

Algebraic grid generation is computationally inexpensive and very simple to implement. After the grid points on the boundaries are obtained with stretching functions such as Vinokur[**8**] stretching, the interior grid is obtained by transfinite interpolation. After this, the gridlines can be blended to be orthogonal near the boundary walls. This was done in this study using the SURCH-algorithm in Fletcher[**9**].

2.5.2 Elliptic Grid Generation

As was the case with algebraic grid generation, the grid points on the boundary can also be obtained using stretching functions. Solving the transformed Poisson equations generates the interior of the grid [**10**]. For 2D grids, the Poisson equations are:

$$\begin{aligned} \alpha x_{\xi\xi} - 2\beta x_{\xi\eta} + \gamma x_{\eta\eta} &= -J^2\left(Px_{\xi} + Qx_{\eta}\right) \\ \alpha y_{\xi\xi} - 2\beta y_{\xi\eta} + \gamma y_{\eta\eta} &= -J^2\left(Py_{\xi} + Qy_{\eta}\right) \end{aligned} \qquad (2\text{-}5)$$

where (ξ,η) represent the coordinates in the computational domain, and P and Q are terms which control the point spacing in the interior of the domain. α, β and γ are metric coefficients and J is the Jacobian of the transformation.

2.6 Conclusion

CFD is a powerful tool to perform simulations of complex flow phenomena in a very economical manner. Computational techniques make it possible to solve the non-linear partial differential governing equations. CFD has major advantages compared with experimental fluid dynamics. One such advantage is the application of boundary conditions to a CFD model that will be very difficult or even impossible to apply in experimental fluid dynamics. Turbulence can be modelled in CFD using one of several turbulence models that differ in complexity. In this study CFD is used in Chapter 4 for a parametric study of boiler operational conditions and in Chapter 5 for the investigation of remedial measures for boiler tube failures due to particle impingement erosion.

3 Boiler Operation, Tube Failures by Erosion and Erosion-Oxidation and Remedial Measures for Tube Failures

3.1 Boiler Operation

3.1.1 Introduction

It is important to be familiar with the operation of a boiler and all its components before one can investigate measures to control boiler erosion. It is also important to know each part of the boiler so that one can better understand the research done by others. Most of the information in this section is adapted from Singer [**11**].

3.1.2 Boiler Operation in a Nutshell

Refer to Figure 3-1 for a schematic of a typical pulverized-coal-fired boiler during the following discussion. Boilers burn pulverized coal to generate heat. This heat is transferred to the walls of the boiler through radiation. The walls of the boiler consist of many vertical tubes through which water circulates. The heat it receives via radiation heats the water in the tubes and the water starts boiling. The steam and water in the tubes are separated in the steam drum. The separated steam is then returned to the boiler for superheating in the superheater tubes. The separated water is returned to the bottom of the boiler through downcomer tubes.

3.1.3 Boiler Components

3.1.3.1 The Furnace

Heat generated in the combustion process appears as furnace radiation. Water circulating through tubes that form the furnace wall lining absorbs a certain percentage of heat. Waterwalls consist of vertical tubes connected at the top and bottom to headers. These tubes receive their water supply from the steam drum by means of downcomer tubes connected between the bottom of the drum and the lower headers. The steam, along with a substantial quantity of water, is discharged from the top of the waterwall tubes into the upper waterwall headers and then passes through riser tubes to the boiler drum. In the boiler drum the steam is separated from the water. The water together with incoming feedwater, is returned to the waterwalls through the downcomer tubes.

3.1.3.2 Superheater Tubes

The purpose of the superheater is to raise the boiler steam temperature above the saturated temperature level. As the steam enters the superheater in an essentially dry condition, further absorption of heat increases the steam temperature. Superheaters designed for high temperatures and pressures require high-strength alloy tubing. This alloy must also have great oxidation

resistance. High operating pressure means increased tube thickness. Thicker tubes are subjected to higher outside metal temperatures and are thus more subject to external corrosion.

3.1.3.3 Economisers

Economisers help to improve boiler efficiency by extracting heat from flue gases discharged from the final superheater section of a radiant unit. In the economiser, heat is transferred to the feedwater supplied to the boiler.

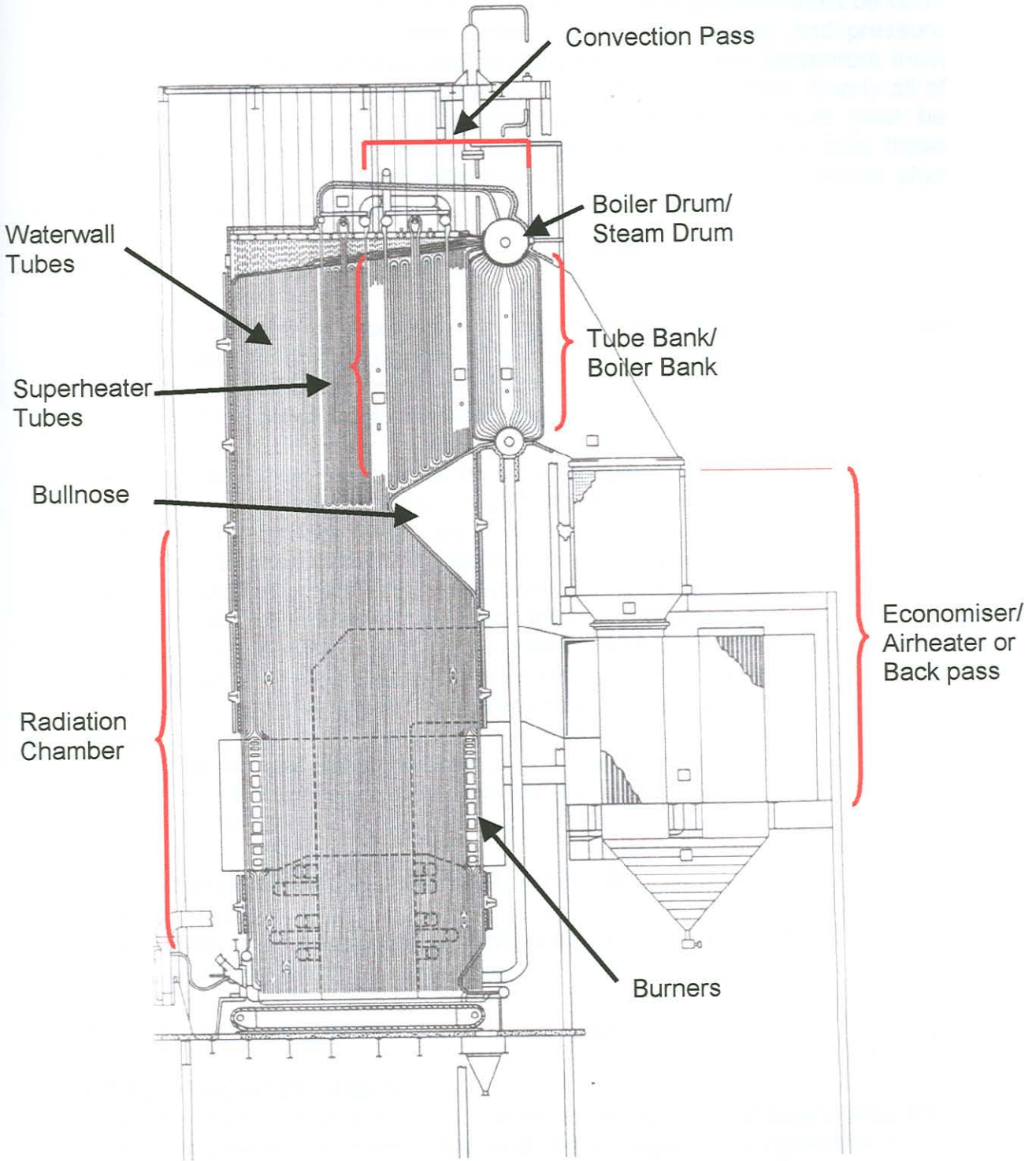

Figure 3-1 A Typical Pulverised-Coal-Fired Boiler [11]

3.1.3.4 Air-Heaters

Air heaters have two functions: they cool the gases before they pass to the atmosphere and at the same time they raise the temperature of the incoming air of combustion. The heating of the incoming air improves the efficiency of the boiler.

3.1.3.5 Steam Drum (Boiler Drum)

Before steam leaves the boiler and enters the superheater, practically all the boiler water must be separated from the steam. This separation must be done within a matter of seconds and under a variety of velocity and pressure conditions. The pressure drop across the steam and water separators must not be sufficient to affect boiler circulation or water-level control. Nearly all of the liquid and solid impurities in the steam and water mixture must be separated from the steam before use. The boiler drum serves both these factors: separating the steam from the water and purifying the steam after being separated from the water.

3.1.4 Water/Steam Circulation

The fact that water is circulating through the tubes of the boiler has been described above. The circulation of the water and steam will be discussed here in more detail because it is an integral part of boiler operation. The whole operation of the boiler is dependent on the circulation system of the boiler.

The term circulation, as applied to steam generators, is the movement of water, steam or a mixture of the two, through heated tubes. The tubes are situated in the furnace walls, boiler banks, economisers, superheaters or reheaters. Adequate circulation results in the cooling fluid absorbing heat from the tube metal at a rate which maintains the tube temperature at or below design conditions. In boilers, circulation through the varied systems of heated tubes can involve either just the flow entering and leaving the system (called once-through flow), or a means of recirculating the fluid, or some combination of these two circulation concepts. The most critical circulating system in a large boiler is that of the furnace walls. The walls are at the same time the area of highest heat absorption rate and a major structural component of the unit. There are three types of furnace wall circulation systems used for steam generation, they are:

- Thermally-induced circulation (natural circulation) with inherent recirculation.
- Thermally-induced circulation, pump-assisted, with recirculation.
- Once-through, with no recirculation.

These systems are now discussed in more detail.

3.1.4.1 Thermal Circulation

This type of circulation is at subcritical pressure. Circulation begins only after heat is applied to the riser tubes and, once begun, is proportional to the amount of heat locally supplied. To maintain the overall system pressure drop as low as possible, boilers using this principle for cooling the furnace

enclosure need large flow areas in downcomers and supply tubes. Thermal circulation boilers can be used at any waterwall operating pressure below critical pressure, as long as there is some finite density difference between the water in the downcomers and the saturated steam-water mixture in the heated circuits.

3.1.4.2 Pump-Assisted Thermal Circulation

This type of subcritical boiler recirculation system uses an external mechanical force, produced by one or more low-pressure-differential pumps, located in the downtake system to supplement the thermal head. Pump-assisted thermal circulation units find particular application at the high subcritical pressure levels, where there is reduced fluid static head energy available to recirculate the furnace wall fluid. The only difference between thermal circulation and pump-assisted thermal circulation boilers is in the circulating systems. Both types share the same kind of firing methods, means of superheating and reheating and controlling superheater and reheater outlet temperatures.

3.1.4.3 Once-Through Circulation

In a once-through boiler, there is no recirculation of water within the unit. In elemental form the boiler is merely a length of tubing through which water is pumped. Heat is applied, and the water flowing through the tube is converted into steam. In actual practice, numerous small tubes arranged to provide effective heat transfer similar to the arrangement in drum-type boilers replace the single tube.

3.1.5 Fuel-Burning Systems

The ideal fuel-burning system would have some of the following characteristics:

- There must not be excess oxygen or unburned fuel after combustion.
- Low energy input necessary for ignition.
- Stable combustion over a wide range of conditions.

For combustion to take place with a stoichiometric quantity of air, infinite resident times at temperatures above the ignition point at which complete burnout of the combustibles takes place, would be necessary. There must thus be excess air during combustion. The less air necessary for complete combustion, the more efficient is the firing system.

The rate and degree of completion of a combustion process (chemical reaction), are greatly influenced by temperature, concentration, preparation and distribution of the reactants, by catalysts, and by mechanical turbulence. All these factors have one thing in common: to increase contacts between the molecules of the reactants. Higher temperature increases the velocity of molecular movement, with a resulting increase in frequency of contact between molecules. At a given pressure, three factors limit the temperature that can be attained to provide the greatest intermolecular contact. These are the heat absorbed by the combustion chamber enclosure, the heat absorbed

by the reactants in bringing them to ignition temperature, and that absorbed by the nitrogen in the air used as a source of oxygen. The higher the concentration of a reactant, the higher is the opportunity for contact between interacting molecules.

There are basically three different configurations of fuel-firing systems: horizontally-fired, tangentially-fired and vertical-fired systems. The first two are the most common and they will be discussed in more detail.

3.1.5.1 Horizontally-Fired Systems

In this configuration of firing, the fuel is mixed with primary combustion air in individual burner registers. Adjustable inlet vanes impart a rotation to the preheated secondary air. The degree of air swirl, coupled with the flow-shaping contour of the burner throat, establishes a recirculation pattern extending several throat diameters into the furnace. The burners are located in rows, either on the front wall only, or they are on both the front and rear walls. The major part of combustion must take place in the recirculation zone. The rate of combustion drops off rapidly as the reactants leave the reaction zone. The air-fuel ratio must therefore be maintained within close tolerances.

3.1.5.2 Tangentially-Fired Systems

The fuel as well as the air is projected from the four corners of the furnace on a line tangent to a circle, lying in a horizontal plane, at the centre of the furnace. When a tangentially-fired system projects a stream of pulverised coal and air into a furnace, the turbulence and mixing that takes place along its path are low compared to horizontally-fired systems. This occurs because the turbulent zone does not continue for any great distance as the expanding gas soon forces a streamlined flow. As one stream impinges on another in the centre of the furnace during the intermediate stages of combustion, they create a high degree of turbulence for effective mixing.

3.1.6 Conclusion

The purpose of a pulverised–coal-fired boiler is to generate steam for industrial applications or power generation. Heat is transferred from the burning coal to the tubes through radiation. The tubes include waterwall tubes, superheater tubes, economiser tubes and boiler bank tubes. Water circulates through the tubes and steam is generated. There exist a few water circulation systems such as thermal-induced circulation and pump-assisted thermal-induced circulation. The steam and water are separated in the boiler drum. There also exist different fuel-burning configurations of which tangentially-fired and horizontally-fired systems are the most common. The boiler discussed in the rest of this dissertation uses thermal-induced circulation and has a horizontally-fired system.

3.2 Boiler Tube Failures

3.2.1 Introduction

Boiler tube failures constitute the major cause of lost availability in steam generating plants world-wide [**12**]. There is plenty of published research on boiler tube failures and on the philosophy of how to prevent these failures. The bulk of the published research covers fire-side tube failures but water-side failures are also dealt with in detail. This study will concentrate on fire-side boiler tube failure mechanisms and especially on impingement erosion. The causes of boiler tube failures are many and varied, as will become evident in the following discussion.

3.2.2 Repeat Failures

Repeat boiler tube failures are frequent, multiple failures with the same physical appearance, occurring in the same flow circuit or even the same tube and resulting from the same failure mechanism and root cause [**13**,**14**]. An alarming number of outbreaks of boiler tube failures are repeat failures [**13**].

Primary factors influencing repeat boiler tube failures are almost always one or more of the following [**13**,**14**]:

- Not following state-of-the-art operation, maintenance, or engineering practices; lack of proper tube failure analysis and root-cause verification.
- Wrong choice of long-term corrective/preventive action.
- Lack of definitive tube-failure reporting and continuous monitoring.

Without a proper understanding of the mechanism of failure, the root cause, and the appropriate corrective actions, it is not possible to apply permanent engineering solutions [**13**].

3.2.3 Mechanisms of Boiler Tube Failures

A mechanism of boiler tube failure is defined as the process which degrades the tube and produces a failure. Determining the correct mechanism of a boiler tube failure is important for the prevention of future tube failures. Proper corrective measures can be undertaken to alleviate the root cause or causes for a failure only when the correct mechanism is known [**15**].

Boiler tube failures can be classified into three broad categories, each forming part of the classic "bath tub curve" describing component reliability [**12**].
The three categories of failures are:

- Wear-out failures
- Failures due to faulty repairs
- Random failures

Wear-out failures are time-dependant failures that describe the natural tendency for the frequency of tube failures to increase as the boiler ages. Faulty repairs are generally the cause of failures due to shortcomings in

quality control at breakdowns or overhauls. Random failures are independent of accumulated operation or starts, being instead the result of transient operational conditions or the development of faults during operation.

Jones[**16**] gives three major reasons for boiler tube failures, i.e.:
- Tube overheating
- Tubes that have been attacked chemically
- Tubes that are thinned down from the fire-side

Dimmer and Dooley[**14**], Mayer[**15**] and Dooley[**17**] give six broad classes of significant boiler tube failure mechanisms and possible reasons of failure:

- Stress rapture – Short-term overheating; high temperature creep
- Water-side corrosion - Hydrogen damage; oxygen pitting
- Fire-side corrosion - Low temperature; coal ash
- Erosion - Fly ash; falling slag; sootblower; coal particle
- Fatigue - Vibration; thermal; corrosion
- Lack of quality control - Maintenance cleaning damage; welding defects; material defects

Colannino[**18**] gives five major modes of fire-side tube failure:
- Ash-induced corrosion
- Reduced-atmosphere corrosion
- Dew-point corrosion
- Impingement erosion
- Stress-corrosion cracking

Each failure given by Colannino[**18**] will be discussed in more detail.

3.2.3.1 Ash-Induced Corrosion
Ash corrosion occurs in the high temperature parts of the boiler such as the superheater section. Under high temperatures, complex chemical reactions occur. The evidence of ash corrosion is metal thinning combined with a chemical analysis that identifies eutectic compounds. Low ash fusion temperatures indicate a potential for ash corrosion. A possible cure for ash corrosion is the operation of the superheater at lower temperatures.

3.2.3.2 Reducing Atmospheres
Corrosion of the waterwall can occur under reducing conditions. Pyrosulfate compounds volatilise at high temperatures, and thus is found in liquids and form only on cool surfaces such as waterwall tubes. The pyrosulfate compounds dissolve the protective oxide coating on the boiler tube. This type of corrosion acts preferentially on the crown of the waterwall boiler tube. The most cost-effective cure for this type of erosion is metal cladding with high-nickel alloys or thermally transparent refractories.

3.2.3.3 Dew-Point Corrosion
Dew-point corrosion can occur wherever metal temperatures are below the dew point of the flue gas. For flue gas containing only water and CO_2, metal

surfaces must be below 100°C. Not even the stack of a boiler is this cool. Thus, other compounds, most notably SO_3, can elevate the dew point to as high as 166°C. Metal components subject to attack by the corrosive dew are economisers and air preheaters. Dew-point corrosion is generally evidenced by smooth corrosion of metal parts. The cure to dew point corrosion is adequate washing to remove sulphur deposits that may cause localised dew-point corrosion.

3.2.3.4 Impingement Erosion

Impingement occurs preferentially where the flue gas is forced to rapidly change direction. Impingement removes the protective oxide layer that all high temperature surfaces must develop for oxidation resistance. As the old oxide layer is abraded, the metal re-oxidises, consuming the underlying metal. This phenomenon is also called erosion-corrosion, which will later be discussed in more detail. The metals exposed to impingement may have a sandblasted or shiny appearance or an undulating surface. The cure for impingement is to reduce the impact of abrasives with metal surfaces. This can be accomplished with changes in materials for the boiler tubes or by the use of deflecting plates or screens.

3.2.3.5 Stress-Corrosion Cracking

Stress-corrosion cracking occurs due to preferential chemical attack along regions of high stress. Chlorides and hydroxides are noteworthy agents for stress-corrosion cracking. Water, superheater and reheater tubes are most prone to attack by stress-corrosion cracking. Boiler tubes are under stress due to internal steam pressures. Stress-corrosion cracking is a microscopic phenomenon and is typically invisible to the naked eye.

3.2.4 Conclusion

All the different mechanisms of boiler tube failures have been discussed. It can be seen that the causes of boiler tube failures are indeed many and varied. What makes boiler tube failures even more complex is the fact that two or more of the above mentioned mechanisms can occur at the same time. In this study, however, boiler tube failures due to impingement erosion are very important and will be concentrated on in the following section.

3.3 Erosion

3.3.1 Introduction

The American Society for Testing and Materials (ANSI / ASTM G40) defines erosion as the *"progressive loss of original material from a solid surface due to the mechanical interaction between that surface and a fluid, a multicomponent fluid, or impinging liquid or solid particles."* [**19**]

There are two basic fields of published research on erosion. The first field is the effect of the particle and environmental characteristics, i.e. hardness, shape, size, velocity, angle of impact etc., on erosion. The second field of erosion research is the response of the target material to impinging particles.

The bulk of the literature covers erosion characteristics at room temperature. Some authors have observed that erosion behaves somewhat differently at higher temperatures. There are authors that performed research on erosion especially in simulated boiler environments [**20**,**21**,**22**,**23**,**24**,**25**].

High-temperature erosive wear is a serious problem in the coal-burning industry as it often leads to unscheduled and costly outages. The problem is especially severe in coal-fired power stations in Southern Africa as the coal has a high quartz content, some of which survives combustion to cause erosive wear damage on its path out of the boiler [**23**].

The wear rate may not be sufficiently high (with the exception of high-ash quartz-rich fuels) to cause tube failures during the first few years of operation, but the wear-damage occurs deep in the economiser and superheater tube banks where it can remain unnoticed [**26**].

3.3.2 Regions where Erosion Occur in a Boiler

Erosion tends to be localised in particular areas of the boiler, and particular parts of a given tube bank. Refer to Figure 3-1 for the tube bank location described in this section. Localisation of erosion by eddy flow around a weld bead on a tube is not uncommon [**27**]. Except for the localised effect of erosion in boilers, the properties of the ash that causes erosion are also important parameters that determine in which areas of a boiler erosion will occur. Erosion also occurs where the ash particles are flung against boiler walls due to inertial forces when the flow direction changes.

3.3.2.1 The Nature of Ash in Erosion Regions

The nature of the interaction of the ash with the boiler tubes changes from a tendency to form a deposit (captive) to one of erosion (non-captive) towards the cooler parts of the boiler [**23**,**26**,**28**]. Failures due to erosion usually occur in the cooler superheater – reheater regions, either towards the top of the furnace or in the back pass [**28,29**].

Erosion wear in pulverised-coal-fired boilers occurs chiefly in the economiser and the primary superheater and reheater sections ('the middle temperature ranges'). The flue gas temperature in these passages is below 1000K [**26**,**30**].

Two essential conditions for erosion must exist wear to take place in the middle-temperature heat-exchanger sections, namely [**26**]:

- Ash particles entrained in the flue gas below 1100K no longer have the propensity for formation of adhesive deposits, and the ash has acquired an erosion-wear property.
- The ash-particle impaction takes place at sufficiently high velocity to cause erosion-wear, leading to subsequent tube failures.

3.3.2.2 Waterwalls

One of the most common areas where fly-ash erosion of waterwall tubes is encountered is around the top of the rear wall of the furnace, where the flue gas is turned to flow through the rear pass [**27**].

3.3.2.3 Tubes

Blockage of the normal gas flow path by slag or ash deposits can result in channelling of the flue gas through the tube banks. Hence fouling can compound erosion problems. Various design features of tube banks can give rise to localised disruptions of the gas flow, and locally turbulent regions may result in associated erosion [**27**]. Some features in the layout of the primary superheaters and reheaters and in the economiser create high velocity zones where erosion usually takes place [**26**,**28**]. Other localities of high-velocity zones of the flue gas flow are created by the gaps between the deep horizontal tube banks and duct walls [**26**]. In the gaps, the lower resistance causes higher velocities [**31**]. Sites of erosion failure are located where local peak gas velocities occur. These are recognised to be very local (on the order of centimetres) and turbulent. The erosion rates at these areas of high velocities are assisted by the muldistribution of ash. Ash-based effects can be considered to be secondary to the peak velocity effects [**17**].

The erosion wear of superheater, reheater and economiser tubes is further enhanced by the tendency of large and erosive fly-ash particles to concentrate in the flue gas stream near the rear wall after the U-turn at the top of the combustion chamber [**26**].

3.3.3 Characteristics of Erosion

From numerous studies of erosion, it appears that the most important variables are what may be termed system variables, such as fly-ash particle velocity and angle of impingement, and operating variables resulting from the type of coal burned and the combustion conditions, which define the size, shape, density and hardness of the fly-ash particles [**27**].

The amount of erosion damage varies, depending on the combination of many factors. In fact, it is the combined effect of these factors that could make the difference between a tolerable erosion rate and a rapid erosion rate that leads

quickly to tube failures. The most critical factor of erosion would have very little effect if other factors were not present to combine to create an erosive condition. The list of better known factors that cause erosion includes [**32**]:

- Particle velocity
- Particle density
- Angle of impingement
- Particle size and shape
- Fluid flow conditions
- Temperature
- Mechanical properties of particles
- Mechanical properties of the target material

In the erosion process, some of the above factors will have greater influence on the erosion rate than others, but all of them have to be taken into consideration in order to understand the mechanism of erosion.

3.3.3.1 Particle Characteristics

It is well documented that erosion rate is a strong function of the angle of attack, velocity, particle size, and particle and target materials.

3.3.3.1.1 Velocity of Impacting Particles

All researchers on erosion agree that the velocity of impacting particles is one of the most important parameters governing erosion wear. Erosion rates vary with particle velocity V according to the power law V^n, where n is on the order of two to four [**27**,**33**], but there is a critical velocity, below which no erosion damage will occur, assuming all other factors are held constant [**32**].

Early investigators of erosion proposed that the erosion process is proportional to the kinetic energy of the oncoming particles. This predicted relationship (i.e., $\varepsilon \sim V^2$) would almost be intuitively expected. Experimental research has however suggested that the velocity exponent is normally greater than two and this is perhaps the single most controversial issue in the study of erosion [**34**].

Table 3-1 contains a summary of research done on the velocity exponents of erosion.

Researcher and Source	Conditions of Study	Velocity Exponent
Grant and Tabakoff[**34**]	20° impact angle 90° impact angle	2.8 4
Shida and Fujikawa[**24**]	304 steel for temperatures of 300 and 650°C. Irregularly shaped silica particles were used as erodent.	2.8
Sun et al.[**35**]	Impact carbon steel, Cu by Al_2O_3, SiO_2 grains (30-40μm). Velocity range: 30-100m.s^{-1}.	2.01-2.69
Raask[**26**]	Carbon steel eroded by 75-125μm quartz sand. Velocity range: 20-30m.s^{-1}. 402°C.	2.5

Table 3-1 Summary of Research Done on Velocity Exponents of Erosion

Raask[**26**] presents a summary of work done by numerous researchers, all of which determined the velocity exponent between 2.0 and 2.9 for carbon steel target material.

This leaves one question: *What is the maximum velocity under which no erosion will occur for flue gas?*

The EPRI Report[**27**] states that typical design values for the average flue gas velocity range from about 20m.s^{-1} for low erosive coals, down to about 12m.s^{-1} for highly erosive coals. Raask[**26**] gives the maximum flue gas velocity for U.S. bituminous coals as contained in Table 3-2.

Type of ash	Weight fraction > 45 μm particles	Range of maximum velocities
Fine fly ash	0.15	12.2 – 19.1m.s^{-1}
Coarse fly ash	0.3	11.4 – 17.1m.s^{-1}
Exceptionally coarse ash	0.5	10.6 – 14.9m.s^{-1}

Table 3-2 Maximum Velocity of Fly Ashes for Various Bituminous Coals

3.3.3.1.2 Particle Impingement Angle

Together with particle velocity, one of the important parameters that affect material erosion is the angle of attack at which particles strike the target surface. Changes in the particle impact angle can have a marked influence on the erosion wear-velocity relationship i.e. the velocity exponent. Ductile and brittle materials also behave differently for different particle impingement angles.

Shida and Fujikawa[**24**] found the maximum erosion rate to be at impingement angles of about 20°-30° for ductile materials and normal impingement (90°) for brittle materials. Kratina et al.[**32**] stated that ductile materials are affected worst at about 30° impact angle, while hard, brittle materials show the greatest loss at a 90° angle of impact.

Work conducted by Grant and Tabakoff[**34**] is widely respected. The abrasives they used were alumina (Al_2O_3) and quartz (SiO_2). For all velocities tested, the angle of maximum weight loss occurs at an angle of approximately 20°. In another study, Tabakoff and Balan[**36**] found it to be between 20° and 25°. As the angle of attack increases from this value, the erosion reduces to a residual value at 90°. The normal component of velocity does not significantly contribute to ductile erosion. The kinetic energy of the particles is dissipated by plastic deformation of the target material without significant material removal [**34**].

Ninham[**37**] used angular quartz particles (70 – 200μm diameter) and silicon carbide particles (250μm average diameter) as erodents in tests to investigate the erosion behaviour of a number of alloys. It was found that the erosion response of high strength materials, particularly those eroded by quartz, is only weakly dependent upon impact angle. Most materials gave rise to a rather flat erosion vs. angle plot, with a peak at roughly 60° impact.

3.3.3.1.3 Particle Concentration

Erosion rate was found by Shida and Fujikawa[**24**] to be a linear function of the particle concentration in the concentration range between 30 and 120g.m^{-3}, tested at 300 and 650°C. The CEA Research Report[**31**] also states that erosion wear is in proportion to particle loading. This is true up to a point where the situation changes from erosion to abrasion of the surface. When the particle loading is large enough, some particles cannot strike the specimen due to the blanketing effect of other particles. Kratina et al.[**32**] also stated that erosion is a linear function of particle density.

3.3.3.1.4 Effect of Different Erodent Size

Research has shown that the particle size does not influence erosion after a certain threshold value is reached. This threshold value is dependent upon both particle velocity and particle size [**26**,**32**,**34**]. Tilly and Sage[**38**] found the plateau to be reached at 45μm for quartz particles and that erosion increases continuously for brittle materials. Raask[**26**], on the other hand, stated that impacting quartz particles smaller than 5μm have little effect on erosion. Fan et al.[**39**] concluded that smaller particles led to a larger value of the velocity exponent than larger particles. It was observed by Tabakoff et al.[**40**] that the erosion damage caused by coal ash particles is much lower owing to their smaller size than compared with erosion damage caused by alumina and quartz particles.

3.3.3.1.5 Effect of Different Erodent Shape

The geometric shape of particles will determine the erosion mechanism involved. Sharp-edged grains are likely to remove material by a cutting action, while spherical grains will cause the most damage by cracking the surface at a 90° impact [**32**]. The role of microcutting is recognised to be significant in case of sharp particles while ploughing occurs in the case of round particles [**41**].

3.3.3.1.6 The Effect of Temperature

The erosion behaviour at 300 and 650 °C does not seem to differ significantly from that obtained at room temperature [**24**]. Kratina et al.[**32**] state that the effect of temperature on erosion rate is less than one might expect.

3.3.3.2 Target Material Characteristics

Surface hardness, modulus of elasticity and scaling stress will invariably affect erosion. They combine to give the material its resistance to abrasion and impact erosion. They also determine the mode or mechanism of erosion involved [**32**].

Erosion behaviour to different heat treatments and materials:

- Brittle and ductile target materials exhibit different mechanisms of erosion [**42**].
- Erosion rate decreases with increasing tempering temperature [**36**,**43**].
- Erosion decreases with increasing spheroidisation [**43**].
- Erosion decreases with increasing proportion of bainite in the bainite-martensite structure obtained by austempering [**43**].

Whereas different heat treatments produce large changes in the mechanical properties, the erosion variation is comparatively small. In general, erosion rate increases with increasing hardness and the ultimate strength, but decreases with increasing ductility [**43**]. The ageing or work-hardening treatments carried out by Ninham[**37**] on the high temperature alloys had essentially no effect on erosion rates.

3.3.3.3 Hidden Factors Contributing to Erosion

There are hidden factors contributing to boiler erosion that can explain why in past cases two identical boilers in the same station experienced completely opposite erosion patterns. These hidden factors include [**32**]:

- Operational load
- Coal properties
- Operation time

These factors affect the gas flow and ash load in the boiler which, in terms of erosion investigation, can be translated into particle velocity and abrasive load.

3.3.4 Conclusion

Boiler tube failures due to erosion occur only in certain areas of a boiler. The properties of the ash particles and high particle velocity are to blame for the high erosion propensity in certain areas. It can also be seen that particle as well as target material characteristics are important factors influencing erosion rate.

3.4 Erosion-Oxidation

3.4.1 Introduction

Fly-ash erosion of primary superheater tubes, reheater tubes in the back pass, waterwall tubes and economiser tubes, is presently a more serious problem than fire-side corrosion [**27**]. It is nevertheless important to know what erosion-oxidation is and what the mechanisms of this phenomenon are.

Describing the phenomenon of erosion-oxidation in a way that makes use of the full breadth of understanding gained from studies of each phenomenon operating separately, is particularly difficult and challenging, because of the generally complex nature of both processes and the many potential combinations of the two phenomena [**44**].

3.4.2 Erosion-Oxidation Regimes

According to Wright et al.[**44**] there are three broad but distinct regimes of possible erosion-oxidation, which may overlap:

- Erosion dominates
- Erosion-oxidation interactions
- Oxidation dominates

These regimes are now discussed in more detail.

3.4.2.1 Erosion Dominates

The rate of oxidation is so slow that oxide removal makes a negligible contribution to the overall material loss, which occurs predominantly by the removal of metal. The presence of an oxide film may modify the erosion-oxidation interaction by changing the physical (for instance, coefficient of friction) or mechanical (for instance hardness) properties of the eroding surface. This regime will be encountered at low temperatures and, for very oxidation-resistant alloys, under conditions of very aggressive erosion where the erosive component completely overwhelms the contribution from oxidation.

3.4.2.2 Erosion-Oxidation Interactions

There are obviously several scenarios whereby interactions between erosion and oxidation can result, depending on the relative rates of oxide growth and the severity of the erosive action. In some circumstances, parts of the erodent particles may become detached and embedded in the target surface. The net result of the erosion-oxidation process in this regime is that the rate of oxidation increases as the scale is thinned locally. The magnitude of the increased oxidation rate depends on the thickness of oxide removed by the erosive impact.

3.4.2.3 Oxidation Dominates

The erosive component removes only the outer part of a continuous and growing oxide scale and effectively reduces the oxide thickness, thereby

leading to a more rapid rate of oxidation than expected. This behaviour may be termed "erosion-accelerated oxidation".

3.4.3 Two Basic Regimes

Rishel et al.[**21**] give only two basic regimes of erosion-oxidation, namely erosion-enhanced oxidation and oxidation-affected erosion.

Erosion-enhanced oxidation occurs where the erosive process interacts with the scale and reduces its rate of thickening, thus promoting higher oxidation rates. Oxidation-affected erosion occurs when the metal surface is deformed by the erosive flux and oxide is removed very rapidly. This prevents the continuous oxide layer from forming on the surface of the metal.

3.4.4 Major Factors that Effect Erosion-Oxidation

Wright et al.[**45**] give a summary of factors that influence the simultaneous action of high temperature oxidation and erosion. The rest of this section is adapted from the paper of Wright et al.[**45**].

3.4.4.1 Effect of Metal Temperature

Even though a change in the gas temperature may or may not materially increase the erosion component, the overall contribution to material loss from erosion-oxidation can be significantly affected by a change in the oxidation (gas or metal) temperature.

3.4.4.2 Particle Size Dependence

In erosion-oxidation, in order for damage to occur, the erodent particle need not have sufficient energy to cut or abrade the metal surface but merely needs to cause the surface oxide to spall, which may require a considerably lower level of kinetic energy. Spallation is the mode of coating failure usually caused by internal stresses. Under these conditions, a change in particle size can have two effects:

- At fixed solids loading, an increase in the particle size leads to a decrease in the frequency of erosion events, hence to an increase in the time interval between erosion events.
- Larger particles imply a higher level of kinetic energy, hence the area over which spallation of the oxide scale occurs may be larger.

Therefore, a strong dependence on the erodent particle size is expected under erosion-oxidation conditions where the major loss is by oxide scale exfoliation. It is expected that the erosion-oxidation rates will increase with increased particle size.

3.4.4.3 Velocity Dependence

It would be expected that increasing the velocity at a given particle size and loading in the gas stream would result in an increase in the frequency of impacts, hence a decrease in the time interval available for oxidation to occur. Thus the overall rate of erosion-oxidation would be expected to increase with increasing velocity.

3.4.4.4 Impingement Angle Dependence

At a given solids loading in the gas stream, the effect of changing the angle of incidence of the erodent onto the alloy target is to alter the effective erodent flux experienced by the target surface. The erosion-oxidation rates will therefore decrease with decreasing angle of impingement.

3.4.5 Erosion-Oxidation of Carbon Steel in the Convection Section of a Boiler

Xie and Walsh[**46**] did some research on the erosion-oxidation behaviour of steels in the convection section of a boiler. It was found that erosion was slowest at the lowest metal temperature, regardless of the oxygen concentration, and slow under strongly oxidising conditions at high temperature and high oxygen concentration. Erosion was most rapid at high temperature in the presence of low oxygen concentration. At low oxygen concentration or temperature, erosion was dominated by the ductile behaviour of the metal, but, as conditions were made more oxidising by increasing oxygen concentration or temperature, the steady thickness of oxide scale and the influence of oxide on the erosion behaviour increased. The oxide was more resistant to erosion than the metal over most of the range of temperatures investigated. Therefore, the transition from metal-to-oxide controlled erosion, with increasing temperature, was accompanied by a decrease in the erosion rate.

3.4.6 Conclusion

This discussion of erosion-oxidation scenarios has suggested why the rate of material loss under such conditions is likely to be significantly greater than for erosion alone, since most of the material loss will be the result of the shedding of oxide scale rather than by the cutting or abrasion of the actual metal surface. The particle kinetic energy required to cause this form of material loss is likely to be lower than that required for metal loss by erosion alone.

3.5 Corrective Action Against Boiler Erosion

3.5.1 Introduction

The operating conditions in a coal-fired power station are conducive to fireside corrosion and erosion, both in the furnace wall and in the superheater and reheater areas, and these effects cause tube wall thinning and premature failure. The problems do not occur uniformly, however, and are concentrated locally within a boiler. Corrosion is influenced by coal quality and combustion conditions. Erosion is even more localised in its effect, and results from dust and ash entrainment in the gas stream. [**47**,**48**]

Traditionally, power utilities used temporary maintenance procedures (like pad welding and tube shields) to remedy fly-ash erosion in fossil-fuel-fired boilers. The EPRI report [**27**] illustrates that reliable, permanent solutions to these problems, though initially costly, may prove more economical in the long run.

Remedial measures for alleviating erosion-wear damage of the superheater, reheater, and economiser tubes by continuous impacting of the flue-gas-borne ash are not easily found [**26**].

3.5.2 Basic Courses of Action for Reducing Fly-Ash Erosion in Boilers

There are basically five courses of action available for reducing fly-ash erosion in any location in a boiler [**27**].

- Reduce the bulk velocity in the boiler. (Achieved by lower excess air levels, reduced operating load and lower levels of hot gas recycle.)
- Even out the gas flow across the boiler section to remove turbulent regions. (Achieved by the use of baffles.)
- Minimise the number of impacts of fly-ash on the tubes by reducing the loading of fly-ash in the gas. (Achieved by washing the coal [**49**].)
- Even out the concentration of fly-ash across the boiler section by eliminating centrifugal stratification. (Can be achieved by baffling.)
- Decrease the erosivity of the fly-ash. (Can be achieved by changing the fineness of the coal.)

3.5.3 Different Remedial Measures

Remedial measures used by utilities to combat fireside erosion include both sacrificial and flow-modification approaches. Sacrificial methods involve a range of approaches, including the use of shields, wear plates, deflectors, coatings, and increased tube wall thickness, but essentially treat only the symptoms of the problem. Flow-modification methods attempt to deal with one of the causes of the problem, and entail the use of hardware (e.g. deflectors, perforated plate, or expanded-metal screens) that reduces local fluid velocities in the regions where erosion is occurring. This approach is considered to have the potential to provide a permanent solution to the problem [**27**]. The CEA

Research Report[**31**] states that the prevention of high local velocities is the best way of preventing localised erosion problems.

Table 3-3 and Table 3-4 obtained from different sources give some remedial measures for boiler tube failures due to fly-ash erosion.

Measure	Effect on erosion	Comment
Decrease of ash content of coal	Could have a significant effect as a result of reduced dust burden and less-abrasive ash	May not be practicable and will increase the cost of fuel
Improved soot blowing	Enhances heat transfer; reduces temperature and velocity of the flue gas; prevents deposit blockages of velocity peaks	Improves the heat transfer and hence the performance of the boiler; Sootblowers may cause erosion by themselves
Removal of ash from superheater and economiser hoppers	Prevents re-entrainment of coarse and abrasive ash from fuel hoppers	Many boilers do not have hoppers
Reduction of combustion air preheat temperature	Would reduce the temperature and hence the velocity of flue gas	Would reduce slagging and corrosion, but may increase the unburned carbon in ash
Baffles for high velocity gaps	Can significantly reduce localised erosion wear	Should be applied as soon as the erosion-wear pattern becomes evident
Application of weld layers, shields, and plasma-sprayed coatings	Will extend the life of tube when erosion wear is localised	Should be applied before the damage becomes extensive

Table 3-3 Different Remedial Measures for Boiler Tube Failures [26]

Location	Symptoms	Causes	Temporary Measures	Recommended Long-Term Measures
• Leading edges of all tubes • All pendant superheater/reheater surfaces especially bottom bends at exit from furnace nose to rear pass • Roof and back wall • At top of rear pass • Rear pass superheater/reheater and economiser, tube bends (all rows) adjacent to back wall of rear pass • Tube rows adjacent to side walls of rear pass • With finned tubes, at base of fins • Near tube bank stiffeners • Tubes immediately after open areas in tube bank • Adjacent to soot-blower runs	• Polishing of leading surfaces of tubes • Smoothing of weld beads • Obvious flattening of leading edges or sides of tubes • Cutting of tube supports where local gas jetting might be expected • Flattened areas of tubes with longitudinal cracks • Thin-edged (longitudinal ductile failure if rate of erosion is rapid)	• Overall (bulk) flue gas velocity too high • Local gas velocity too high due to blockage or plugging, or design faults • Local turbulence • Misalignments of tubes (maintenance) • Plugging of flow passages • Very high fly-ash loading in flue gas • Stratification of fly-ash • Unusually erosive fly-ash • Malfunctioning of soot-blowers (poor alignment, insufficient maintenance) • Use of excessive pressure with sootblowers	• Reduce bulk velocity by operating at reduced load • Padweld or shield damaged areas and monitor closely • Replace tubes and monitor closely • Encase critical areas in refractory	• Blend or wash coal to decrease ash loading • Reduce flue gas velocity by reducing excess air • Reduce flue gas velocity by redesigning tube bank • Remove tubes • Increase spacing between tubes • Eliminate tube fins • Install flow control screens • Install baffles at entrance to back pass to redistribute fly-ash • Institute detailed tube thickness monitoring and remaining life calculations • Improve maintenance of sootblowers • Set proper operating procedures for sootblowers

Table 3-4 Remedial Measures for Fly-Ash Erosion of Superheater, Reheater and Economiser Tubes [27]

3.5.3.1 Sacrificial Remedial Measures

3.5.3.1.1 Coatings

The high cost and long lead-time in obtaining special tubes, coupled with the incidental costs of tube replacement, make the application of the surface coatings with specific properties an attractive proposition [**47**]. Care must be taken, however, because in some instances the usage of coatings is ineffective [**50**].

The materials used as coatings need to be effectively protected against corrosion and erosion. They must have a high thermal conductivity in order to provide a good service behaviour and effective and economic maintenance layout [**51**].

Coatings are not viewed with enthusiasm by some utilities, because of the experience of poor performance of coatings applied by faulty techniques [**27**]. One of the most important parameters when applying coatings, is the spray angle, or angle of incidence of the spray material on the substrate. Site spraying is further complicated by the closeness of the tubes in the boiler [**47**]. Care is required so that any heat treatments to cure or harden the coatings do not affect the base material properties [**29**].

It is important to know what influence the coating has on the heat transfer of boiler tubes. Nguyen[**52**] tested the heat transfer characteristics of three different coatings: ceramic coating, black plasma coating and a metallic coating. The ceramic coating and black coating transferred more heat than a bare tube whilst the metallic coating transferred less heat than a bare tube.

Levy and Wang[**53**] determined that small grain size, low porosity and the absence of cracks were the microstructural features that enhanced erosion resistance of coatings. Hardness levels and composition have a secondary effect on coating performance.

3.5.3.1.2 Shields

Because the areas where erosion occur are associated with high-velocity, turbulent gas flow, the proper fixturing of shields is important. Shields which are too large, misaligned, or which can move out of position, and fixturing which further disturbs the gas flow, can lead to an enhancement of the erosion problem [**27**]. Stainless-steel erosion shields give some protection to the plain carbon-steel tube, but care must be taken to shield the whole damaged area [**29**].

3.5.3.1.3 Pad-Welding

Pad-welding should be discouraged, since it is one of the causes of a large number of repeated failures [**27**], due to:

- insufficient material remaining in the tube wall,
- dissimilar metal effects, and
- copper embrittlement.

Pad-welding should not be considered a permanent fix, but should only be used in an emergency situation to extend tube life until the next scheduled outage for maintenance [**17**,**27**].

3.5.3.1.4 Alternative Materials

Where corrosion rates are high, the need for frequent replacement of tubes can be reduced by the use of a higher grade material with improved corrosion resistance, or, in the case of erosion, wrappers may be used [**47**]. Boiler tubes can be manufactured from materials specially designed for erosive/corrosive boiler application [**50**,**54**,**55**].

3.5.3.2 Flow-Modification Approaches

The basic cause of boiler tube failure is that the flue gas velocity is too high for the ash erosion wear propensity of given fuel supply, and once the boiler plant is built, the velocity of flue gas flow in erosion-affecting passages cannot be greatly reduced. There are, however, some measures that should be considered for reducing the overall velocity of the flue gas and eliminating the high velocity zones where the ash impaction erosion occur [**26**]. The second basic cause of fly-ash erosion, where flow-modifying approaches can be used to reduce erosion, is particle concentration [**49**].

3.5.3.2.1 Flow-Modifying Screens and Baffles

Expanded-metal screens are installed in order to control erosion by modifying the flow velocity, reducing excessive gas velocities and redistributing the ash load. As already mentioned, the erosion of a metal surface by a particle-laden flow is influenced by the physical properties of the fly-ash particles and the metal, particle impact angle and the incident particle speed. Erosion is linked to one of these factors and a predominance of any one of these factors leads to an increase in the erosion potential. Thus the control of the carrier gas velocity is important. Due to the boiler geometry, flows with skewed velocity distributions develop and this leads to high velocities and channelling in sections of the boiler. This channelled flow contains a higher concentration of fly-ash leading to erosion problems in those areas. The erosion can be controlled by modifying the flow within the boiler through the use of screens, particularly in the critical areas of high gas velocity [**56**]. Refer to Figure 3-2 for an example of screen location.

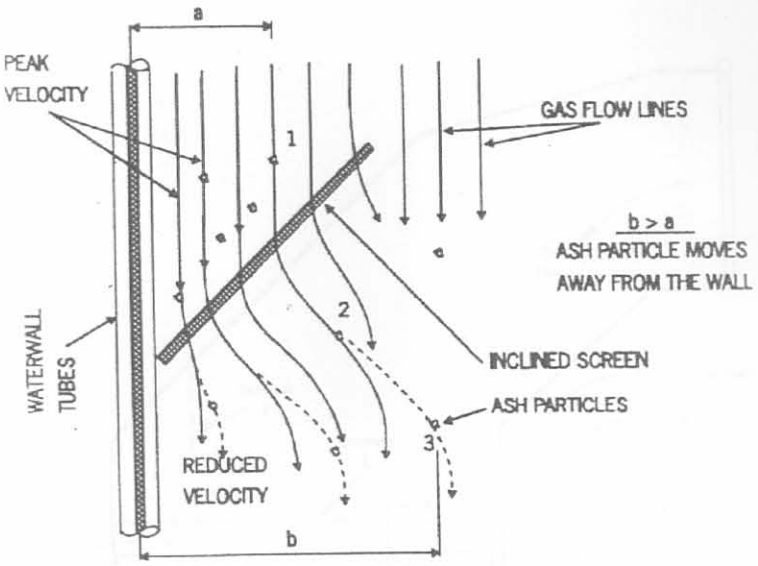

Figure 3-2 Schematic Showing of Expected Screen Behaviour [56]

Typically, screens are used to modify fluid flow by creating or eliminating large-scale velocity or pressure non-uniformities and for the production or for the reduction of turbulence. The placement of the screen requires knowledge of flow turning and the redistributing capabilities of the screen.

The installation of horizontal baffle plates are used to block open areas and reduce non-uniform gas flow. The use of totally solid baffles can cause movement of the erosion to an adjacent area, thus expanded stainless wire meshes would be preferable. Care must be taken to ensure that the local high velocity is not transferred to other locations [**29**].

Baffles intended to effectively prevent gas flow between the tube banks and to the walls have sometimes acted to deflect and concentrate a stream of fly-ash onto adjacent tubes, with the result that highly-localised wastage has been experienced. Such secondary effects can be minimised if sufficient clearance can be maintained between the baffles and the downstream tube bank so that jets and eddies induced by the baffles are dissipated ahead of the tubes. Baffle plates containing holes (punched plate) to allow some gas flow, and so reduce the deflection/concentration effect, are also used but have introduced a new problem. Depending on the positioning of these baffles with respect to the downstream tubes and the resistance to flow imposed by the plate, flow through the holes may result in concentration of the fly-ash and accelerated erosion of the first tubes to intersect the gas flow downstream [**27**].

3.5.3.2.2 Flow Modification in Boiler Back Pass

Figure 3-3 shows the positions of screens intended to minimise economiser erosion in the boiler back pass [**27**]. The gap between the tube bundles can be seen in the detailed view of Section A-A in Figure 3-3. Figure 3-4 shows the application of the screen over the gap in the centre of the economiser in Figure 3-3.

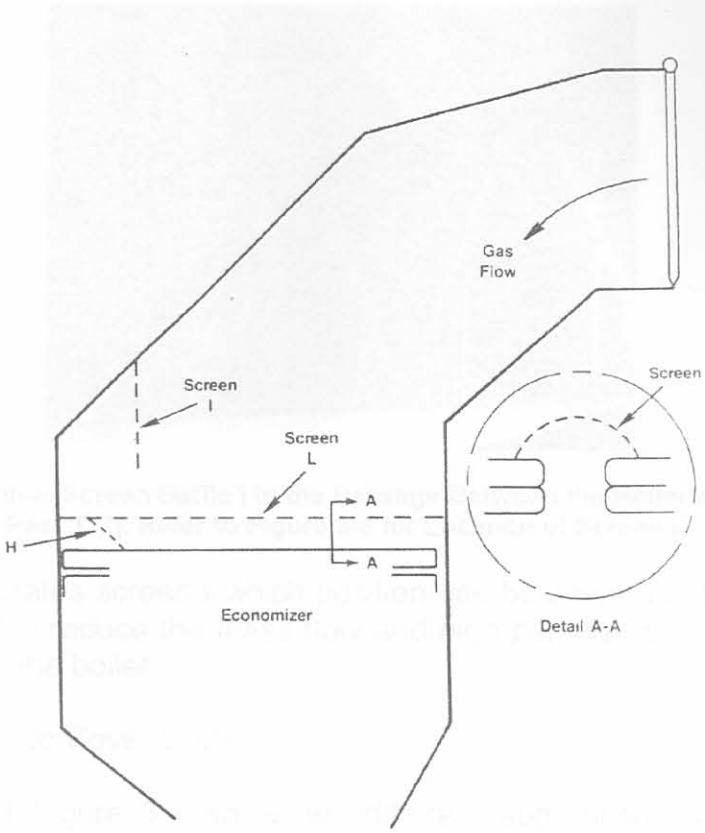

Figure 3-3 Boiler Geometry for Economiser Section – Fly-Ash Erosion Protection through the use of Screens[27]

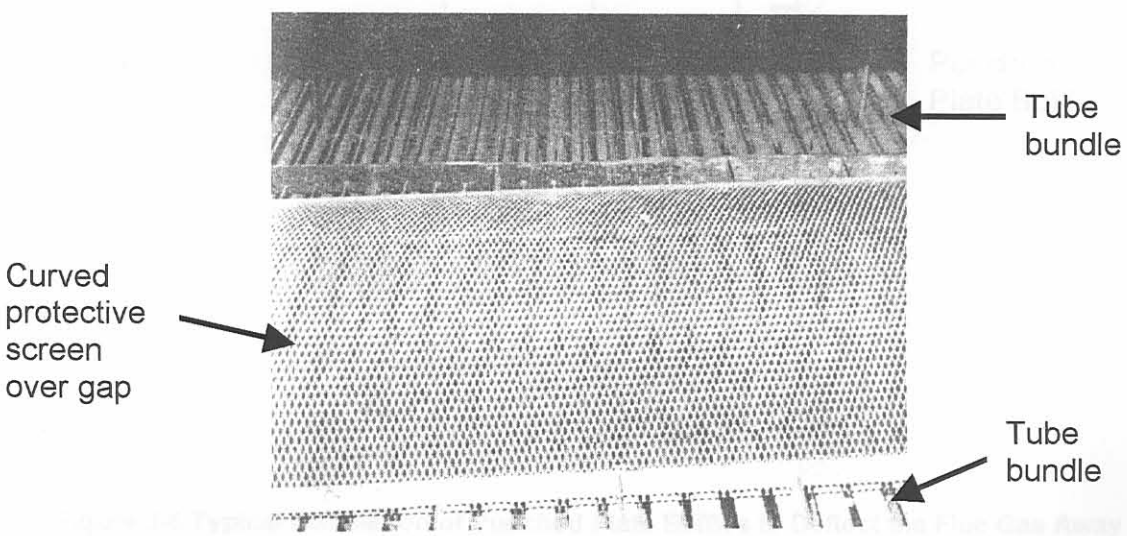

Figure 3-4 Protective Screen L Over the Gap Between Tube Bundles in the Centre of the Economiser [27]. Refer to Figure 3-3 for Location of Screen L

The screen is curved to provide a variable resistance and as such the high velocity and ash are redistributed to obtain a uniform velocity and a uniform ash concentration [**32**].

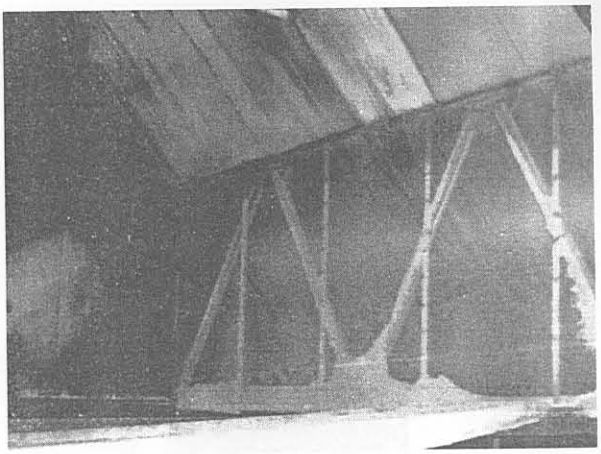

Figure 3-5 Vertical Screen Baffle I in the Passage Between the Boiler and the Back Pass [27]. Refer to Figure 3-3 for Location of Screen I

Figure 3-5 illustrates screen I which position can be seen in Figure 3-3. This screen is used to reduce the mass flow and high particle concentration near the back wall of the boiler.

3.5.3.2.3 Baffles to Cover Gaps

Figure 3-6 and Figure 3-7 show two different applications to cover gaps between tube banks and boiler walls.

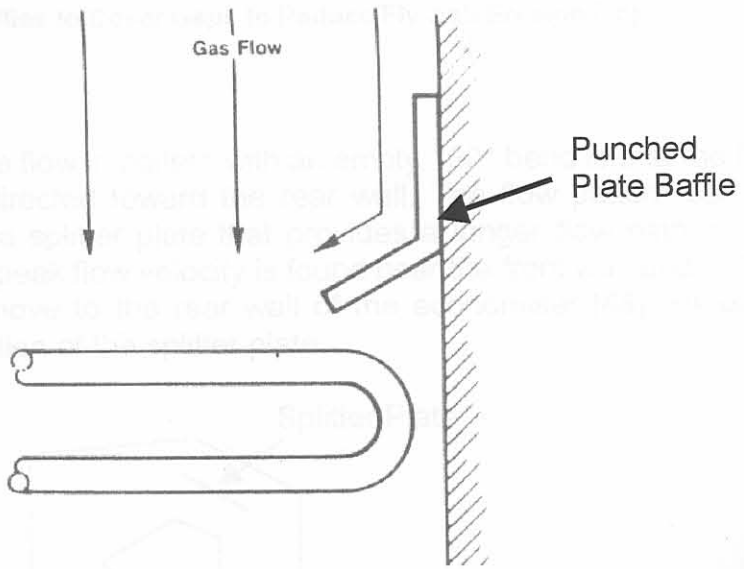

Figure 3-6 Typical Installation of Punched Plate Baffles to Deflect the Flue Gas Away from the Gap Between the Tube Bank and Boiler Wall [27]

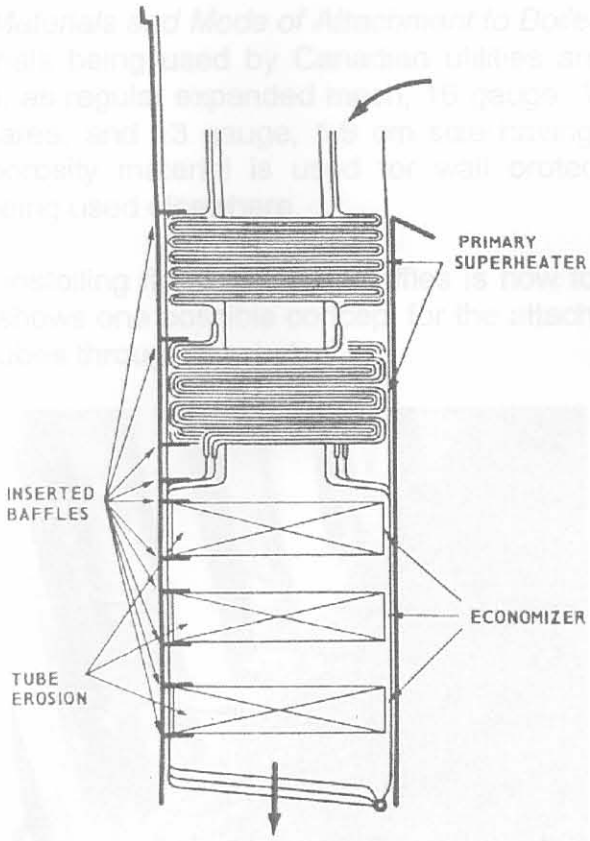

Figure 3-7 Baffles to Cover Gaps to Reduce Fly-Ash Erosion [26]

3.5.3.2.4 Splitter Plate

The main feature of the flow in boilers with an empty 180° bend is that the flue gas and fly-ash are directed toward the rear wall. The flow pattern can be modified by inserting a splitter plate that provides a longer flow path at the bend. In this case the peak flow velocity is found near the front wall and not all the fly-ash particles move to the rear wall of the economiser [**48**]. Refer to Figure 3-8 for the location of the splitter plate.

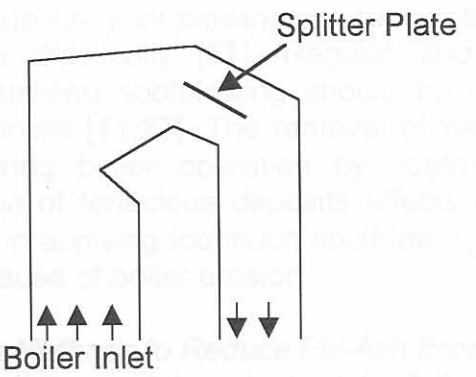

Figure 3-8 Splitter Plate to Defelect Flow in the Upper Part of a Boiler[48]

3.5.3.2.5 Screen Materials and Mode of Attachment to Boiler Tubes

The screen materials being used by Canadian utilities are stainless steels, typically Type 304, as regular expanded mesh, 16 gauge, 1.3 cm size having 47 percent open area, and 13 gauge, 1.9 cm size having 75 percent open area. The high porosity material is used for wall protection, with the 47 percent material being used elsewhere.

A predicament of installing flow-modifying baffles is how to attach them in a boiler. Figure 3-9 shows one possible concept for the attachment of protective screens to boiler tubes through brackets.

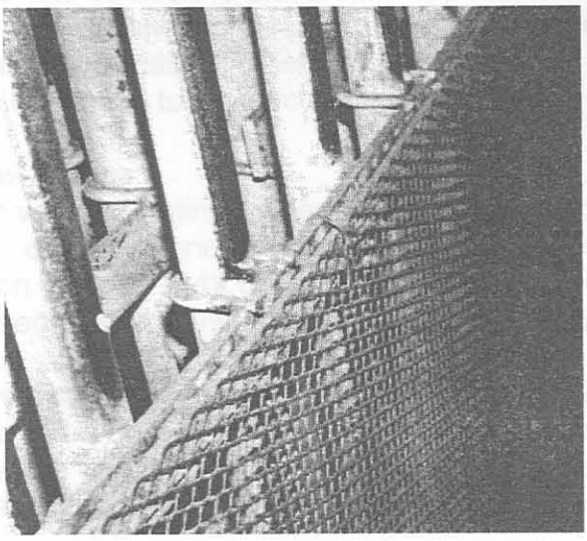

Figure 3-9 Mode of Attachment for Protective Screen through the use of Brackets[27]

Care must be taken when applying flow-modifying screens, because when screens are applied wrongly they can cause severe erosion. Erosion can be inflicted on the tubes where they are attached to the screens [**49**].

3.5.3.3 Other Remedial Methods

3.5.3.3.1 Sootblowing

If used in the right sequence, soot blowing can reduce boiler tube erosion and plant operating costs drastically [**57**]. Regular and properly sequenced (upstream and downstream) sootblowing should be capable of preventing plugging by loose deposits [**11**,**27**]. The removal of weakly bonded deposits can be achieved during boiler operation by sootblowing. However, the extensive accumulation of tenacious deposits affects boiler availability [**58**]. Care should be taken in applying too much sootblowing because sootblowing can itself be a major cause of boiler erosion.

3.5.3.3.2 Maintenance Methods to Reduce Fly-Ash Erosion

No matter what precautions are taken, boiler tube failures are going to occur. However, the service life of boiler tubing can be extended through proper maintenance and care [**16**].

Many authors propose maintenance visions to prevent boiler tube failures [**12**,**13**,**14**,**15**,**16**,**17**,**18**,**57**,**59**,**60**,**61**,**62**,**63**,**64**]. These visions include new management and maintenance plans to reduce boiler tube failures as well as expert systems to predict boiler tube failures and boiler tube life.

Accurate prediction of the lives of boiler tubes is difficult because of uncertainties associated with loading conditions, erosion/corrosion rates, geometry of the eroded/corroded areas, and material properties [**64**].

Techniques and strategies employed to overcome tube degradation are many and varied, and no one solution is universally applicable. Where decay rates are low it is often most economic simply to replace the worn tube with new material of similar specification when routine surveys indicate that the effective thickness has fallen to a particular level [**47**].

3.5.3.3.3 Cold Flow Studies

The use of cold air velocity testing to identify turbulent velocity areas, followed by installation of diffusing and distribution screens, provide permanent solutions for erosion problems [**49**,**65**]. The great advantage of this technique is that it can be used after the installation of the flow modification devices to test their efficiency. Velocity readings must be taken on a large-scale grid across various levels of the boiler as was done by Black and McQuay[**66**] and the CEA Research Report[**67**], and on a fine grid in areas where high velocities are known or expected to be present [**27**]. This technique has been applied very successfully to many boiler units in a number of countries [**17**].

The results of the research done by MacDonald[**67**] confirms the usefulness of cold air velocity testing in abatement of erosion and boiler tube failures. The results indicate a major requirement for cold flow tests to detect local flow conditions. The measurement of cold air flows is the most important task and the most critical variable in erosion control programs.

Drennen et al.[**68**] summarised a program to control and prevent boiler tube failures from fly-ash erosion. The heart of the program is the cold air velocity test in the boiler. The program is used to identify the type and placement of flow control devices that redistribute ash and gas to reduce the erosion potential. Refer to Figure 3-10 for a road map of activities for the control and prevention of fly-ash erosion through the usage of cold air velocity testing.

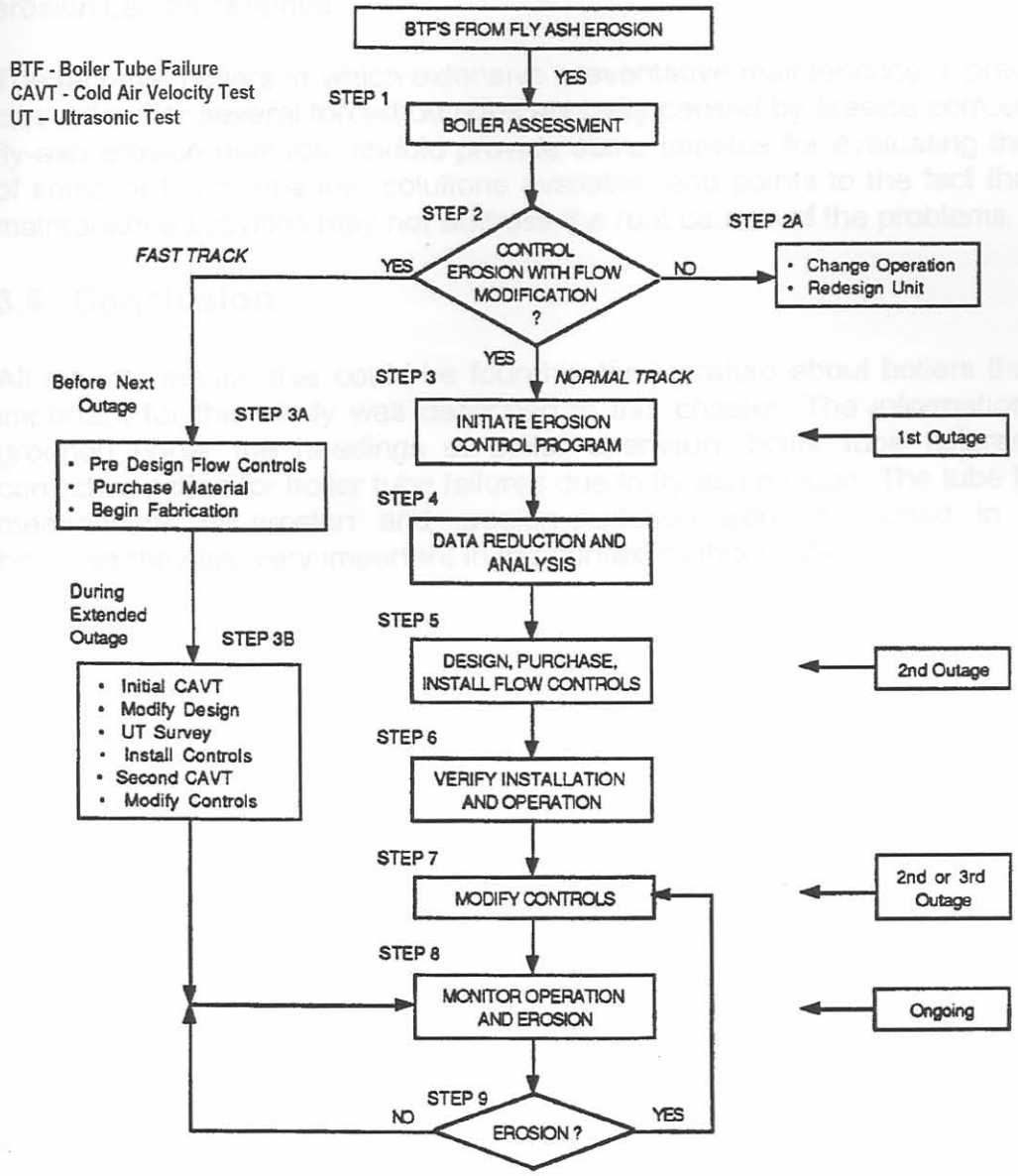

Figure 3-10 Road Map of Activities for Control and Prevention of Fly-Ash Erosion [68]

3.5.4 Conclusion

There are basically two different fields of approaches for corrective action of fly-ash erosion in pulverised-coal-fired boilers. These fields of corrective action are either sacrificial approaches or flow-modifying approaches. Sacrificial approaches include the usage of coatings, shields, pad-welding or the use of more suitable alternative materials. These corrective approaches essentially treat only the symptoms of the problem and do not provide permanent solutions. Flow modification approaches usually provide more permanent solutions, through the use of screens and baffles. The aim of flow-modification approaches is to redistribute the ash load and to prevent channelling of the flue gas. Through the use of cold flow studies together with

the use of flow-modification approaches, permanent solutions to fly-ash erosion can be obtained.

The fact that boilers in which extensive preventative maintenance is practised can still suffer several forced outages annually caused by fireside corrosion or fly-ash erosion damage, should provide some impetus for evaluating the use of some of the permanent solutions available, and points to the fact that the maintenance activities may not address the root causes of the problems.

3.6 Conclusion

All the information that could be found in the literature about boilers that are important for this study was described in this chapter. The information was grouped under the headings of boiler operation, boiler tube failures and corrective action for boiler tube failures due to fly-ash erosion. The tube failure mechanisms of erosion and erosion-oxidation were discussed in detail because they are very important in the context of this study.

4 CFD Modelling of Boiler

4.1 Two-Phase Flow and Flow in Tube Banks

4.1.1 Introduction

Due to the fact that most of the erosion occurs in and around boiler tube banks is it important to know how two-phase flow behaves around these tubes. A fair amount of research has been done on erosion of single tubes as well as of multiple tubes. The multiple tubes are configured either in a staggered or an in-line arrangement. Table 4-1 gives a summary of literature on flow through tube banks.

Tube Arrangement	Source
Single Tube	**[69,70]**
Staggered	**[71,72]**
In-line	**[73,74,75,76]**
Staggered and In-line	**[39,77,78,79,80,81,82,83,84,85]**

Table 4-1 Literature Research Sources on Flow Around Tubes

These references will now be discussed in more detail.

4.1.2 Two-Phase Flow

The presence of solid particles in many industrial applications has a detrimental effect on the performance of the components. The problem of particulated flow in any flow system can be divided into three parts. The first part consists of the particle trajectories. The second is the effect of the presence of the particles on the fluid behaviour. The third part consists of the nature of the solid surface impact and the material erosion [**69**].

4.1.3 The Effect of Particles on Fluid Flow Properties

4.1.3.1 Around Tubes

The presence of particles in a fluid could affect flow properties such as streamline patterns, vorticity, coefficient of drag, separation angle, and recirculation eddies. With an increase in particle size, there is a larger difference in relative velocities between that of the particle and the air because of higher inertia, thus resulting in higher interphase forces. This leads to a change in the fluid velocities, resulting in an increased coefficient of drag of a tube in cross-flow. Thus, the influence of the particles on the fluid flow depends on the size and number of particles present for a given mass fraction. With an increase in particle mass fraction, the size of the recirculation zone increases. With larger-diameter particles, the length of the recirculation eddy is decreased with an increase in the particle concentration [**69**].

4.1.3.2 In the Rest of the Boiler

Gas flow patterns are determined primarily by the air inlet geometry and conditions are not greatly modified by liquor sprays and in-flight combustion [**86**].

4.1.4 Particle Rebound Phenomenon of Particles

The erosion of metals impacted by small dust particles as well as the rebound dynamics of these particles can only be described in a statistical sense [**34**,**40**]. This becomes obvious when one examines the number of geometric situations that might occur at impact [**34**]. Quartz sand was used in the research of Grant and Tabakoff[**34**]. The value of the velocity of a particle and the direction of its motion as it rebounds from the surface after collision must be known so that the solution of the particle equations of motion may be continued beyond the points of collision [**69**]. Equations (4-1) and (4-2) are the results obtained by Grant and Tabakoff[**34**].

$$\frac{V_{N_2}}{V_{N_1}} = 0.993 - 1.76\beta_1 - 1.56\beta_1^2 - 0.49\beta_1^3 \qquad (4\text{-}1)$$

$$\frac{V_{T_2}}{V_{T_1}} = 0.988 - 1.66\beta_1 + 2.22\beta_1^2 - 0.67\beta_1^3 \qquad (4\text{-}2)$$

The symbols of Equations (4-1) and (4-2) are defined in Figure 4-1.

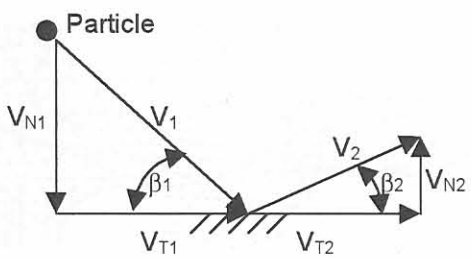

Figure 4-1 Velocity and Angle Notations for Particle Rebound Characteristics

4.1.5 Effect of particles size on particle trajectory in an in-line tube bank

Transverse and longitudinal tube spacing, cylinder diameter and the flow velocity of the gas seem to be important factors affecting particle trajectory, impact, and erosion when particle properties are fixed [**35**,**80**]. Two numerical simulations [**73**,**81**] are now discussed in more detail, as their results bear resemblance to the CFD simulation performed by the author to be presented later in this dissertation.

4.1.5.1 Numerical Simulation 1

This numerical simulation of two-phase flow in a tube bank was conducted by Jun and Tabakoff[**73**]. The flow and geometry specifications are as follows:

Flow Reynolds number (Re)	= 400 (Laminar)
Air density	= 1.23kg.m^{-3}
Particle size	= 40μm and 100μm
Particle density	= 2444kg.m^{-3} (sand); 1666kg.m^{-3} (Fly-ash)
Tube arrangement	= transverse- , longitudinal pitch = 2×cylinder diameter

Figure 4-2 shows the particle trajectories of 100μm sand. For these large particles, most of the rebounded particles from the first cylinder cross the mainstream and impact on the neighbouring cylinder surface either on the first or second row. Therefore a considerable amount of secondary impact occurs on the first cylinder surface either on the front side or on the backside relative to the main stream. Particles introduced in the wake do not change the direction significantly because the particle inertia is dominant compared to the aerodynamic forces acting on it. Impact occurs mostly on the front side of the first cylinder while it occurs less frequently on the front side of the second cylinder and on the backside of the first cylinder. According to the results from the simulation, the maximum erosion occurred at 40° to 70° from the leading edge, even though the maximum impact frequency occurred at 0° to 50° from the leading edge.

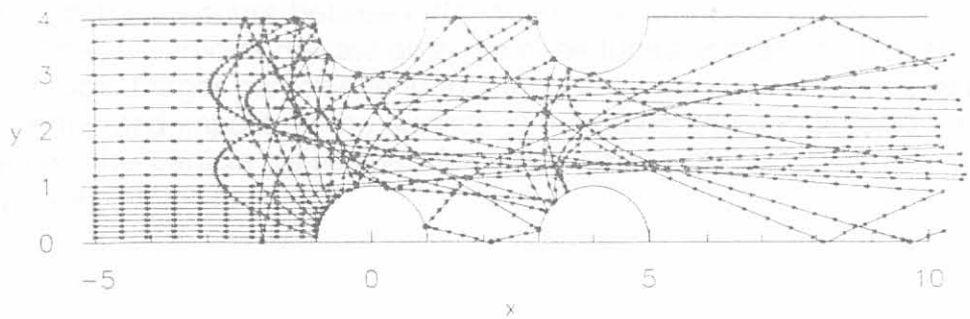

Figure 4-2 Particle Trajectories Over In-Line Tube Bank (Re=400); 100μm Sand [73]

Figure 4-3 shows the particle trajectories of 40μm fly-ash. For these smaller size particles, most of the impact on the first cylinders are primary impacts, while most of the impacts on the second cylinders are secondary impacts from the first row of cylinders. An interesting feature of the impacts on the second cylinders is that they are concentrated in a limited area on the tube surface in this particular case. The local maximum erosion on the second row of tubes occurs around 60° to 70° from the leading edge.

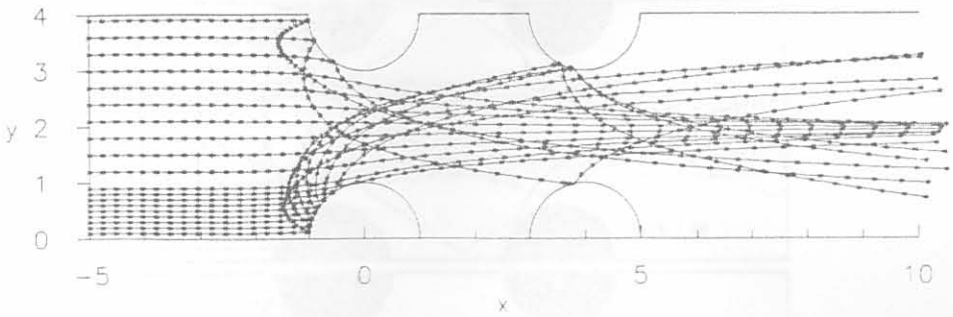

Figure 4-3 Particle Trajectories Over In-Line Tube Bank (Re=400); 40μm Fly-ash [73]

4.1.5.2 Numerical Simulation 2

This numerical simulation of two-phase flow in a tube bank was conducted by Fan et al.[**82**]. The simulation properties are as follows:

Particle material	= coal ash
Gas velocity	= 6.1m.s^{-1}
Air density	= 1.23kg.m^{-3}
Particle size	= 20, 30, 40, 50, 100, 200μm
Particle density	= 2450kg.m^{-3}
Tube arrangement	= transverse-, longitudinal pitch = 2×cylinder diameter

Erosion damage occurs between 40° and 60° in the case of the first row of tubes. Smaller particles deviate away from the tubes and do not impact on the tube surface. Larger particles tend to keep their initial momentum because of their inertia, and impact on the surface of the tubes and get deflected. Figure 4-4 shows the particle trajectories for particle sizes of 0.02, 0.05 and 0.1mm respectively.

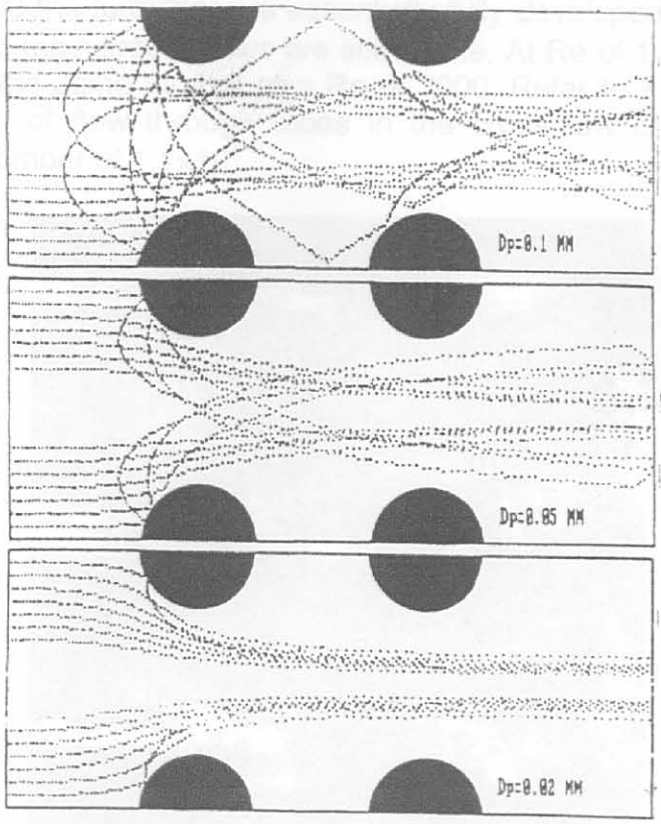

Figure 4-4 Particle Trajectories in Two-Phase Flow Around In-Line Tubes (V_∞=10m/s) [82]

4.1.6 Observations of Flow Phenomena in an In-Line Tube Bank

Here are some observations made by other researchers regarding flow phenomena in in-line tube banks:

- Fujii and Fujii[**74**] found that an almost fully-developed flow pattern is attained behind the first row of tubes. Weaver and Abd-Rabbo[**75**] observed flow patterns for an in-line array of four tube rows over a wide range of Reynolds numbers. Flow visualisation showed that the flow development is a function of not only Reynolds number but also of the row number of tubes.
- From pressure drop experiments conducted by Traub[**84**], it follows that the drag coefficient is almost independent of the inlet turbulent intensity over a wide range of Reynolds numbers.
- Flow visualisation by Weaver and Abd-Rabbo[**75**] shows that the flow pattern around the first and second row tubes is not typical of that around the third and subsequent rows. For Re = 30, the wake regions between the tubes appears essentially stagnant. As Re is increased, the wakes are seen to consist of two stable vortices with clear straight flow lanes between the columns. At a Re of about 150, these vortices begin to become unstable, with the flow crossing the wake region and the vortices periodically being swept into the mainstream flows. There is no evidence that the mainstream flow is significantly affected by the developing turbulence in the wakes. At Re = 400, the wakes become fully turbulent. At

a Re of 3000 the turbulence is essentially fully developed by the third row although the mainstream flows are still visible. At Re of 1.1×10^4 the flow is essentially the same as that at a Re of 3000. Refer to Figure 4-5 for the visualisation of flow through tubes in the cross-flow configuration at a Reynolds number of 1.1×10^4.

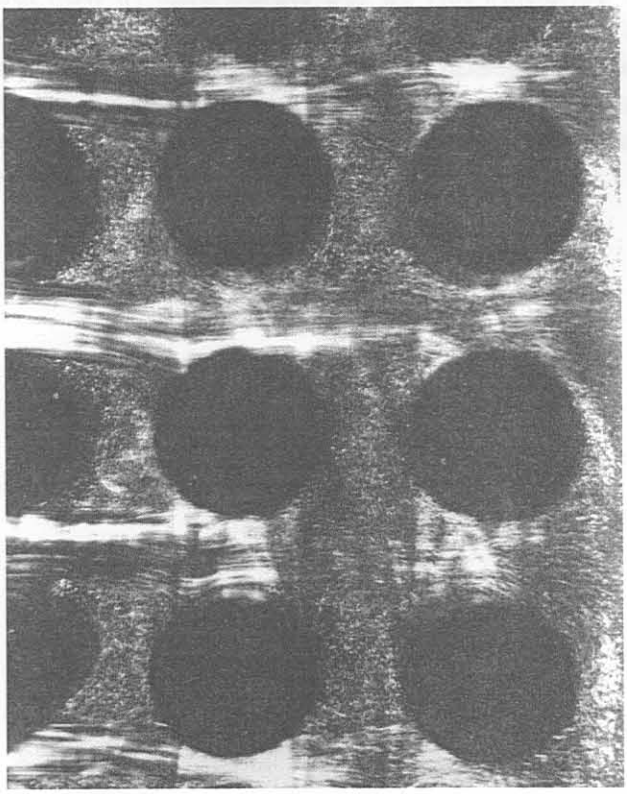

Figure 4-5 Flow Visualisation in an In-Line Tube Bank (Re=1.1×10^4) [75]

- The flow is steady at the entrance of the tube banks, but becomes oscillatory downstream of the onset location of vortex shedding [**79**].
- Tube erosion damage by particle impaction depends on the particle size and the free stream velocity [**72**].
- Flow visualisation by Nishimura et al.[**78**] shows that the flow changes from steady to unsteady at about Re=100 due to vortex shedding for in-line as well as staggered tube arrays.

4.1.7 The Effect of a Gap Between Tube Rows of an In-Line Tube Bank

Gaps between adjacent layers of crossflow in-line tube banks are sometimes required because of manufacturing feasibility or soot blowing lanes. Only one paper could be found that deals with the effect of a gap between rows of an in-line tube bank. Zhang and Chen[**87**] did research on how a gap influences heat transfer of tubes in a tube bank. No literature was found however that deals exclusively with erosion or flow patterns in a tube bank with a gap between adjacent tube rows. Zhang and Chen[**87**] found that the existence of

a gap enhanced the heat transfer of those tubes just adjacent to the gap by 10 to 30%.

4.1.8 Conclusion

Particles can affect flow in tube banks but do not influence large-scale boiler flows. Two-phase flow in in-line tube banks is dependent on tube spacing as well as particle size. Smaller particles do not impact tubes in tube banks, as do larger particles. It was also discovered that flow in in-line tube banks is fully turbulent at a Reynolds number of 3000 and the flow field remains essentially the same for larger Reynolds numbers.

4.2 CFD Modelling of Erosion and Boiler Flow

4.2.1 Introduction

There are a few papers available in the literature on erosion in boilers and the nature of flow through the boiler using CFD. Because CFD will be used in this study, it is important to know what other researchers had done, what assumptions they made and how accurate their results were compared to measurements.

4.2.2 Boundary Conditions, Heat Transfer and Two-Phase Flow

As already discussed in Chapter 2, is it important to apply the correct boundary conditions to obtain realistic results.

4.2.2.1 Inlet Boundary Conditions

The following assumptions were made by other researchers regarding boiler inlet conditions:

- In all the research found on CFD simulation of flow through a boiler, a uniform inlet flow velocity profile and geometry was assumed [**48**,**88**,**89**,**90**,**91**]. Figure 4-6 illustrates an example of a uniform velocity inlet as applied to boiler CFD models.
- Shen et al.[**89**] also assumed a uniform inlet temperature distribution.
- Tu et al.[**48**] assumed a uniform inlet fly-ash concentration distribution.
- Inlet turbulence intensity is taken to be 5% by Tu and Fletcher[**88**], and 10% by Shen et al.[**89**].

The following conclusions were drawn from studies by other researchers regarding boiler inlet conditions.

- Shen et al.[**89**] concluded during upper boiler studies that different inlet velocity and temperature profiles do not significantly alter the velocity field and temperature distributions through a boiler.
- Vakkilainen et al.[**91**] used a variety of inlet velocity profiles and temperature profiles to determine the sensitivity of the results to chosen inlet conditions. Results from this work show that predicted temperature profiles and velocity profiles at the boiler bank and superheater heat transfer surfaces were not affected significantly by these inlet conditions. Flow features like channelled flow, tangential swirling and recirculation zones can be very strong in the lower furnace near the air jets, but dissipate somewhat due to turbulent shear in the upper furnace.

4.2.2.2 Outlet Boundary Conditions, Heat Transfer and Ash Particles

This section describes some assumptions made or conclusions reached by other researchers regarding boiler outlet conditions, heat transfer and ash particles in simulated boiler environments.

- The normal gradient of all dependent variables is set to zero at the outlet of the computational domain [**48**,**88**].
- Shen et al.[**89**] found that radiation heat transfer in boilers can be omitted in CFD simulations without influencing flow patterns through the boiler.

- The solid particles are assumed to have no influence on the gas flow [**89**].
- Fly-ash particles are assumed to be spherical [**48**].

4.2.3 Computational Grids

As discussed in Chapter 2.5, the grid must be of an appropriate quality to obtain reliable CFD results. The rest of this section gives a summary of grid sizes used by other researchers. An example of a computational grid is also illustrated. This information will give guidelines of what grid are required in boiler CFD models.

- Shen et al.[**89**] used 50 410 cells (71×71×10) in the CFD model. The geometry of the computational domain can be seen in Figure 4-6.

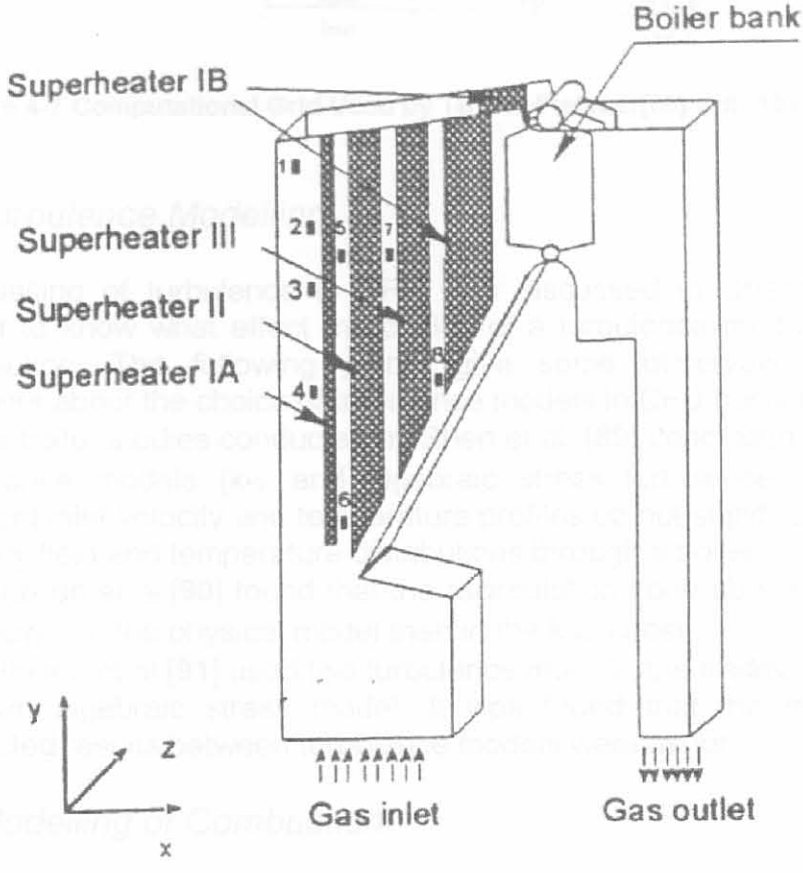

Figure 4-6 Schematic of Modelling Geometry used by Shen et al.[89]

- Tu et al.[**48**] used 117000 cells (30×130×30) in a domain almost similar to the one illustrated in Figure 4-7.
- Vakkilainen et al.[**90**] used 21888 cells (32×36×19) extending from below the bullnose to the exit of the boiler bank.
- Vakkilainen et al.[**91**] used 50000 nodes extending from below the bullnose to the entrance of the economiser.
- Tu and Fletcher[**88**] used a grid of 103168 cells (62×52×32). This grid is shown in Figure 4-7.

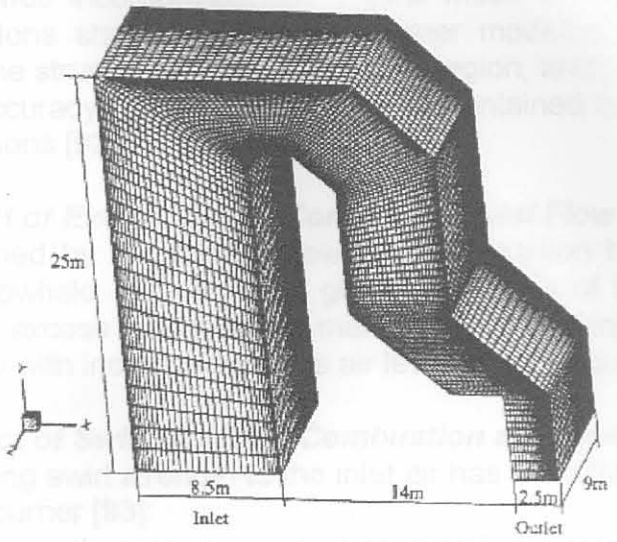

Figure 4-7 Computational Grid Used by Tu and Fletcher[88] with 103 168 cells

4.2.4 Turbulence Modelling

The modelling of turbulence in CFD was discussed in Chapter 2.3. It is important to know what effect the choice of a turbulence model has on the CFD solution. The following points give some observations by other researchers about the choice of turbulence models in CFD boiler models.

- Upper boiler studies conducted by Shen et al. [**89**] concluded that different turbulence models (k-ε and algebraic stress turbulence models) and different inlet velocity and temperature profiles do not significantly alter the velocity field and temperature distributions through a boiler.
- Vakkilainen et al.[**90**] found that the recirculation zone above the bullnose was larger in the physical model than in the k-ε model.
- Vakkilainen et al.[**91**] used two turbulence models, the traditional k-ε model and an algebraic stress model. It was found that the differences in predicted results between turbulence models were minor.

4.2.5 Modelling of Combustion

Because the modelling of combustion is very complex as will become evident in the rest of this section, ways must be investigated to simplify the modelling of combustion and what effect this simplification will have on the flow field through a boiler.

Grace et al.[**86**] found that gas flow patterns are determined primarily by the air inlet geometry and conditions, and are not greatly modified by liquor sprays and in-flight combustion.

4.2.5.1 Burner Modelling

The CFD solver STAR-CD has been used successfully by other researchers to assess NOx production and char burnout trends in boilers. A detailed

burner geometry was incorporated into a CFD mesh of 420000 cells. The STAR-CD predictions show that detailed burner modelling is essential to reproduce the flame structure in the near-burner region, and provided that this is done, a high accuracy of predictions can be maintained in the scale-up to multiburner conditions [**92**].

4.2.5.2 The Effect of Excess Air on Combustion and Flow

The results obtained by Gupta[**93**] show that combustion has a significant effect upon the flowfield. Although the general features of the flowfield are unaffected by the excess air level, the maximum mean temperatures decay much more rapidly with increased excess air level than its counterpart.

4.2.5.3 The Effect of Swirl of Air on Combustion and Flow

The effect of varying swirl strength to the inlet air has the following features of the flow near the burner [**93**]:

- Higher swirl strength promotes a higher centrifugal force, and hence a larger central recirculation zone core diameter.
- Increased swirl strength reduces or eliminates the size of the corner recirculation zone and increases the central toroidal recirculation zone.
- Combustion reduces the length and width of the central recirculation zone, under similar conditions of swirl to the airflow.

4.2.6 Other Observations of Flow through Boilers using CFD

4.2.6.1 The Effect of the Tube Bank on Flow through the Boiler

The points discussed next are observations and assumptions made by other researchers on the effects of the tube bank on the flow pattern through the boiler.

- If the tube bank is not included in the CFD model, the channelled flow narrows at the exit of the superheater and the temperatures in the recirculation zone are moderately higher. In addition, if the flue gas is assumed to have a constant density, the temperatures in the recirculation are moderately lower [**89**]. Shen et al.[**89**] treated the tube bank as a lumped heat exchanger with non-isotropical heat transfer coefficients and pressure loss coefficients.
- Tu et al.[**48**] showed that it is possible to obtain a good indication of regions of high erosion rate without the need of modelling tube banks, thus greatly simplifying the calculations. The quality of the solutions in boilers without tube banks is sufficient to provide an insight into the flow phenomena and erosion patterns within coal-fired boilers.
- Vakkilainen et al.[**90**] concluded that the modelling of flow without boiler internals such as the superheater tubes and tube bank give better results for the flow field through the boiler than models with internals, where the tube bank was modelled using a porous cell approximation.

4.2.6.2 The Effect of the Bullnose on Flow through the Boiler

The purpose of the bullnose is to protect the superheater tubes from furnace radiation [**90**]. The design of the upper boiler and the shape of the bullnose result in a large recirculating flow above the bullnose which greatly reduces the convective heat transfer [**89**,**90**]. It was found, however, that the velocity

and temperature distributions are sensitive to the shape and size of the bullnose [**89**]. The effect of size and shape of the bullnose on gas temperature and velocity were investigated for three sizes and three shapes by Vakkilainen et al.[**91**]. Both the size and the shape of the bullnose affected gas flow.

4.2.6.3 Inertia of Particles

Here are some observations made by other researchers regarding particles in boiler flows through the use of CFD.

- The flue gas and fly-ash entrained into the economiser are thrown to the rear wall of the economiser due to centrifugal forces. The velocities of both flue gas and fly ash are highest in this region [**48**].
- Smaller fly-ash particles are more influenced by the gas flow, and, with increasing particle size, the larger particles are accelerated by the centrifugal force and flung outwards [**88**].

4.2.7 Conclusion

CFD has previously been used by researchers to model erosive boiler environments with success. Good results can be obtained with assumptions such as uniform inlet velocity and temperature profiles. Radiation can also be omitted in CFD boiler simulations without affecting the flow pattern through the boiler significantly. Combustion can therefore be ignored in CFD models for upper boiler erosion studies. Boiler internals, such as the tube bank, do not have to be modelled to indicate regions of high erosion rate. The effect of the turbulence model used in boiler flows has a negligible effect on the flow field apart from small changes in the sizes of recirculation zones. From all the information gathered in this section, it becomes obvious that great simplifications can be made to boiler CFD models.

4.3 CFD Analysis : A Parametric Study for Different Conditions of Flow Through a Boiler

4.3.1 Introduction

The following section is a parametric study of the influence that certain parameters like inlet velocity, inlet geometry and porosity of boiler internals have on the flow field through the boiler. The effect of particle size on particle trajectories is also investigated. This section of this study does not simulate real boiler operating conditions of the Babcock boilers but it is done to become familiar with boiler flows and to see the effect of different parameters on the flow field through the boiler.

4.3.2 2D Analysis of the Boiler

The first CFD analysis of the boiler is a 2D simulation of the flow through the boiler. A 2D grid is used because it produces fast results and should be efficient to visualise the flow field through the boiler. The 2D simulation is a very useful first analysis.

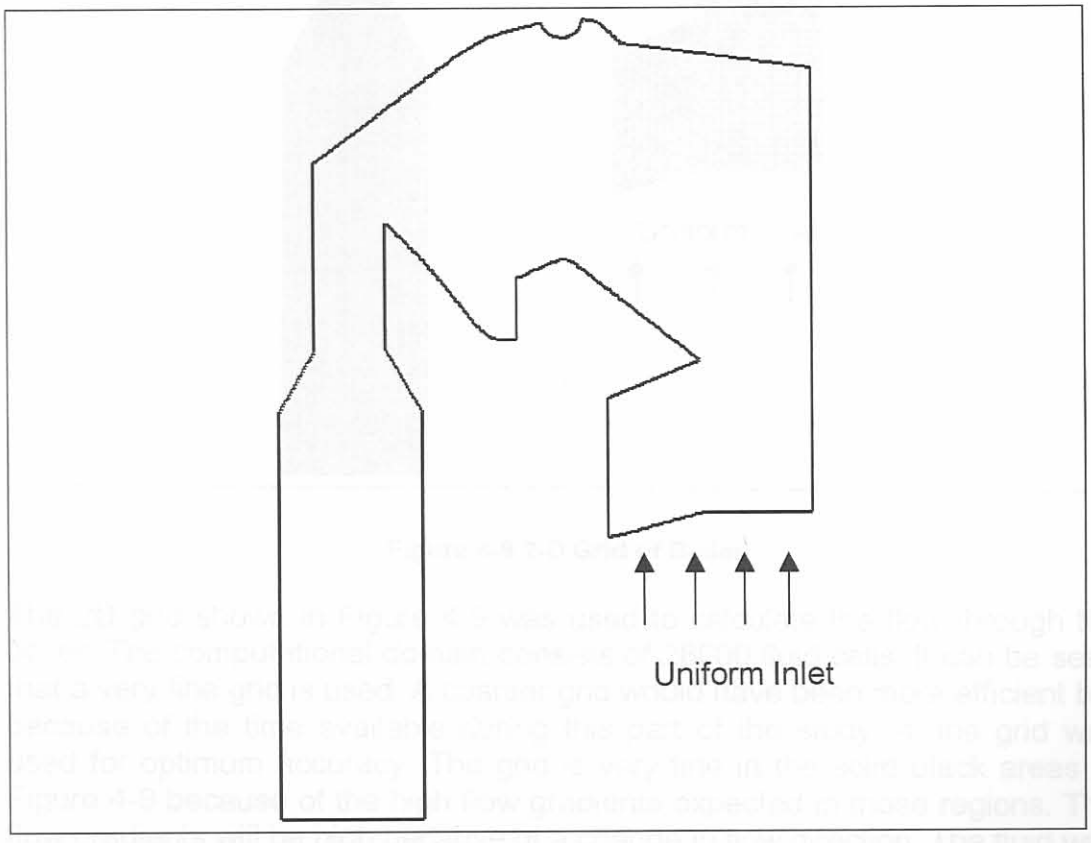

Figure 4-8 Edge Plot of 2-Dimensional Boiler Geometry

Figure 4-8 shows the outline of the boiler that is used for the 2D CFD simulation. A uniform inlet geometry and velocity distribution below the bullnose and a outlet boundary after the airheater are used as was used by

Tu et al.[**48**], Tu and Fletcher[**88**], Shen et al.[**89**] and Vakkilainen et al.[**90**,**91**].

4.3.2.1 The Effect of Inlet Velocity on the Flow

To interpret CFD results it is vital to do a sensitivity analysis of boiler flows to certain boiler operating parameters. If the flow pattern through the boiler doesn't change much when the inlet velocity is changed, for example, one knows that the flow field in the boiler is relatively stable and would not change if other inlet conditions were used. The solution is then Re-number independent.

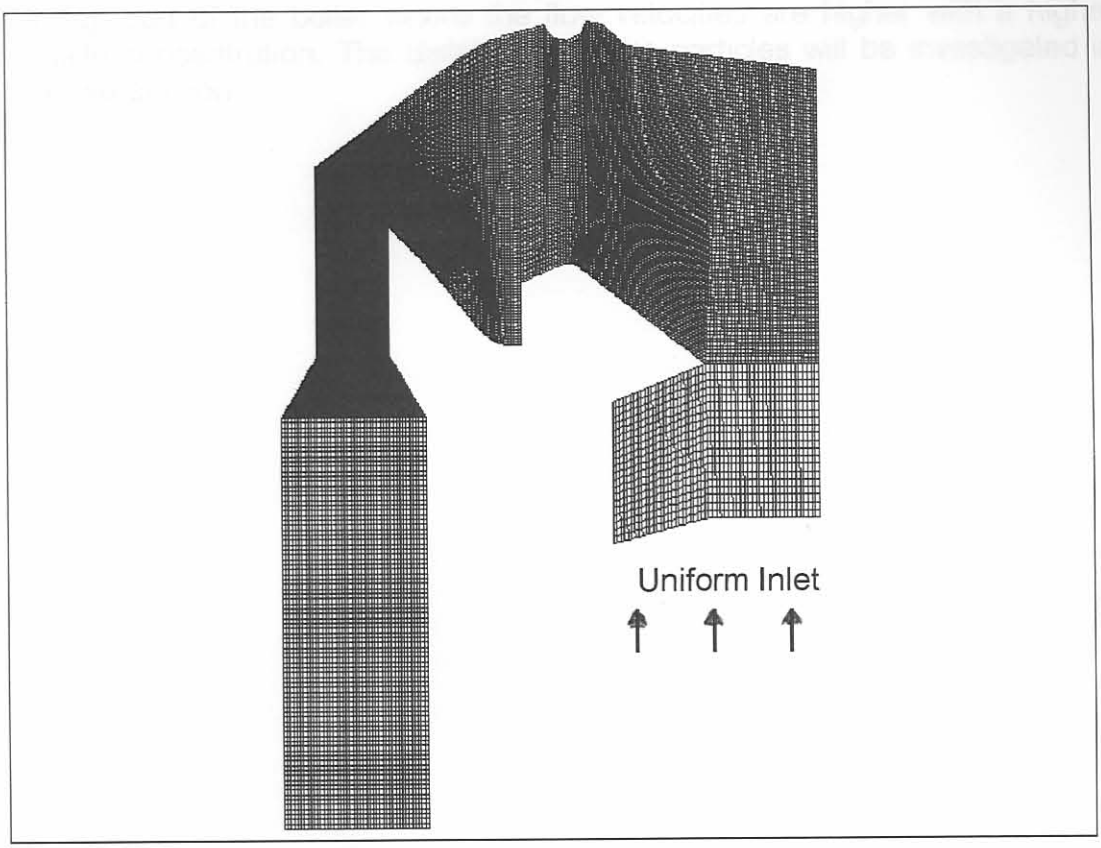

Figure 4-9 2-D Grid of Boiler

The 2D grid shown in Figure 4-9 was used to calculate the flow through the boiler. The computational domain consists of 28000 fluid cells. It can be seen that a very fine grid is used. A coarser grid would have been more efficient but because of the time available during this part of the study, a fine grid was used for optimum accuracy. The grid is very fine in the solid black areas of Figure 4-9 because of the high flow gradients expected in those regions. The flow gradients will be high because of a change in flow direction. The fluid was simulated as incompressible air with no heat transfer. The turbulent model used was the k-ε model.

Figure 4-10 and Figure 4-11 illustrate the flow fields for the different inlet velocities. Only plots of velocity magnitude are shown because velocity is one of the most important parameters influencing erosion [**24**,**26**]. It can be seen

that the flow fields are exactly the same for the two different input velocities. Inlet velocity is thus not an important factor when determining where the areas of localized high velocity are. As expected, there is a major recirculation zone above the bullnose that extends from the tip of the bullnose to the inlet passage of the airheater. Only the top half of the tube bank therefore transfers heat efficiently. This is consistent with the findings of Shen et al.[89] and Vakkilainen et al.[90].

Erosion is a direct consequence of the flow pattern caused by the shape and size of the bullnose. The bullnose causes the large recirculation zone and the flow is therefore not uniform across the tube bank. There is channeled flow in the top part of the boiler where the flow velocities are higher with a higher particle concentration. The distribution of the particles will be investigated in the next section.

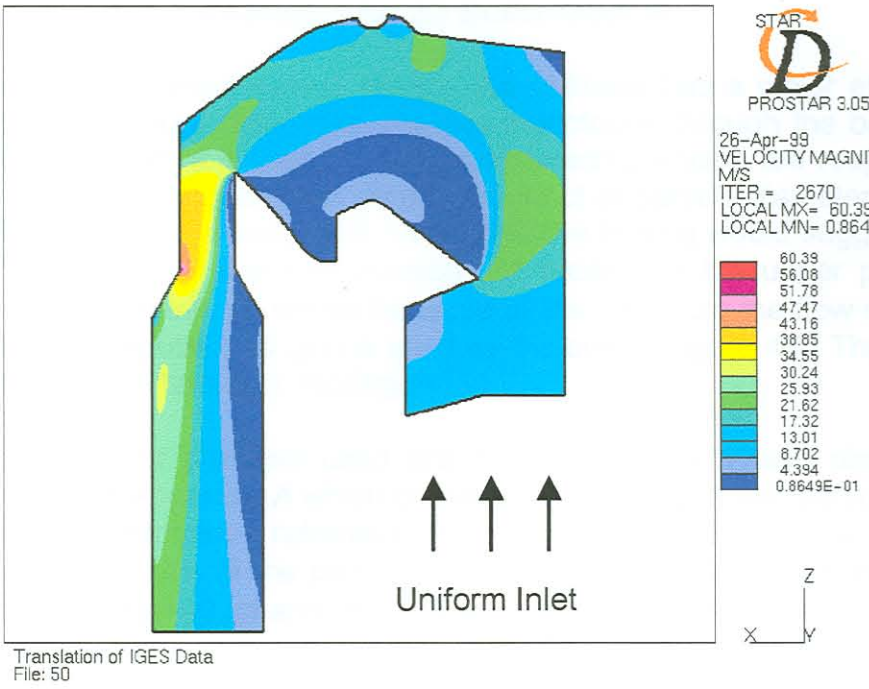

Figure 4-10 Velocity Magnitude Plot (10m.s^{-1} at Inlet)

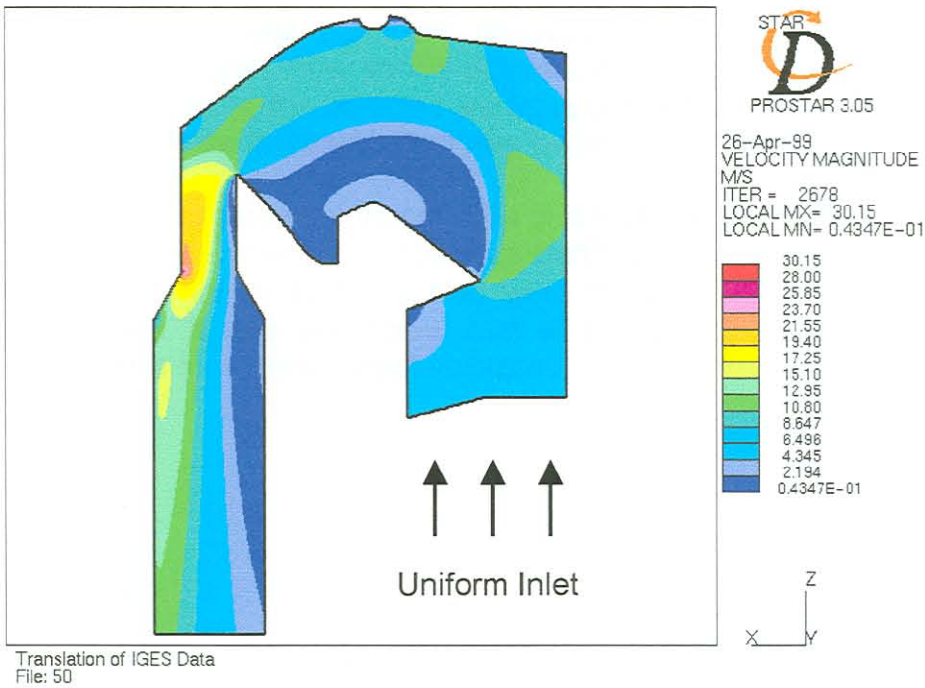

Figure 4-11 Velocity Magnitude Plot (5m.s^{-1} at Inlet)

4.3.2.2 Particle Trajectories for 2D Boiler Models

As discussed in the previous section the bullnose has a major effect on the flow pattern through the boiler. Particle trajectories through the boiler will be investigated next. It is important to know which particles are responsible for material loss through erosive wear. The effect of particle diameter on particle trajectories is also investigated. One's intuitive feeling would suggest that the larger particles are more responsible for erosion in the upper parts of the boiler due to centrifugal forces because of the 180° turn the flow must follow. The same computational grid is used as the one in Figure 4-9. The density of the particles are taken as 1650kg.m^{-3}.

The diameter of particles used are 10 and 100μm. These diameters are obtained from Appendix A which contains the analysis of ash particle diameter for fly-ash samples retrieved from the Babcock boilers at Sasol. Approximately 10% of the particles are 10μm and smaller and about 10% of the particles are 100μm and larger. The bulk of ash diameters are between 10 and 100μm.

Figure 4-12 to Figure 4-15 show the particle trajectories for 10 and 100μm particles for 10 and 5m.s^{-1} inlet velocities respectively. It can be seen that the smaller particles follow the gas streamlines, whereas the larger particles are flung outwards due to centrifugal forces.

The 10μm particles follow almost exactly the same trajectories for both the 5m.s^{-1} and 10m.s^{-1} inlet boundary conditions. For the 100μm particles, however, the trajectories differ for the different inlet conditions. For the case of the higher inlet velocity, the particles are flung outwards towards the top of the boiler more than is the case with the lower boiler inlet velocity.

This results are in agreement those of Tu and Fletcher[**88**]. The particle sizes used by Tu and Fletcher[**88**] to calculate particle trajectories are between 5 and 150μm. The larger particles also were flung outwards more than the smaller particles. It was also found that all the particles follow almost the same trajectories for different input velocities.

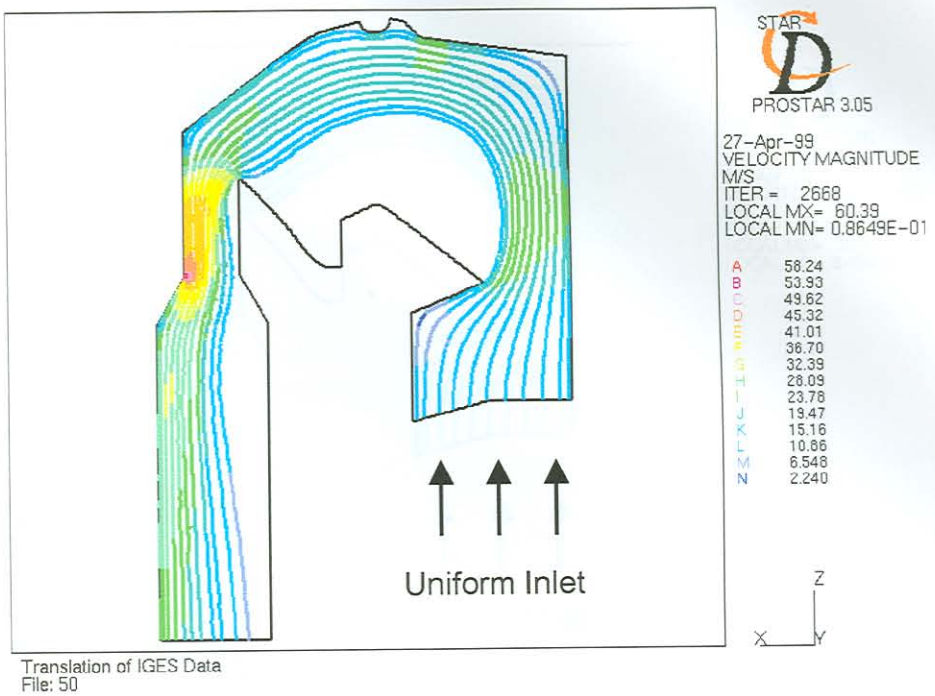

Figure 4-12 Particle Trajectories for 10μm Particles (10 m.s^{-1} Uniform Inlet)

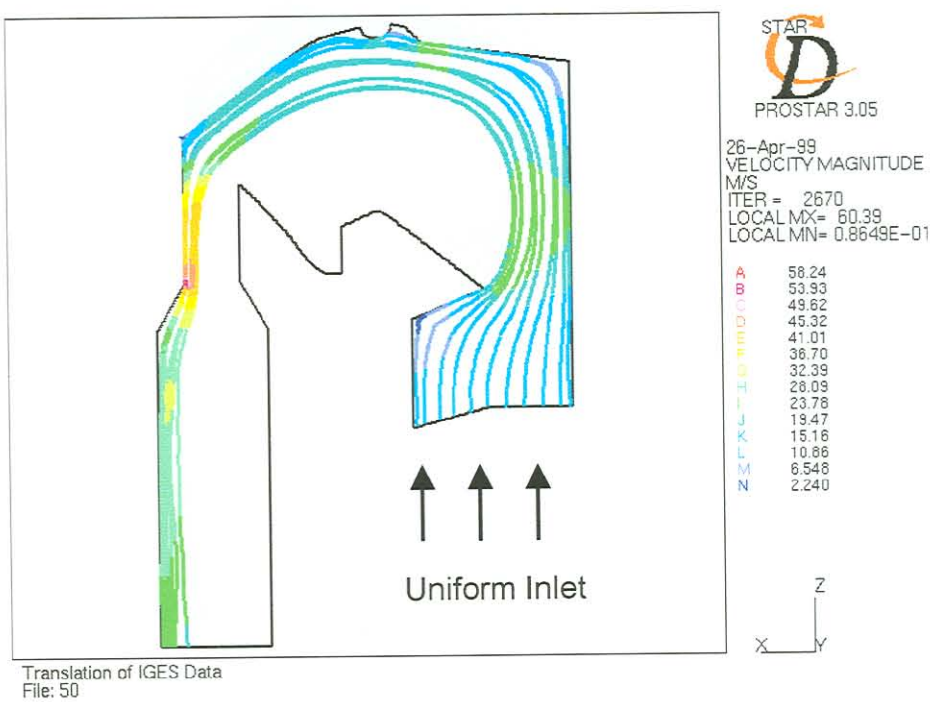

Figure 4-13 Particle Trajectories for 100μm Particles (10m.s^{-1} Uniform Inlet)

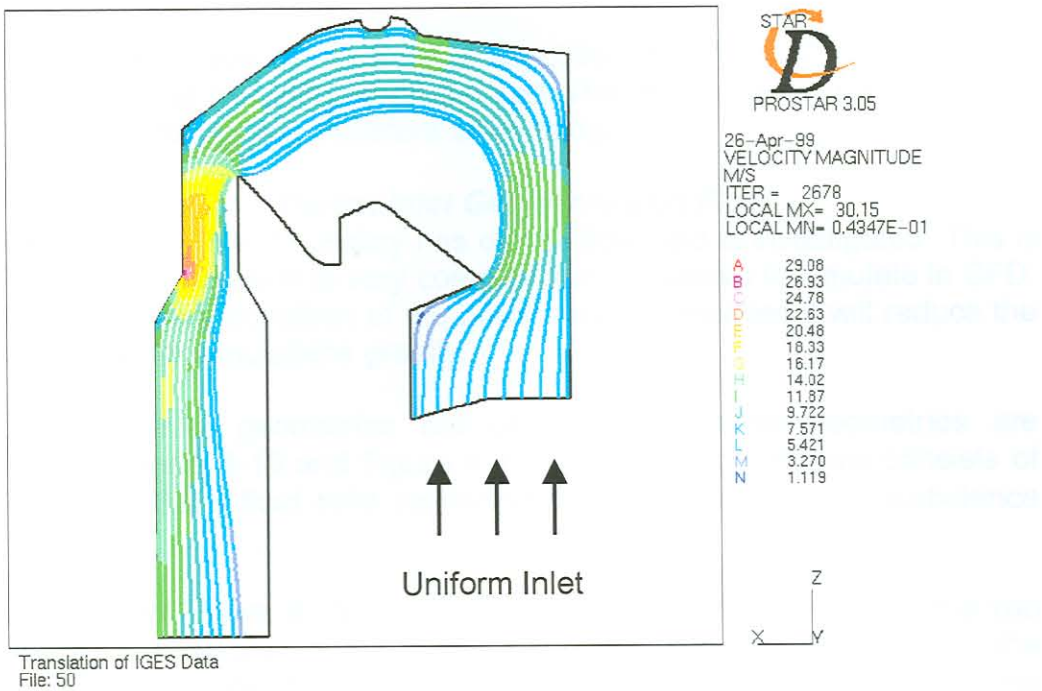

Figure 4-14 Particle Trajectories for 10μm Particles (5 m.s^{-1} Uniform Inlet)

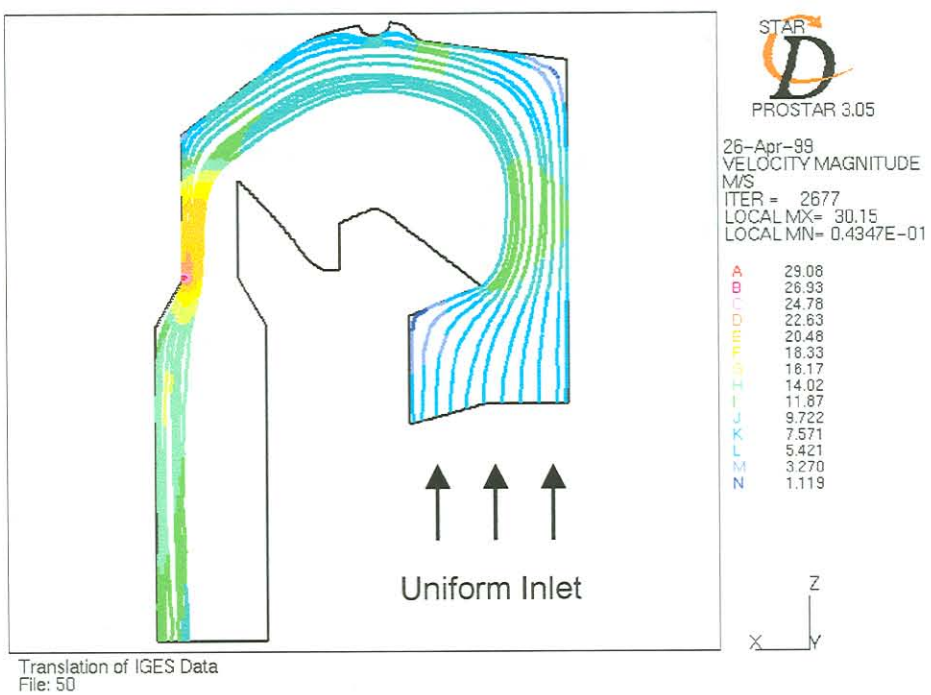

Figure 4-15 Particle Trajectories for 100μm Particles (5m.s^{-1} Uniform Inlet)

4.3.3 3D Analysis of the Boiler

In the previous section the boiler was simplified to only a 2D model. In this section a 3D boiler geometry is considered. The differences between 2D and 3D CFD boiler models can therefore be investigated.

4.3.3.1 The Effect of Different Inlet Geometries on Flow

The effect that the inlet boundary has on the flow field is investigated. This is done because combustion is very complex and expensive to simulate in CFD. If the inlet boundary condition of the boiler can be simplified it will reduce the cost of CFD boiler simulations greatly.

Two different inlet geometries are used. These boiler geometries are illustrated in Figure 4-16 and Figure 4-17. These two geometries consists of 186324 and 243296 fluid cells respectively. Once again the k-ε turbulence model is used.

Figure 4-18 and Figure 4-19 show the velocity magnitude plots for the two different boiler inlet geometries at the symmetry plane of the boiler for the same volume flow rate through the boiler. The only major differences in the flow fields are in the radiation chamber below the bullnose, which is obviously due to the different inlet geometries. The flow fields in the upper boiler, above the bullnose, are nearly the same. The recirculation zone above the bullnose for both cases has nearly the same shape and size. When these results are compared to the 2D results of the previous section, it is clear that there are no great differences in the flow patterns for the different dimensional CFD models.

Shen et al.[**89**] found that the inlet velocity and temperature profiles do not significantly alter the velocity field distribution through a boiler. Vakkilainen et al.[**91**] also used different inlet conditions and it was concluded that flow features like channelled flow, tangential swirling and recirculation zones can be very strong in the lower furnace near the air jets, but dissipate due to turbulent shear in the upper furnace. The results obtained in this section are thus in good agreement with other researchers' findings.

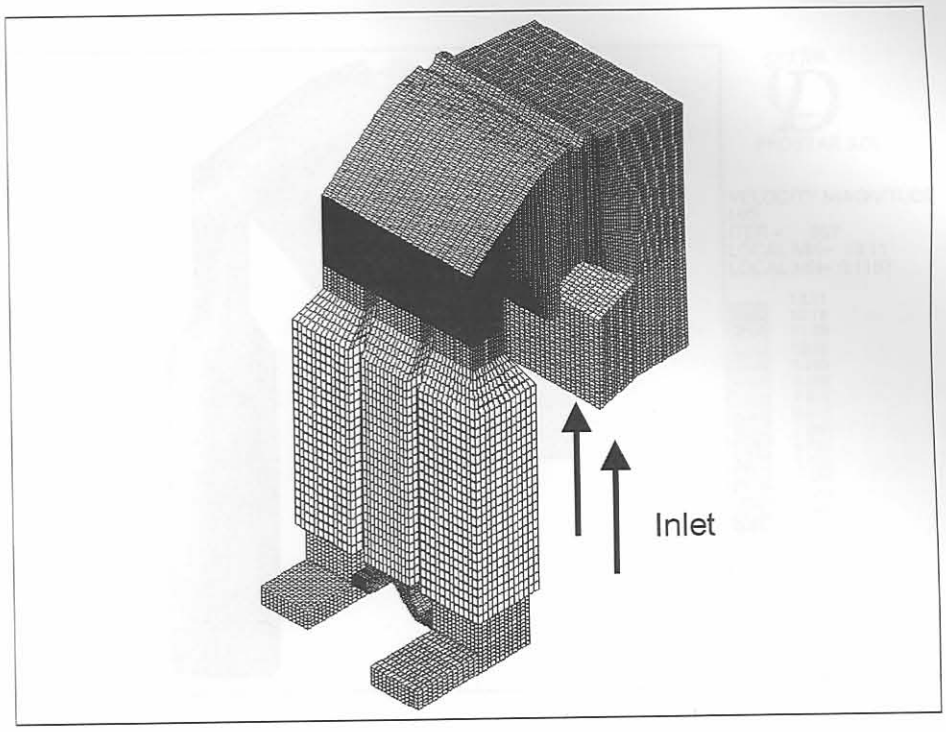

Figure 4-16 3-D Computational Grid with Uniform Inlet

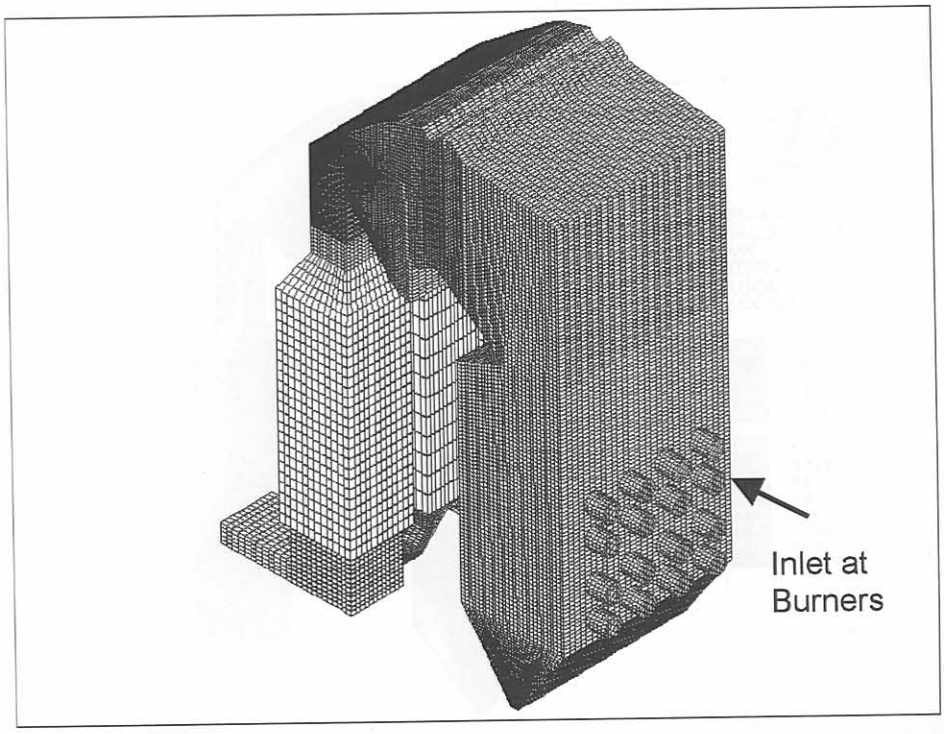

Figure 4-17 3-D Computational Grid with Inlet at Burners

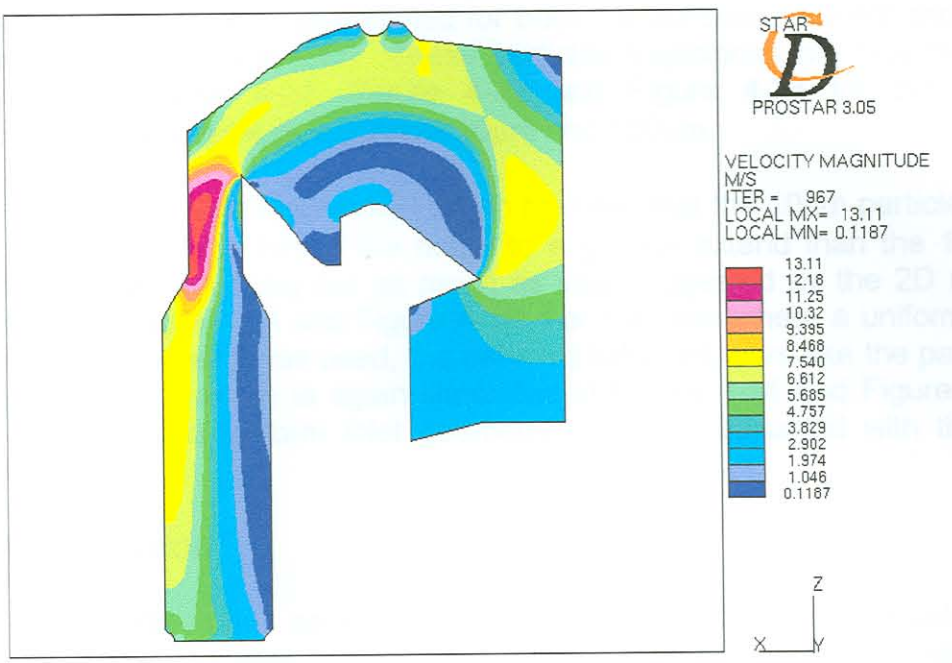

Figure 4-18 Centreline Velocity Magnitude Plot with Uniform Inlet (Mass flow rate of 216.59kg.s^{-1})

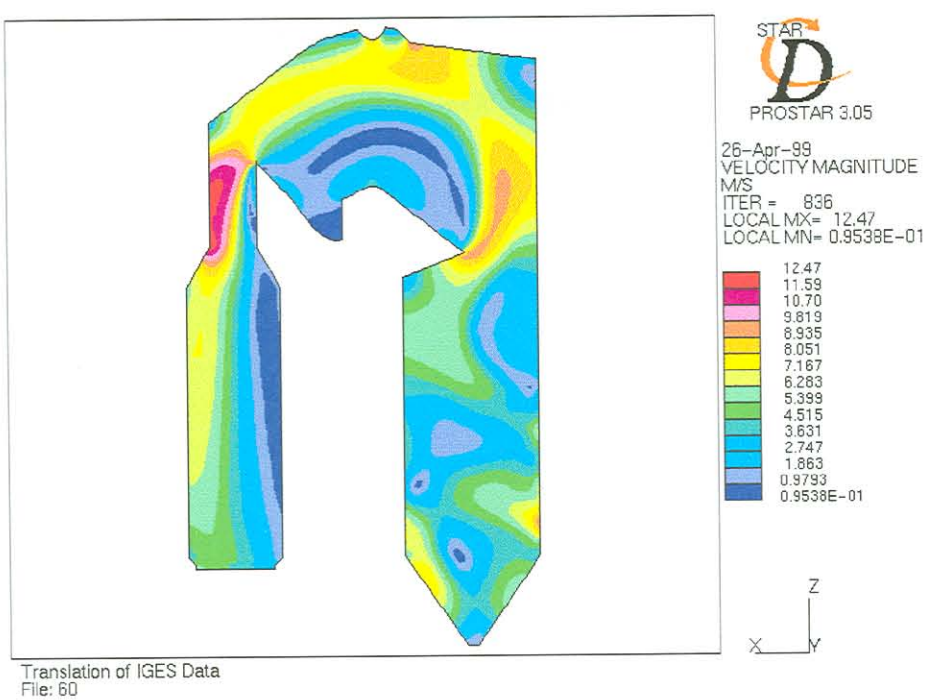

Figure 4-19 Centreline Velocity Magnitude Plot with Inlet at Burners (No Swirl) (Mass flow rate of 216.59kg.s^{-1})

4.3.3.2 Particle Trajectories for 3D Boiler Models

Particle trajectories were determined for both the 3D boiler models shown in Figure 4-16 and Figure 4-17. These particles trajectories are illustrated in Figure 4-20, Figure 4-21, Figure 4-22 and Figure 4-23 for both inlet geometries and particle diameters of 10μm and 100μm.

From Figure 4-20 and Figure 4-21 it can be seen that the 10μm particles are flung outwards to the top of the boiler to a greater extend than the 100μm particles. It was not flung out as much as was suggested by the 2D model illustrated in Figure 4-14 and Figure 4-15. For the case where a uniform inlet velocity and geometry was used, the particles behaved more like the particles of the 2D model, which is again illustrated in Figure 4-14 and Figure 4-15. This is because a uniform inlet geometry was also assumed with the 2D model.

4.3.4 Conclusion

From the results in this section, it can be seen that different inlet velocities does not in any way alter the flow field through the boiler. It can therefore be assumed that the flow field will remain approximately the same for other inlet velocities. If different inlet geometries are used in 3D CFD models, the flow fields are approximately the same in the upper boiler above the bullnose. It was also found that the flow fields do not differ much for 2D and 3D models in the centre plane of the boiler. It is expected though that the flow field will differ near the boiler walls. In both 2D and 3D models, the trajectories of particles behave the same for 10μm and 100μm particles. The 10μm particles follow the streamlines of the flow while the 100μm particles are flung outwards towards the top of the boiler due to centrifugal forces.

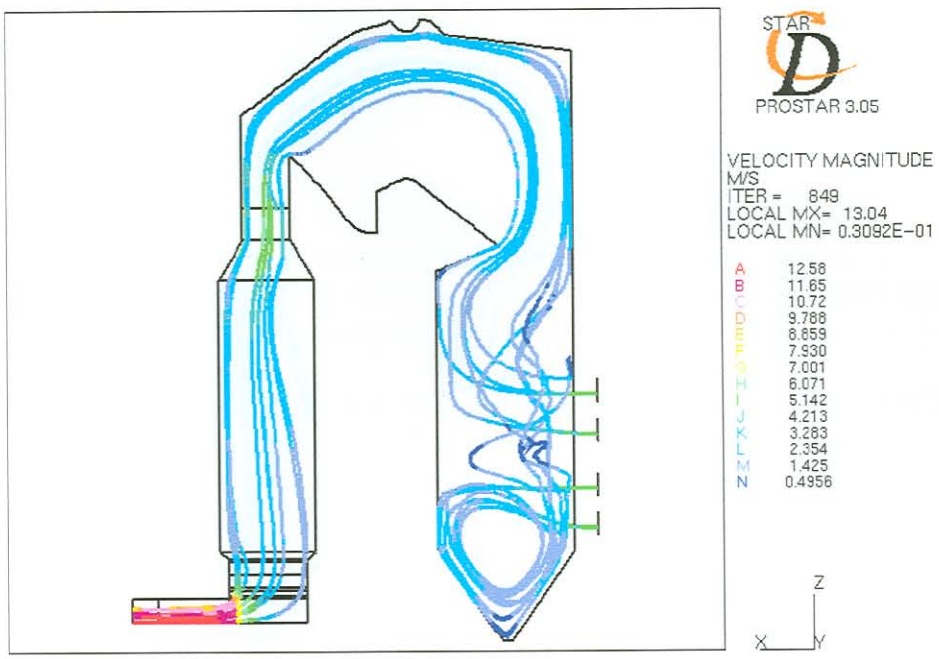

Figure 4-20 Particle Trajectories for 10μm Particles

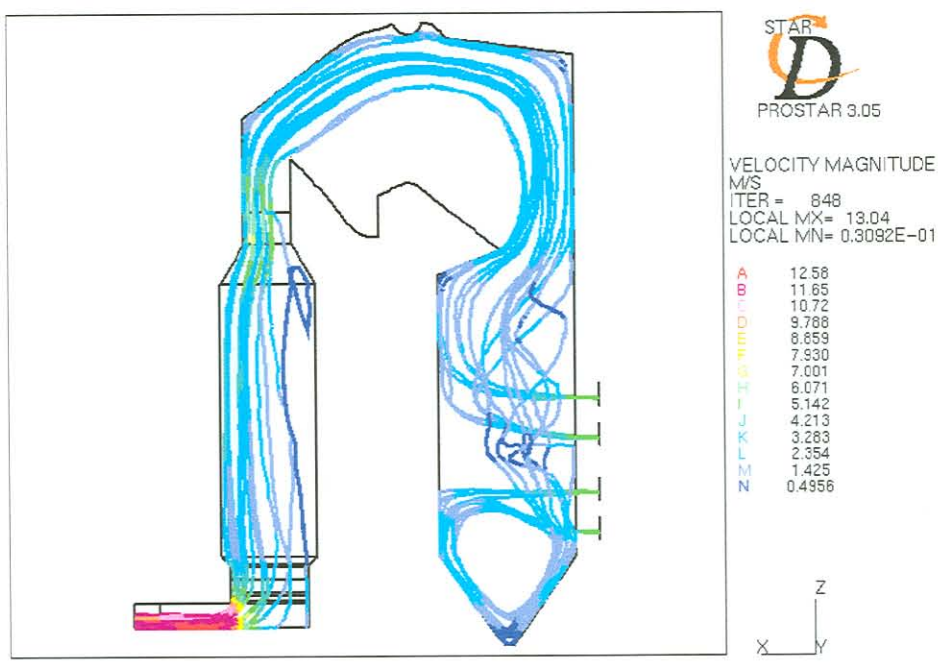

Figure 4-21 Particle Trajectories for 100μm Particles

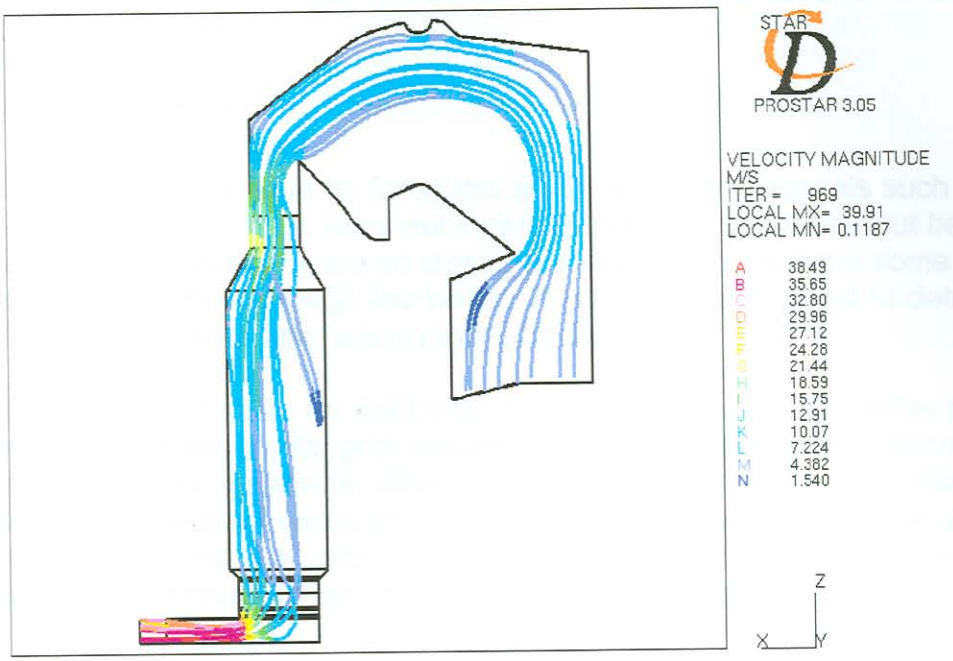

Figure 4-22 Particle Trajectories for 10μm Particles

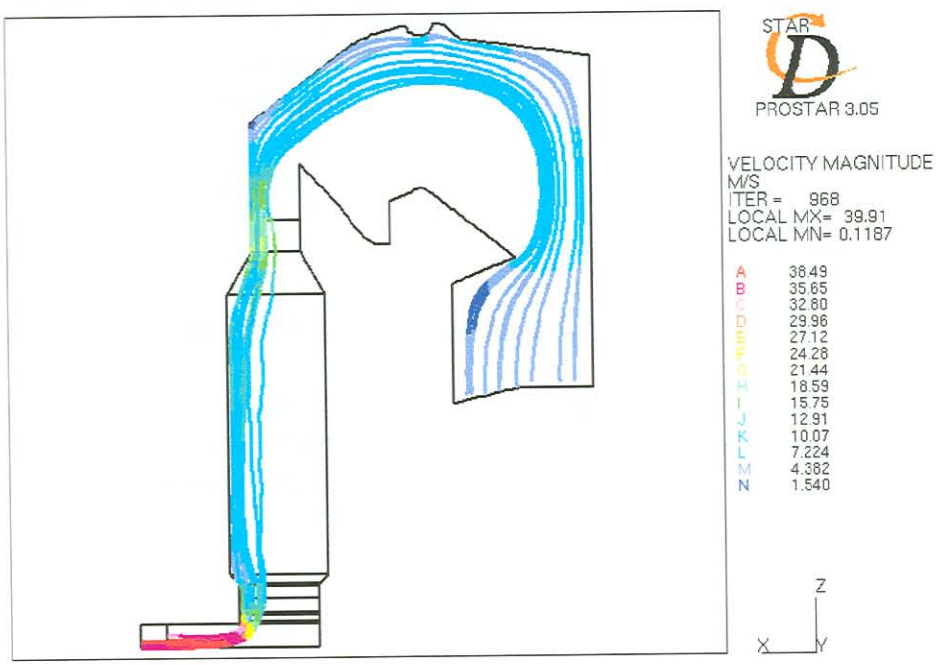

Figure 4-23 Particle Trajectories for 100μm Particles

4.4 Modelling of Boiler Internals through the use of Porosity Coefficients

4.4.1 Introduction

In the CFD analyses done so far in this study, the boiler internals such as the airheaters and boiler bank were not included in the CFD models. But because the tubes of the tube bank are so closely packed, they must have some sort of influence on the flow through the boiler. This section is devoted to determine the effect of the boiler internals on overall boiler flows.

It is not feasible to solve for the boiler internals directly in CFD boiler models because of the fine-scale grid required near the boiler tubes. Because of computer memory limitations, alternative methods must be used to model the boiler internals without using small-scale grids. This is done through the use of porous sections that replace the boiler internals, but have the same pressure drop versus velocity characteristics as the tubes they replace.

One usually uses porous cells in a CFD code if there exists fine-scale geometrical structures in a flow field. The effect of these structures is usually too small to resolve numerically within the overall calculation. Examples of these include[**3**]:

- Flows in porous media, such as packed-bed chemical reactors.
- Heat exchangers of the shell-and-tube type, where the calculation is to encompass the entire assembly, containing a large number of tubes/plates. (In this study the porous cells are used for this reason.)
- Flows in fibrous materials.
- Filters.
- Honeycomb structures.

In this study porous sections are used to replace the tube banks of the boiler.

4.4.2 Calculation of Porosity Coefficients

The assumption is made that everywhere within the volume containing the distributed resistance, there exists a local balance between pressure and resistance forces such that:

$$-K_i \cdot u_i = \partial p / \partial \xi_i \qquad (4\text{-}3)$$

Where:

$\xi_{i.}$ ≡ Orthotropic directions (i. = 1,2,3)
K_i ≡ Permeability
u_i ≡ Superficial velocity in direction $\xi_{i.}$

The permeability K_i is assumed to be a quasilinear function of the superficial velocity magnitude $/v/$ of the form:

$$K_i = \alpha_i \cdot /v/ + \beta_i \qquad (4\text{-}4)$$

Where α_i and β_i are user-specified coefficients.

If Equation (4-4) replaces the K_i in Equation (4-3), the following relationship exists:

$$\partial P = \alpha v^2 + \beta v \qquad (4\text{-}5)$$

where ∂P is the pressure drop in the flow direction and v is the inlet velocity. The coefficients α and β are obtained from the pressure drop versus velocity characteristic obtained from the detailed hydraulic model of a tube row. The coefficients for the tube bank and airheater will be determined in the following sections.

4.4.3 Porosity Characteristics for Boiler Bank Tubes

4.4.3.1 Porosity Characteristics Across Boiler Bank Tubes in Crossflow

The porosity coefficients for the tube bank in crossflow are determined in this section through the use of a CFD hydraulic model. One row of tubes is used to determine the pressure drop versus velocity characteristics of the tube bank. This setup is illustrated in Figure 4-24. The computational domain used in the CFD analysis in this section is the green crosshatched region in Figure 4-24. The figure only shows a few tubes in the flow direction for clarity. In the real model there are 26 rows separated in the middle by a gap.

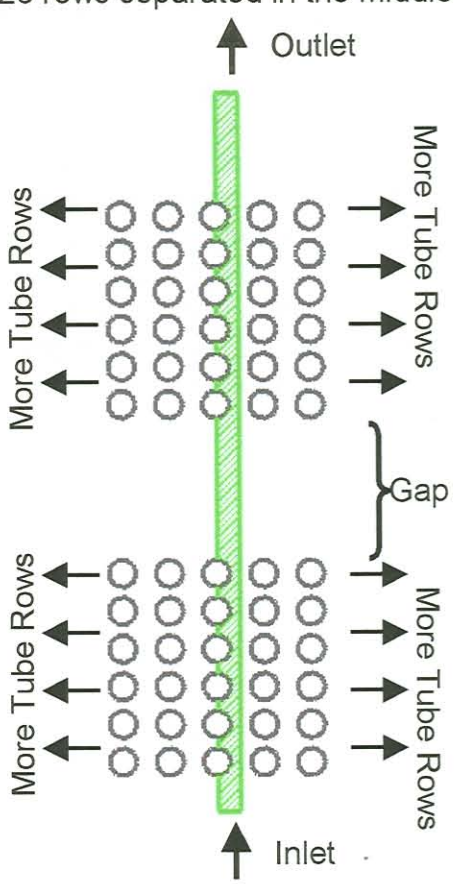

Figure 4-24 Computational Domain to Determine Dressure Drop Characteristcs for Crossflow Configuration

The computational grid around one tube of the domain shown in Figure 4-24 can be seen in Figure 4-25. The whole computational domain consists of 44100 fluid cells. Incompressible air is used as the fluid. The k-ε turbulence model is used and no heat transfer is assumed in the CFD model.

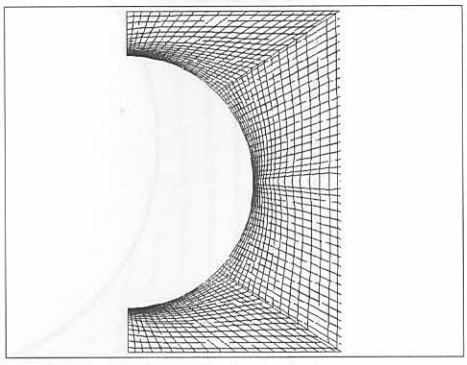

Figure 4-25 Computational Grid for Cross Flow Around One Tube in a Tube Bank (88.9 mm Tube Diameter)

The velocity flow field around only one tube can be seen in Figure 4-26 and Figure 4-27 for an inlet velocity of $7 m.s^{-1}$. Figure 4-26 contains less velocity vectors for clarity but was obtained using the same grid density as in Figure 4-27. The point of separation is clearly visible. No information was found in the literature that gave a correlation for the determination of separation point on a tube for flows in tube banks for the verification of the results. The flow pattern repeats almost identically for subsequent tubes, as can be seen in Figure 4-28. This is consistent with the results of Weaver and Abd-Rabbo[**75**] which stated that turbulence is essentially fully developed by the third row of tubes at high Reynolds numbers. The pressure drop across the whole tube bank for one tube row is illustrated in Figure 4-29. The pressure drops because of the friction drag of the tubes. The pressure is also dropping because of the losses incurred by all the recirculation zones behind the tubes. The pressure drop is a function of fluid flow velocity, number of tube rows, tube spacing in the transverse and longitudinal directions, tube diameter and fluid properties [**85**].

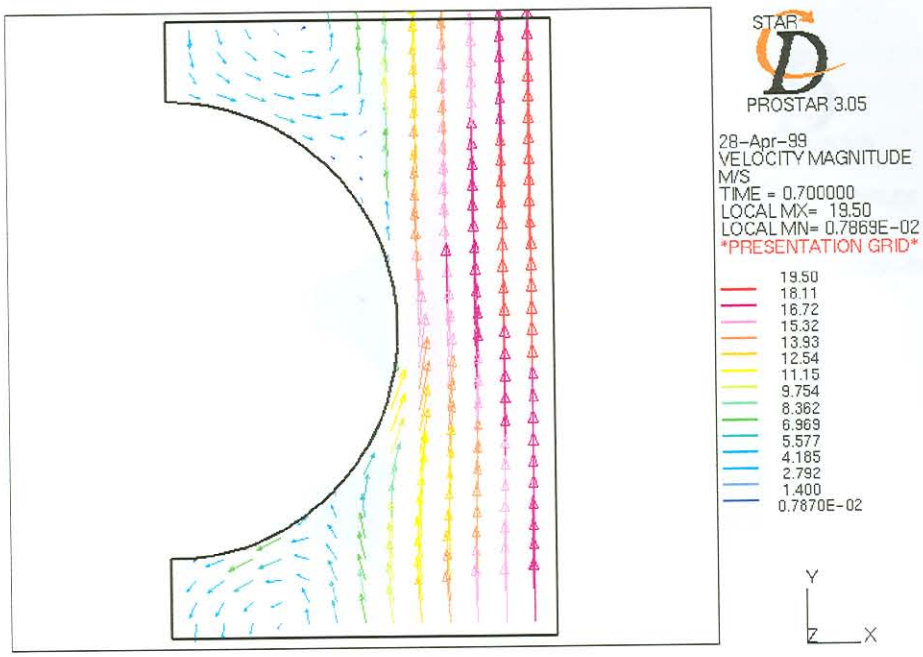

Figure 4-26 Velocity Vectors for Presentation Grid around One Tube of the Boiler Bank for a Crossflow Configuration (7m.s^{-1} Inlet Velocity)

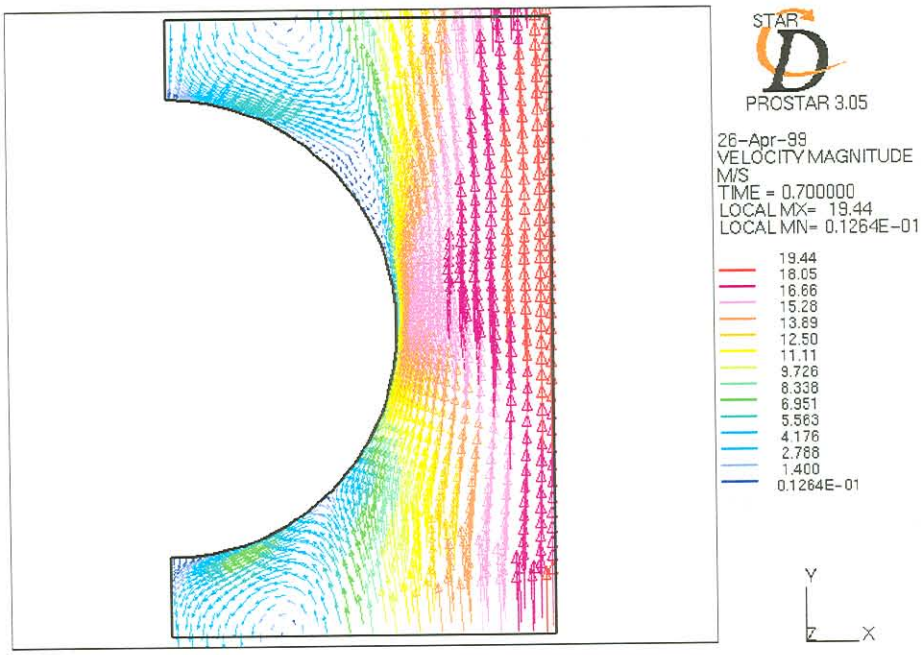

Figure 4-27 Velocity Vectors for actual grid around one tube of the boiler bank for a crossflow configuration (7m.s^{-1} Inlet Velocity)

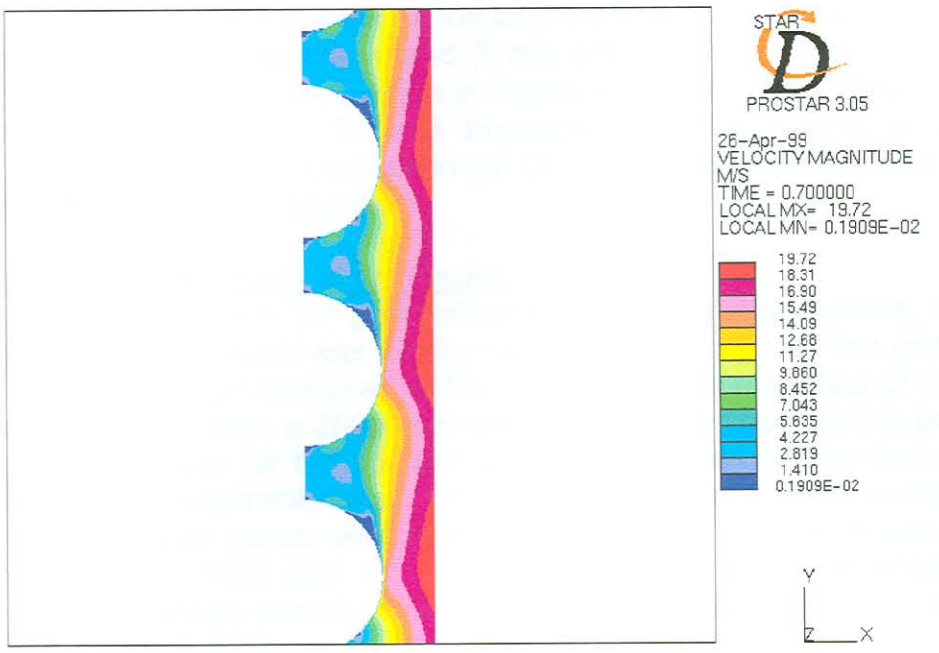

Figure 4-28 Velocity magnitude contour plot for flow around a few tubes of the boiler bank for a crossflow configuration (7m.s^{-1} Inlet Velocity)

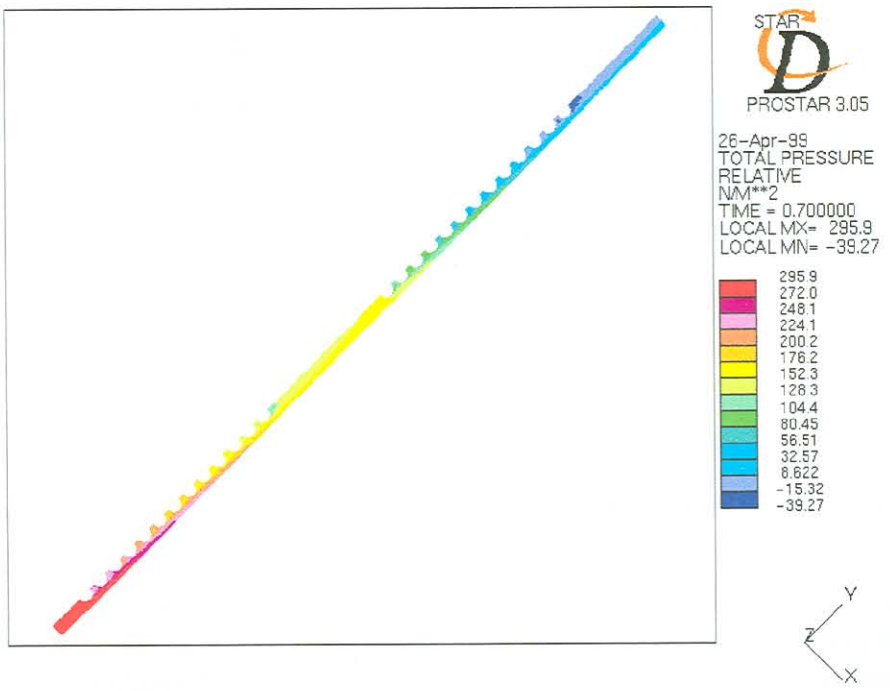

Figure 4-29 Relative pressure distribution over whole computational domain of the boilerbank for a crossflow configuration (7m.s^{-1} Inlet Velocity)

Calculation of the Porosity Coefficients

The pressure drop characteristics of the tube bank in crossflow is illustrated in Figure 4-30. The coefficients α and β are obtained from a second order polynomial curve fit through the data in Figure 4-30. The coefficients α and β from the plot in Figure 4-30 and Equation (4-5) are 1.0436 and 5.84 respectively. This data can be used in the CFD model to model porosity in the crossflow direction of the tube bank.

The Effect of Grid Refinement on Results

It is important to check for grid refinement to see if the solution is grid independent. The analysis was run for two different grid sizes. The grid used in the previous section contained 44100 cells. To check the effect of the grid size on the flow solution, a 25000 cell grid is used. The values of the porosity constants were lower for the coarser grid than was the case for the refined grid. The point of separation was not as clearly defined with the coarse grid and the recirculation zones were smaller. The point of separation was better resolved with the finer grid and thus better results were obtained. The pressure drop versus velocity characteristics for the two different cases is illustrated in Figure 4-30.

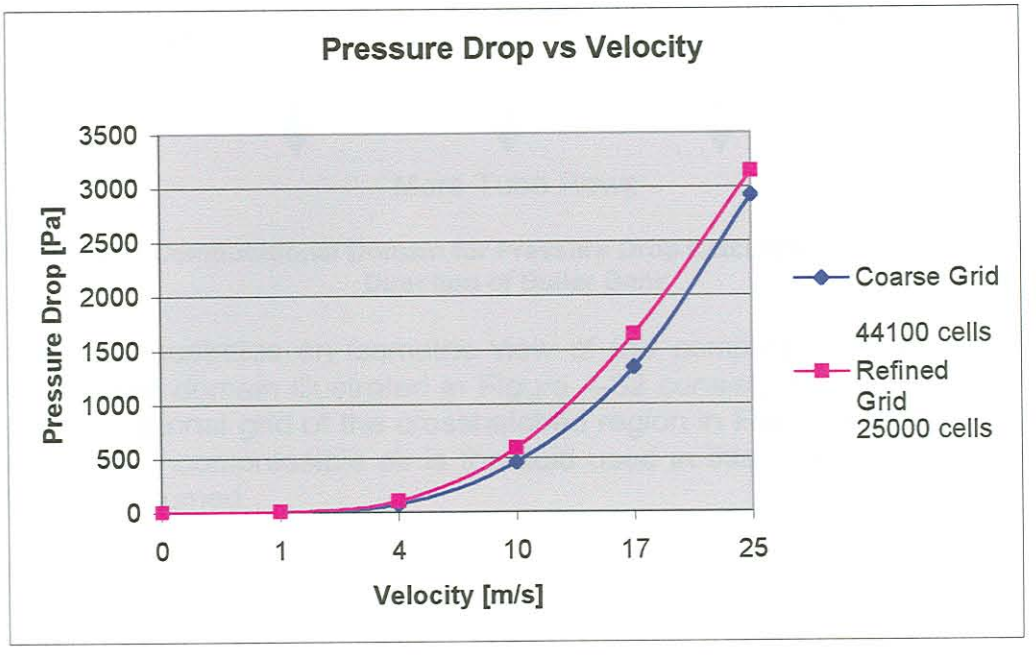

Figure 4-30 Pressure drop versus velocity characteristic for the whole tube bank for a crossflow configuration.

Because of some difficulties with stability in the CFD model with boiler internals, which will be discussed later, it was decided to determine the porosity coefficients in the longitudinal directions of the tubes as well. Although the pressure drop will be much less in this direction compared to the cross flow direction, it is important to obtain this resistance to the flow. This will simulate the porosity characteristics of the tube bank much more accurately.

4.4.3.2 Porosity Characteristics of Flow in the Longitudinal Direction of Tubes

The domain for the calculation of pressure drop in the longitudinal direction of a tube bank is illustrated as the green crosshatched region in Figure 4-31. Symmetry boundary conditions are used in all four directions shown in Figure 4-31. The flow direction in Figure 4-31 is into the page.

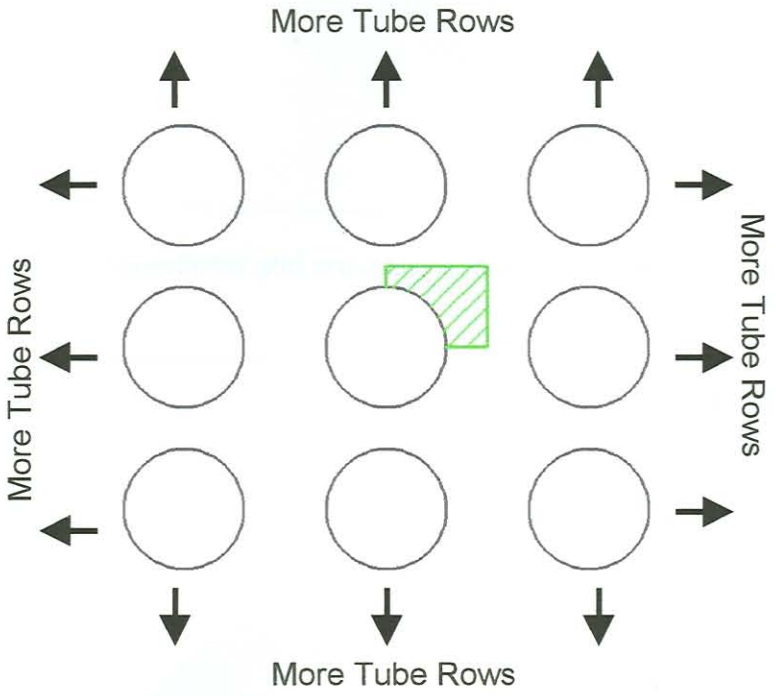

Figure 4-31 Computational Domain for Pressure Drop Calculation in Longitudinal Direction of Boiler Bank

Figure 4-32 illustrates an isometric view of the computational domain. The computational domain illustrated in Figure 4-32 consists of 25500 fluid cells. The computational grid of the crosshatched region in Figure 4-31 is shown in Figure 4-33. Incompressible air is the fluid used in this analysis and no heat transfer is assumed.

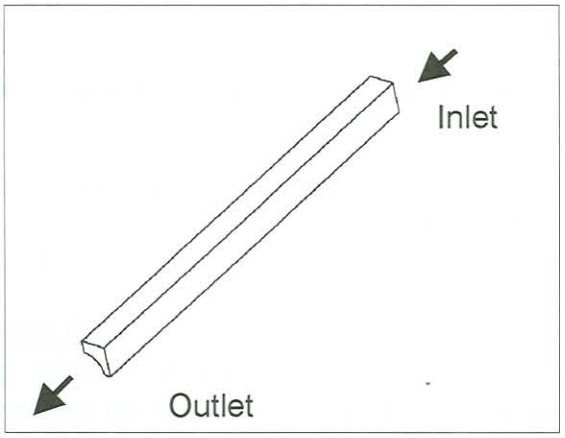

Figure 4-32 Edge plot of computational domain for flow parallel to the boiler bank tubes

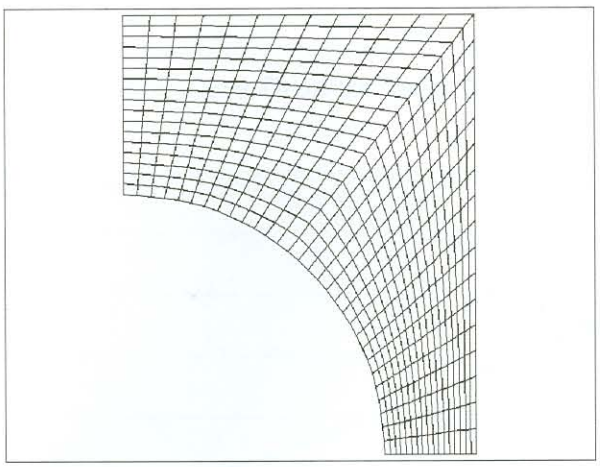

Figure 4-33 Computational grid around one tube for flow parallel with the tube

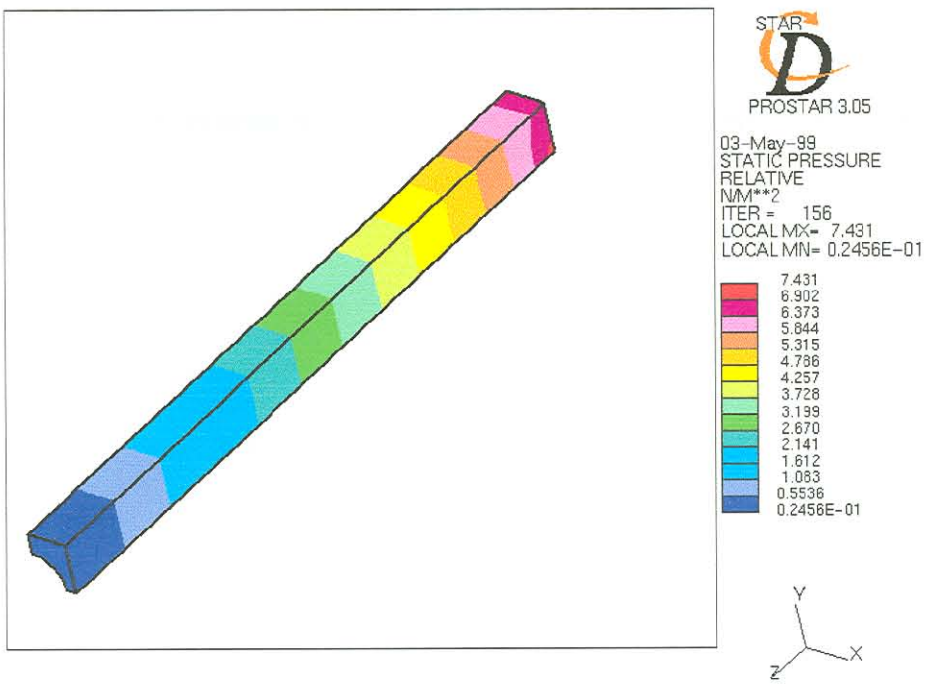

Figure 4-34 Pressure drop in the longitudinal direction around one boiler bank tube ($10m.s^{-1}$ Inlet Velocity)

The pressure drop across the computational domain for a unit length of tube is illustrated in Figure 4-34 for an inlet velocity of $10m.s^{-1}$. The pressure drops because of tube wall friction.

Calculation of Porosity Coefficients

The pressure drop versus velocity characteristic of the tube bank in the longitudinal direction can be seen in Figure 4-35. The porosity coefficients α and β are obtained from a second order polynomial curve fit through the data in Figure 4-35. From the data in Figure 4-35 and Equation (4-5), the two porosity coefficients, α and β, are 0.0194 and 0.5016, respectively.

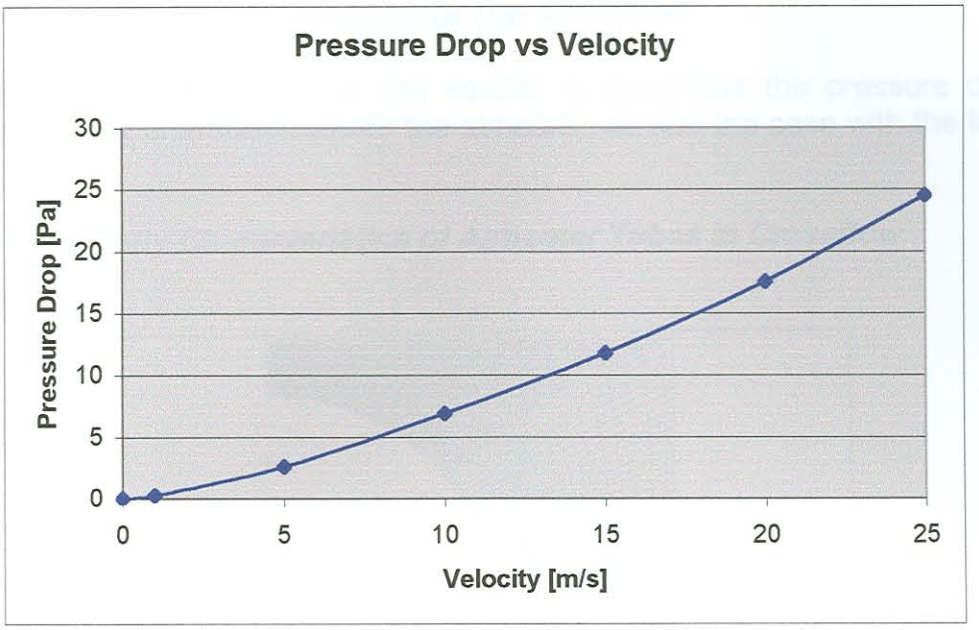

Figure 4-35 Pressure drop versus Velocity characteristic for boiler bank tubes in the longitudinal direction

4.4.4 Porosity Characteristics for the Airheater

The same method is used in this section to determine the pressure drop versus velocity characteristics for the airheater, as was the case with the tube bank.

4.4.4.1 Porosity Characteristics of Airheater Tubes in Crossflow

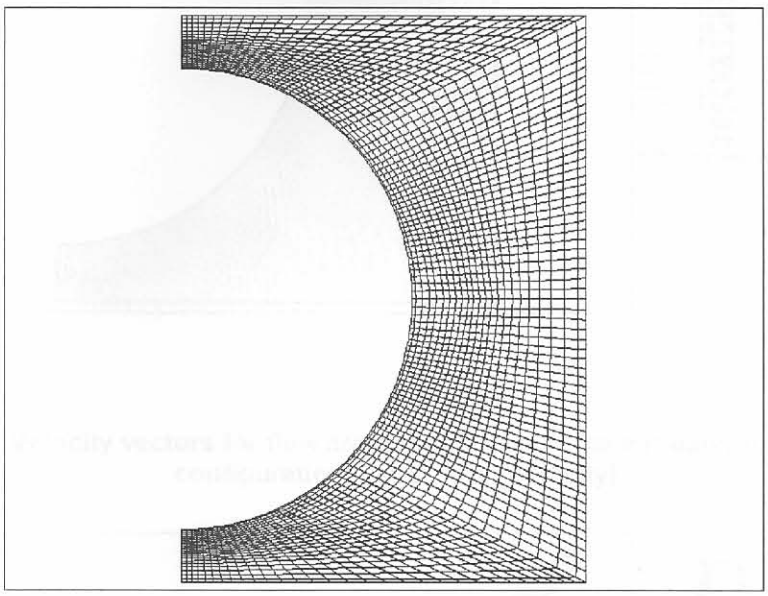

Figure 4-36 Computational grid for the airheater around one tube for a crossflow configuration. (57mm Tube Diameter)

The computational domain for this CFD analysis consisted of 28000 fluid cells. The computational grid around one tube can be seen in Figure 4-36. The velocity vector field around one tube is illustrated in Figure 4-37 for an inlet velocity of $7m.s^{-1}$. The recirculation zones in front and at the back of the tube is clearly seen. The recirculation zones and tube wall friction are the main factors contributing to pressure contour plot across the computational domain. The pressure drop across some of the airheater tubes is illustrated in Figure 4-38.

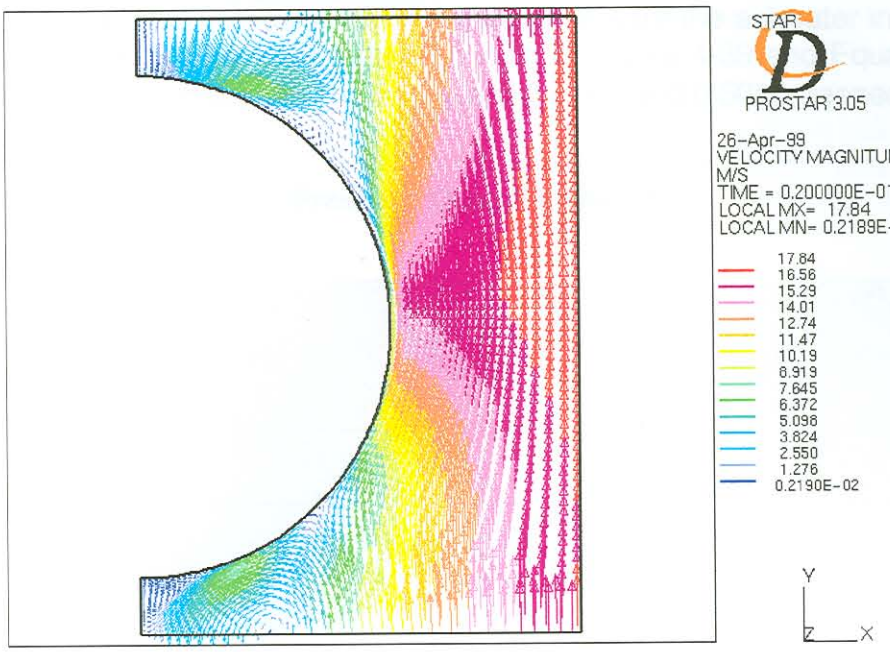

Figure 4-37 Velocity vectors for flow around one tube of the airheater for a crossflow configuration (7m.s^{-1} Inlet Velocity)

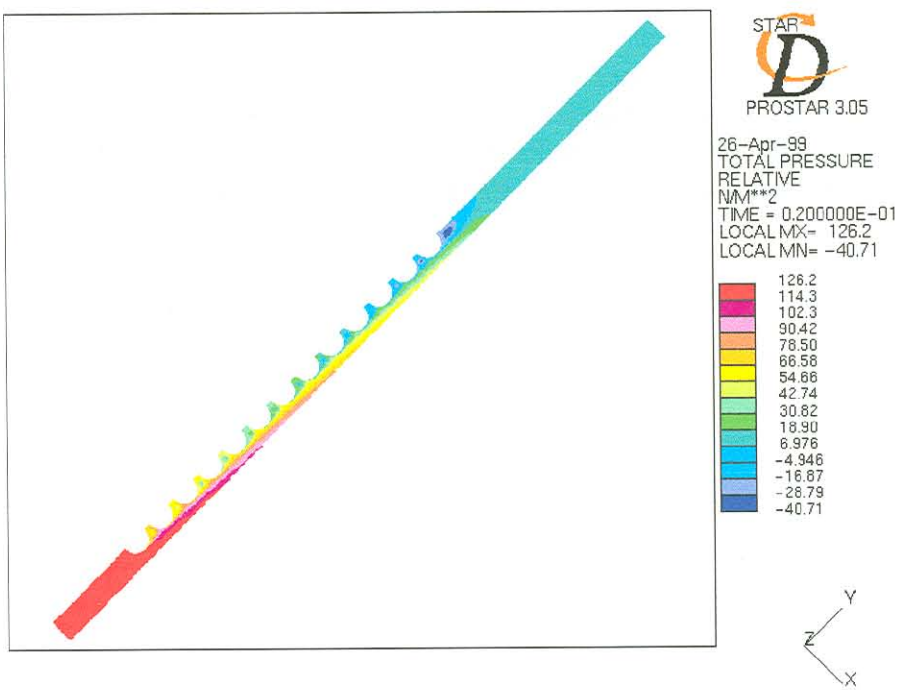

Figure 4-38 Pressure drop across tubes of the airheater for a crossflow configuration (7m.s^{-1} Inlet Velocity)

Calculation of Porosity Coefficients

The pressure drop versus velocity characteristics for the airheater in crossflow is illustrated in Figure 4-39. From the data in Figure 4-39 and Equation (4-5) the two porosity coefficients, α and β, are 0.0194 and 0.5016, respectively.

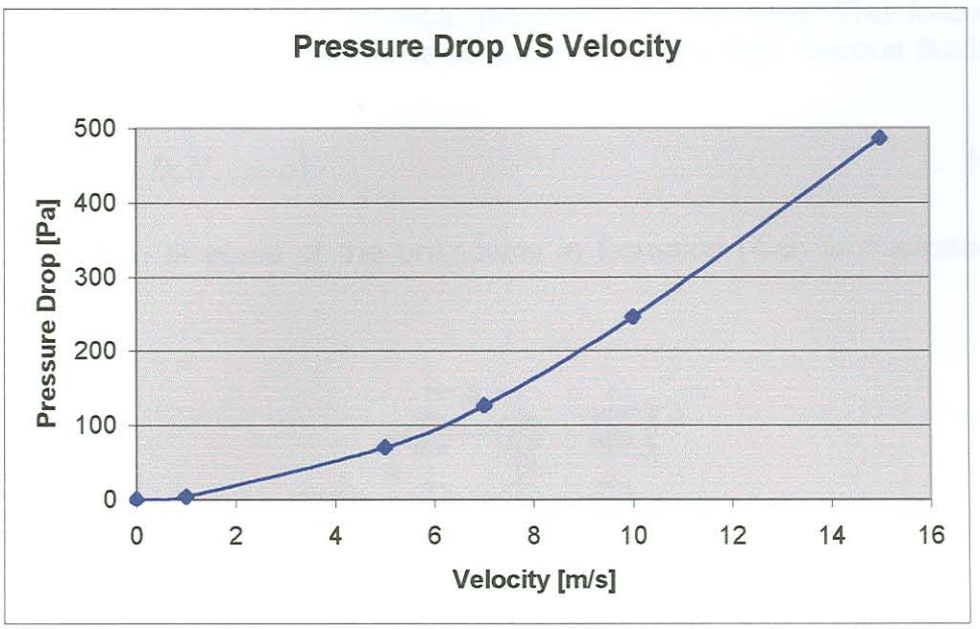

Figure 4-39 Pressure Drop versus Velocity characteristic for the air heater for a crossflow configuration

Because of stability problems in the CFD model of the overall CFD boiler model, the pressure drop versus velocity characteristics was not determined for the airheater tubes in the longitudinal direction. This also proved unnecessary because it was decided not to include the effect of the airheater in the overall boiler CFD model.

4.4.5 Comparison of Numerical Results to Empirical Data

Zukauskas[**85**] studied the hydraulic resistance of tube banks. He said that the total pressure drop across a bank of tubes is a function flow velocity, tube bank arrangement and the physical properties of the fluid. The following functional relation expresses the resistance of a bank with viscous fluids of constant density:

$$\Delta p = f\left(V, S_T, S_L, D, N_L, \mu, \rho\right) \tag{4-6}$$

The description of some of the unknowns in Equation (4-6) is illustrated in Figure 4-40.

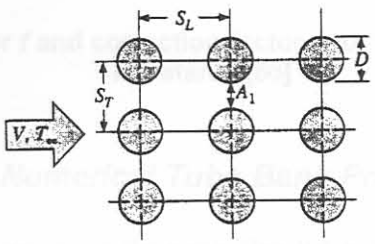

Figure 4-40 Tube Arrangement Parameters [94]

The dimensionless form of the relation discussed above are:

$$Eu = \phi\left(\mathrm{Re}, \frac{S_T}{D}, \frac{S_L}{D}, N_L\right) \tag{4-7}$$

The pressure drop across a bank of tubes can be expressed as:

$$\Delta p = N_L \chi \left(\frac{\rho V_{\max}^2}{2}\right) f \tag{4-8}$$

The values of f and χ are obtained from the Moody-type graph in Figure 4-41 and the value of V_{max} is obtained from Equation (4-9):

$$V_{maks} = \frac{S_T}{S_T - D} V \tag{4-9}$$

V_{max} is used because the correlations are based on maximum fluid velocity within the tube bank. For an in-line tube bank, V_{max} occurs at the transverse plane A_1 of Figure 4-40.

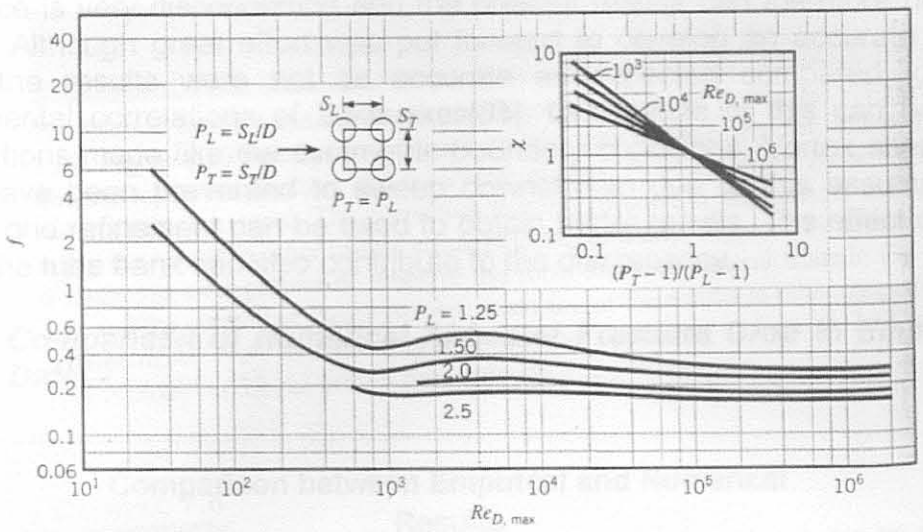

Figure 4-41 Friction factor *f* and correction factor χ for the calculation of hydraulic resistance[86]

4.4.5.1 Comparison of Numerical Tube Bank Pressure Drop to Empirical Pressure Drop

The calculation of pressure drop through the tube bank using the correlations developed by Zukauskas[**85**] can be seen in Appendix B. A MS Excel macro was used to determine the pressure drop. The same solution strategy was followed as was used by Incropera and DeWitt[**94**].

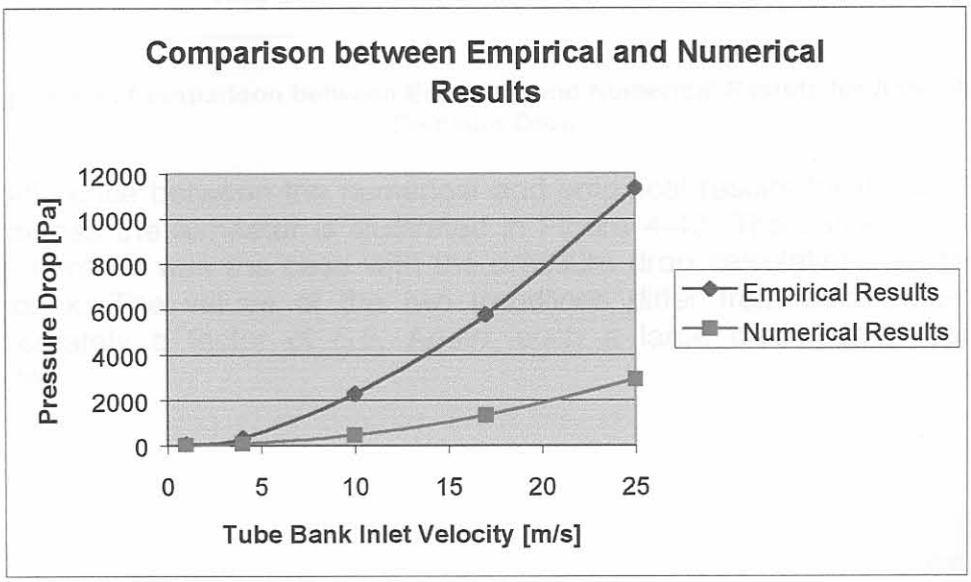

Figure 4-42 Comparison between Empirical and Numerical Results for Tube Bank Pressure Drop

The numerical results obtained in Chapter 4.4.3.1 for the tube bank and the results from the experimental correlations of Zukauskas[**85**] are plotted in Figure 4-42. The empirical correlation predicts a pressure drop with a factor of 4 higher than the numerical results obtained in this study. This large

difference is very disconcerting and the present results can therefore not be trusted. Although great effort was put forward to develop an accurate CFD model the results were not as accurate as expected compared to the experimental correlations of Zukauskas[**85**]. One cause of this can be the assumptions made like the symmetric boundary conditions. Vortex shedding could have been prevented to sweep downstream due to this assumption. Further grid refinement can be used to obtain better results. The effect of the gap in the tube bank can also contribute to the discrepancy.

4.4.5.2 Comparison of Numerical Airheater Pressure Drop to Empirical Data

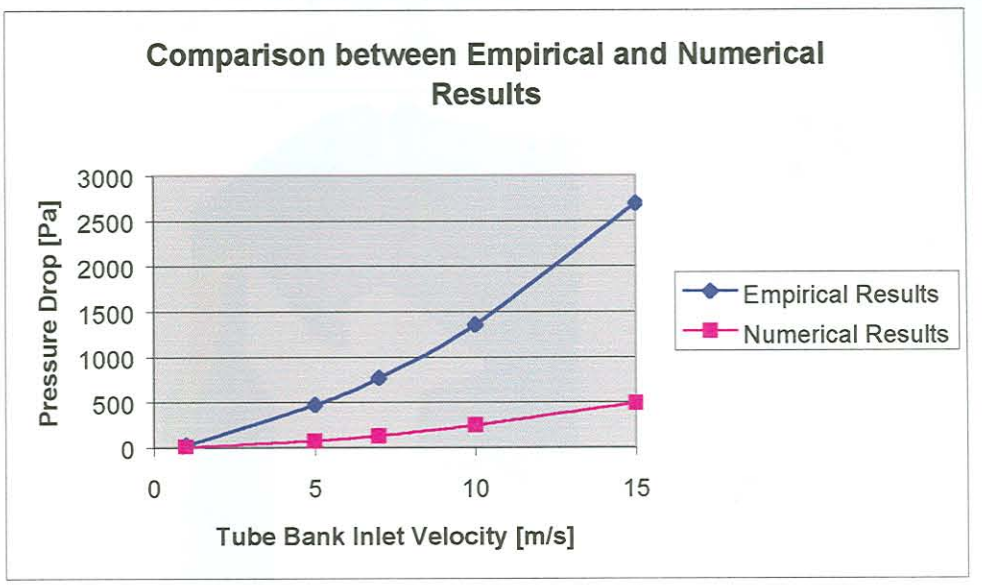

Figure 4-43 Comparison between Empirical and Numerical Results for Airheater Pressure Drop

The difference between the numerical and empirical results for the pressure drop across the airheater is illustrated in Figure 4-43. The same trends are visible here as was the case with the pressure drop calculations across the tube bank. The values of the two trendlines differ from each other with approximately a factor of 5.5. Again, such a large discrepancy was not expected.

4.4.6 Application of Porosity Coefficients to Boiler Internals

Although the porosity coefficients determined for the boiler internals are not trustworthy, porous sections will still be used in the CFD boiler models to see what effect they have on the flow pattern through the boiler.

4.4.6.1 Application of Porosity Coefficients to the Boiler Bank

To simulate the effect of the boiler bank, porous cells were placed in the location of the boiler bank. The characteristics of the porous cells were determined in Chapter 4.4.2. The same approach was followed by Vakkilainen et al.[**90**] with the use of porous cells to replace the boiler bank in the CFD model of the boiler.

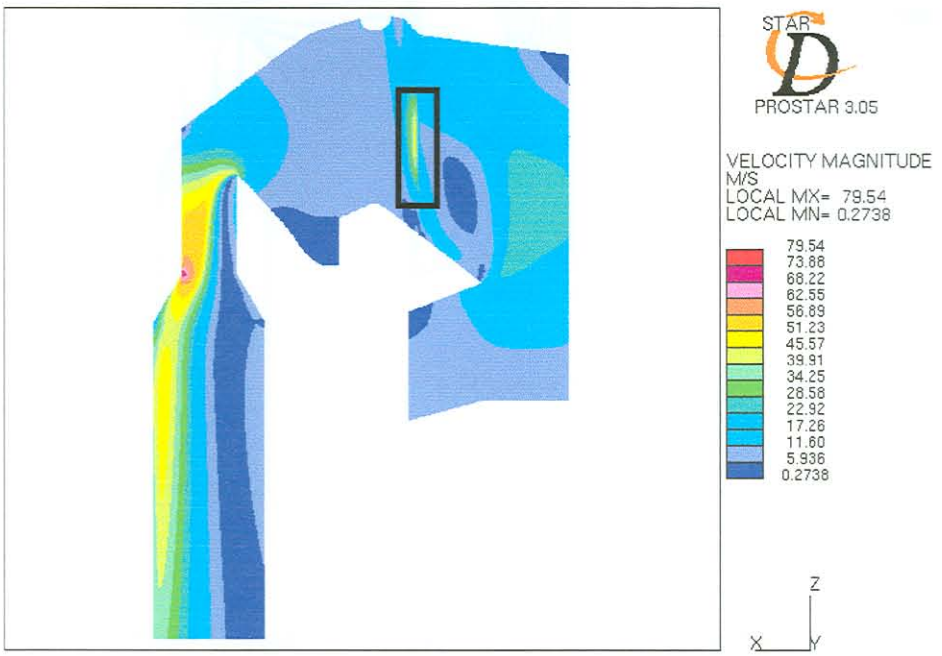

Figure 4-44 Velocity Magnitude Plot for Boiler Model with Porous Cells to Replace Tube Bank (10m.s^{-1} Inlet Velocity)

The velocity magnitude plot for the boiler model with boiler bank modelled as porous cells, is illustrated in Figure 4-44. As can be seen in the rectangle in Figure 4-44 for an inlet velocity of 10m.s^{-1}, the flow field at the entrance of the boiler bank is not realistically represented. Because the resistance of flow in the vertical direction of the tube bank is less than in the cross-flow direction, the flow is turned vertically downwards to follow the path of least resistance. This is due to the directional properties of the porous cells used to 'replace' the boiler bank. Except for the flow that is indicated in the rectangle in Figure 4-44, the rest of the flow field seems to be realistic. Vakkilainen et al.[**90**] found that the modelling of flow without boiler internals gave better results for flow patterns through boiler than models with internals. The results of this study are thus in agreement with other researchers' work.

Figure 4-45 and Figure 4-46 illustrate the particle trajectories for 10μm and 100μm particles respectively. The result in Figure 4-45 does not resemble erosion patterns that were observed during boiler shutdown. The porous section in the CFD model redistributes the ash particles across the whole crossflow area of the tube bank. Better results were obtained where no boiler internals were modelled. Refer to Figure 4-12 for the illustration of particle trajectories where no boiler internals were used. The particle trajectories for 100μm particles illustrated in Figure 4-46 are more consistent with observed erosion patterns during boiler shutdown.

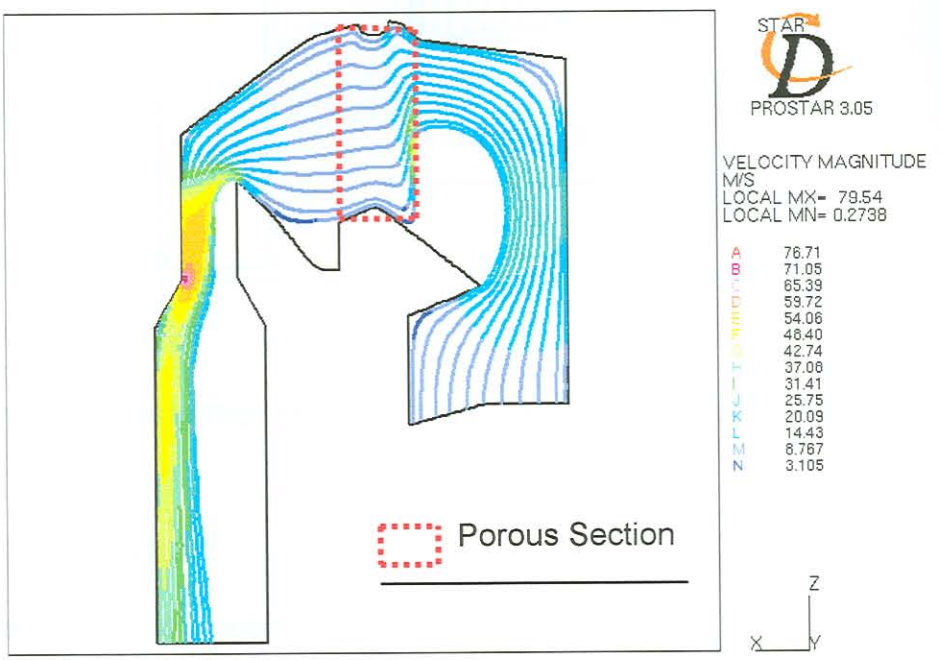

Figure 4-45 Particle Trajectories for 10μm Particles with Porosity Model included for the Boiler Bank

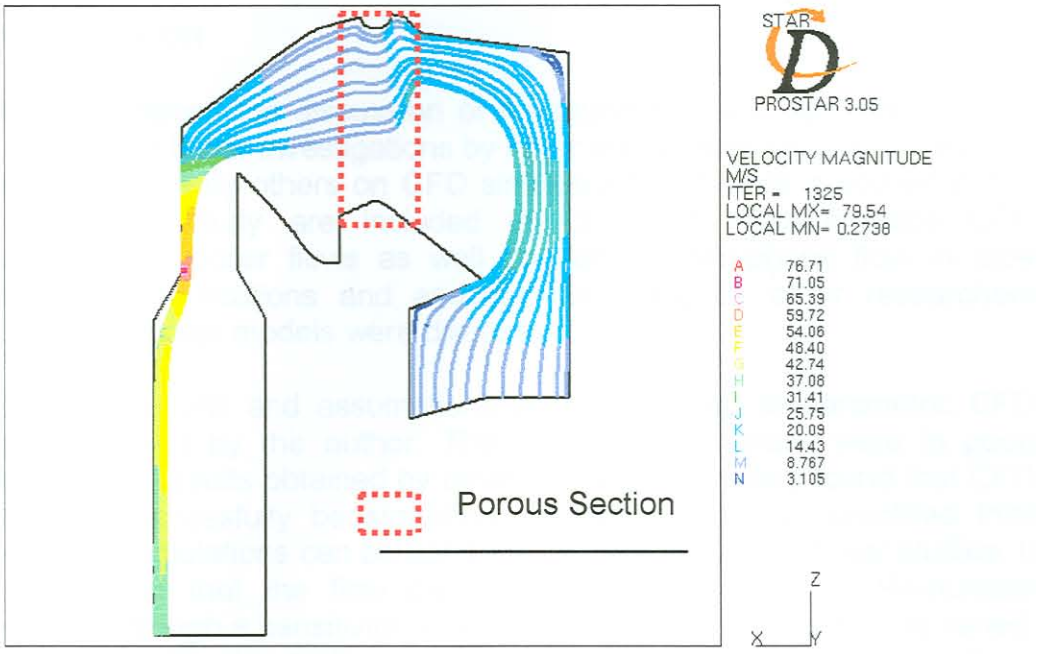

Figure 4-46 Particle Trajectories for 100μm Particles with Porosity Model included for the Boiler Bank

4.4.7 Conclusion

In this section ways were investigated to simplify boiler internals in boiler CFD models. The proposed method was to determine the pressure drop versus velocity characteristics in a detailed hydraulic model of one row of the boiler bank. The pressure drop versus velocity characteristics were then used to define porous cells in the CFD model with the same pressure drop characteristics. The results obtained numerically differ from the experimental correlations of Zukauskas[**85**]. No concrete explanation can be given for the large difference in the computational and experimental results. When the porous cells were included in the 2D CFD model, the results were reasonable with the exception of the flow field at the inlet of the tube bank. It can be concluded, however, that the usage of porous cells to replace boiler internals gives rise to too many uncertainties to use them in detailed CFD boiler models. Due to time constraints to complete this thesis it was decided to not use porous sections for the further CFD analyses in this study. For future work following this study, it is recommended that the uncertainties arising from this study be investigated in more detail to obtain reliable methods to replace boiler internals. The advice of Tu et al. [**48**] is followed in this study that it is possible to obtain a good indication of regions of high erosion rate without the need of modelling tube banks. Tu et al. [**48**] stated that the quality of solutions in boilers without tube banks is sufficient to provide an insight into the flow phenomena and erosion patterns within coal-fired boilers.

4.5 Conclusion

Chapter 3 contained the discussion of the found that was applicable to this study, except for boiler investigations by other researchers regarding CFD. All the research done by others on CFD simulations that were important in the context of this study are included in Chapter 4. This includes CFD investigations on boiler flows as well as detailed two-phase flow in tube banks. The simplifications and assumptions made by other researchers regarding CFD boiler models were discussed.

These simplifications and assumptions were compared to parametric CFD studies performed by the author. The results of this study were in good agreement with results obtained by other researchers. It was found that CFD models can successfully be simplified through the use of simplified inlet geometry. 2D simulations can be used with success in centre boiler studies. It was also found that the flow pattern through the boiler is Re-number independent through a sensitivity analysis where the inlet velocity was varied. It was also found in this CFD parametric study that larger particles are flung towards the top of the boiler to a larger extent than smaller particles due to higher inertial forces.

In the section that concluded this chapter, boiler internals were simplified through the use of porous sections. The pressure drop versus velocity characteristic of the boiler internals were obtained through a detailed hydraulic model. These results did not compare well to experimental data published by another researcher and more work is necessary to obtain more reliable results. This can include the comparison of the results to other experimental correlations.

5 Using CFD to Investigate Remedial Measures for Boiler Tube Erosion

5.1 Introduction

All the research done so far in this thesis supports the research to be presented in this chapter, and served to give a broad background on erosion in boilers. In Chapter 3, the mechanisms of boiler tube failures were discussed. As erosion is identified as the leading cause of boiler tube failures at Sasol, the mechanisms of erosion were investigated in detail. Remedial measures proposed by other researchers were then investigated. In Chapter 4, two-phase flow was investigated in tube banks. Numerical simulations of other researchers were studied to see which size particles contribute the most to tube erosion. Boiler CFD modelling done by other researchers were then discussed. A CFD parametric study was done to see what influence certain operating conditions had on boiler flows. It was clear that larger particles were flung outwards towards the top of the boiler and are probably the cause of erosion in those areas. In this chapter ways are investigated from the knowledge gained so far in this study to solve the unique erosion problems encountered in the boilers at Sasol.

5.2 Erosion in Centre of the Tube Bank

5.2.1 Introduction

A useful first analysis is to recreate the flow conditions in the tube bank without any remedial measures. If the location of erosion can be predicted in this CFD analysis and it relates to observed erosion patterns during boiler shutdown, then remedial measures can be implemented in the CFD boiler model to minimise erosion.

5.2.2 Flow in the Center of Tube Bank without Remedial Measures

Figure 5-1 illustrates the horizontal cross section of the boiler bank at the centre of the boiler. There is a larger than usual gap in the centre of the boiler. There is also a large gap between the tube banks in the horizontal plane. This gap is aligned 90° to the flow direction. The computational domain for the CFD model is the green crosshatched region in Figure 5-1 with symmetrical boundaries to the left and right of the domain. The 8 tube rows on the right of the computational domain have a coarser grid due to memory limitations, while a fine grid is used for the 6 tube rows next to the centre gap. The computational domain illustrated in Figure 5-1 consists of 374812 cells. Incompressible air is used as the fluid in this study. The computational grid around one tube of the denser grid is illustrated Figure 5-2.

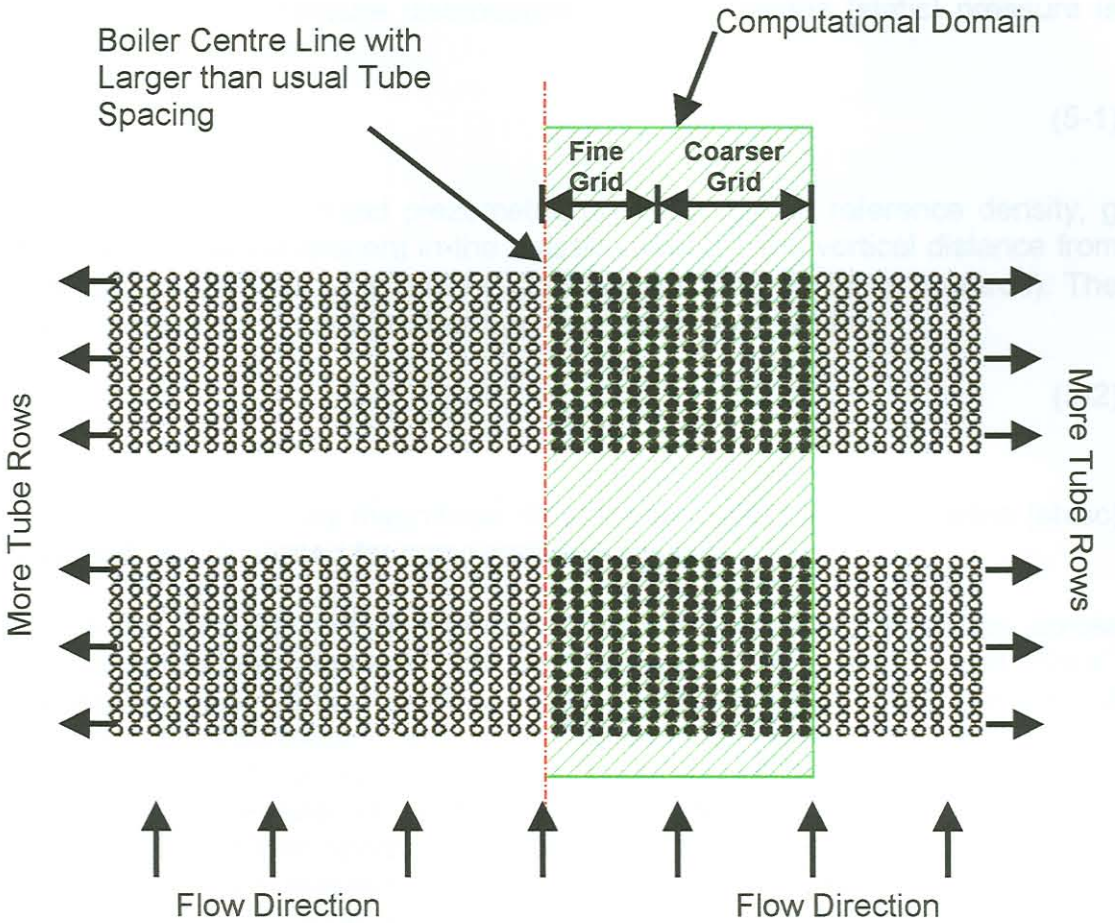

Figure 5-1 Computational Domain of Centre of Boiler Bank

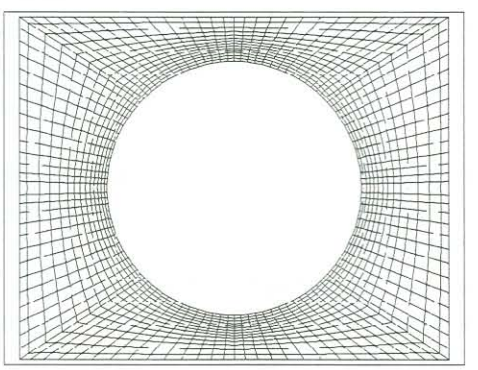

Figure 5-2 Computational Grid around One Tube in the Boiler Bank (Fine Grid)

The pressure distribution across the computational domain is a good indication that the interface between grids with different densities is of an appropriate quality. If sudden changes do not occur in the pressure distribution across grid interfaces of different densities then the grid interface is usually of an appropriate quality.

The four following pictures indicate the piezometric pressure distribution and the total relative pressure distributions. The piezometric (static) pressure is calcutated as follows:

$$p_s = p_p + \rho_0 g z \tag{5-1}$$

where p_p is the computed piezometric pressure, ρ_0 the reference density, g the gravitational component in the z-direction and z the vertical distance from a datum level where ρ_0 is defined (the z-axis points vertically upwards). The total pressure for incompressible flow is calculated as follows:

$$p_{tot} = p_s + \frac{1}{2}\rho V^2 \tag{5-2}$$

where V is the velocity magnitude. Both these pressures, piezometric (static) and total, are illustrated for comparative purposes.

Figure 5-3 and Figure 5-4 give the piezometric pressure distribution across the computational domain for inlet velocities of $10m.s^{-1}$ and $5m.s^{-1}$ respectively. The vertical black line indicates the position where the grids of different densities meet. There is no indication of sudden pressure changes across the interface indicated by the black line of different grid densities. Figure 5-5 and Figure 5-6 illustrate the total relative pressure distribution for the two different inlet conditions. Once again, there is no indication of sudden pressure changes across the interface. It can therefore be assumed that the interface between the different cell densities at the interface is appropriate.

The velocity magnitude distribution can be seen in Figure 5-7 and Figure 5-8 for different inlet velocities of $10m.s^{-1}$ and $5m.s^{-1}$ respectively. It can be seen from these figures that there are high peak velocities in the centre gap of the tube bank for both cases. It is also evident that the higher velocity magnitude region extends a few tube rows adjacent to both the centre gap as well as the gap between the two tube bundles.

The velocity magnitude at the right of the computational domain for both cases is very low. The blue regions on the velocity magnitude plots indicate this low velocity. This is due to the chosen boundary conditions. The best possible solution would have been obtained if the whole boiler bank were included in the CFD model. Due to memory limitations this was not possible. Because the velocities are high in the centre gap the mass flow is greater in this region. As a consequence, for the continuity equations to be satisfied, the flow rate must be less at the boundary furthest away from the centre gap. As the region of interest is close to the centre gap, the boundary conditions assumption is sufficient to provide quantitative results. Other boundary conditions or larger tube banks with coarser grids can be investigated in the future.

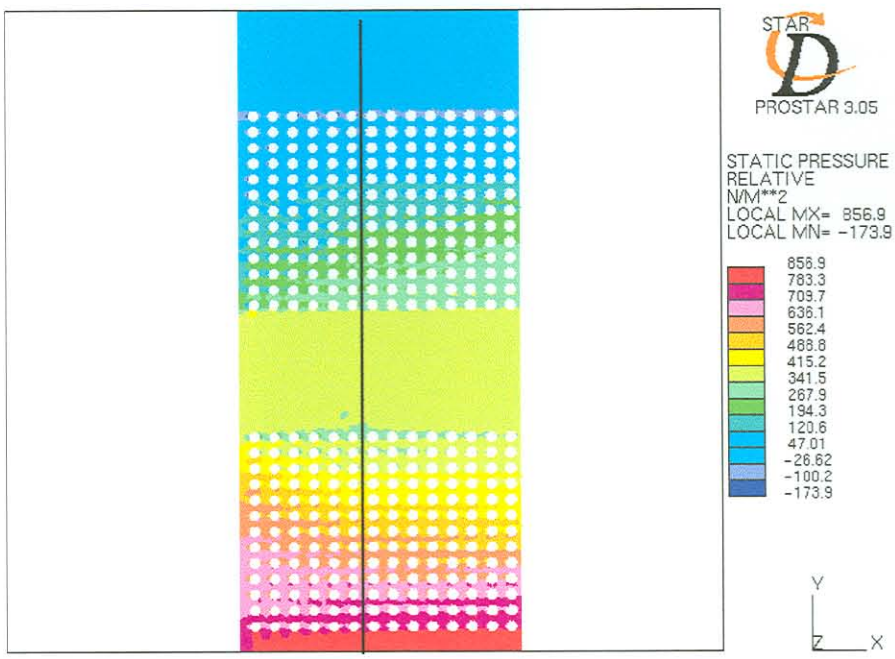

Figure 5-3 Piezometric Pressure Distribution for Flow across the Whole Computational Domain for 10m.s^{-1} Inlet Velocity

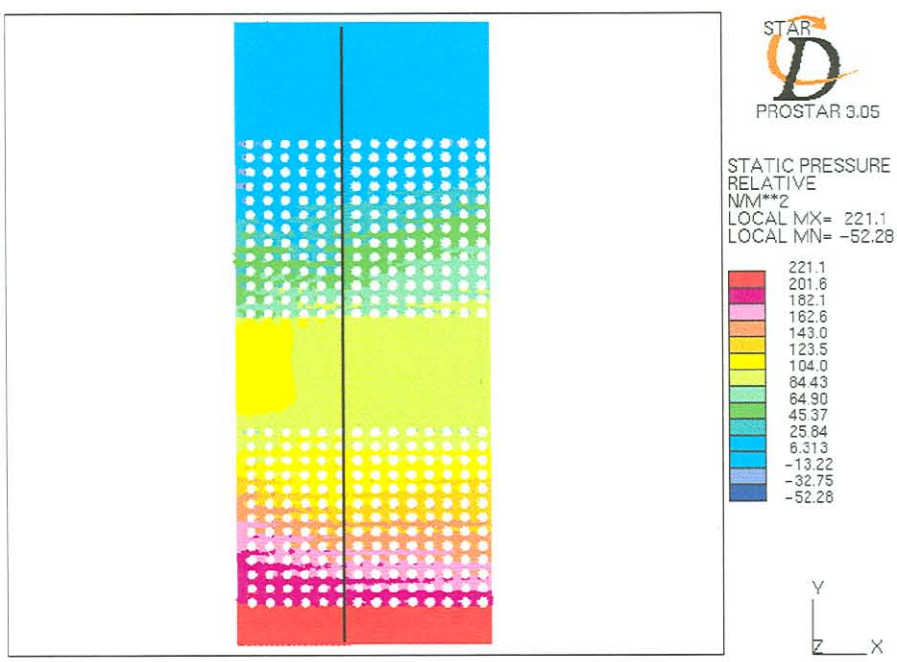

Figure 5-4 Piezometric Pressure Distribution for Flow across the Whole Computational Domain for 5m.s^{-1} Inlet Velocity

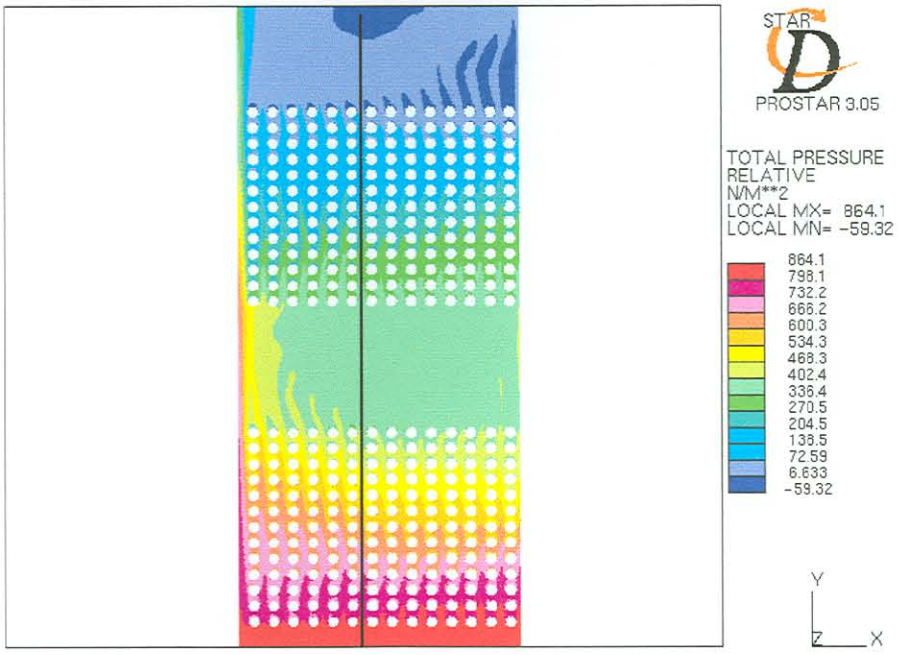

Figure 5-5 Total Relative Pressure Distribution for Flow across the Whole Computational Domain for 10m.s^{-1} Inlet Velocity

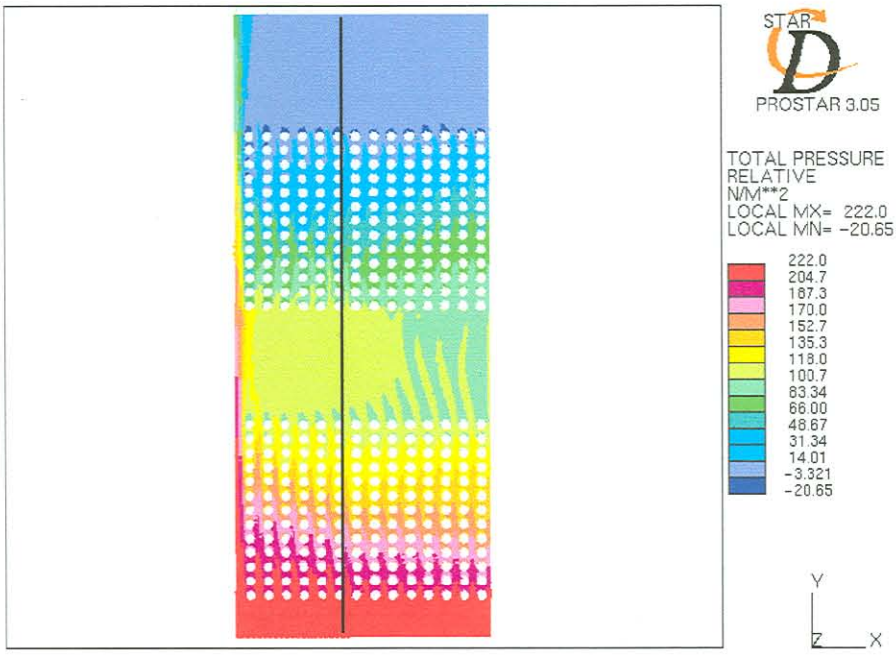

Figure 5-6 Total Relative Pressure Distribution for Flow across the Whole Computational Domain for 5m.s^{-1} Inlet Velocity

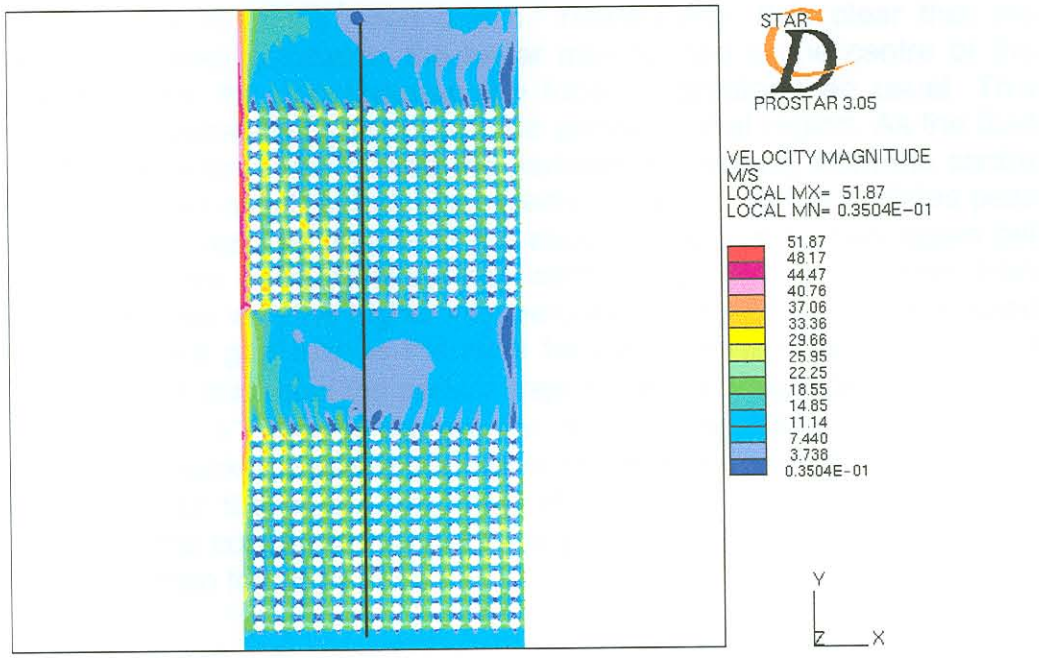

Figure 5-7 Velocity Magnitude Contour Plot for Flow across the Whole Computational Domain for 10m.s^{-1} Inlet Velocity

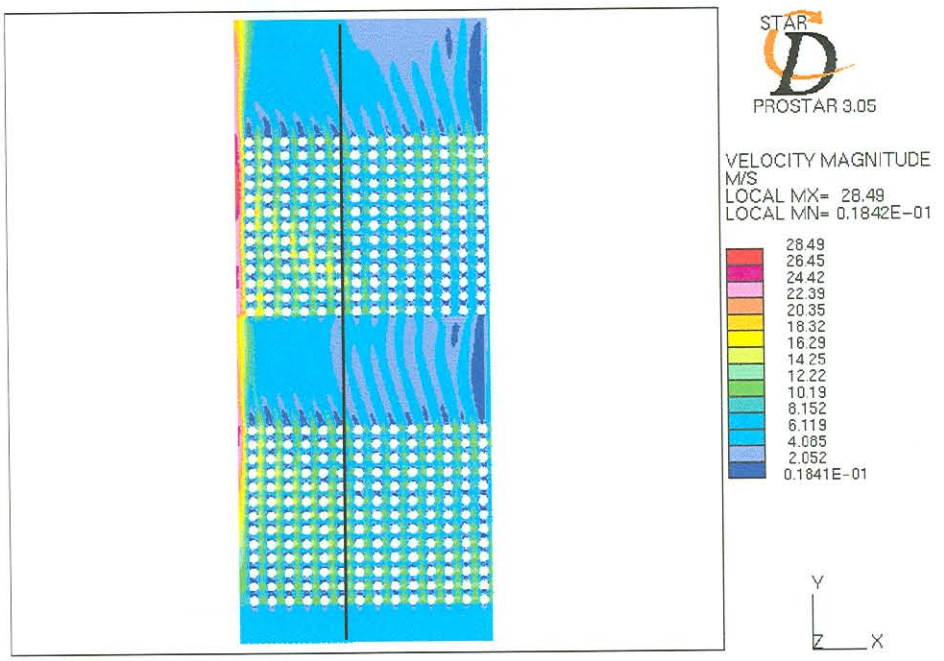

Figure 5-8 Velocity Magnitude Contour Plot for Flow across the Whole Computational Domain for 5m.s^{-1} Inlet Velocity

Figure 5-9 and Figure 5-10 illustrate the particle trajectories for 10μm particles at inlet velocities of 10m.s^{-1} and 5 m.s^{-1} respectively. It is clear that the particles are sucked in towards the faster moving fluid in the centre of the boiler bank where the gap between the tubes is greater than usual. This causes the concentration of particles to be greater in that region. As the fluid moves into the second tube bundle the particles move away from the centre gap and tend to get redistributed more evenly. However, as the particles pass approximately through the middle of the second tube bundle they again get sucked to the centre because of the high centre velocity. It can be seen from Figure 5-9, the case with the higher inlet velocity, that the particles get sucked more to the centre gap than is the case for the lower inlet velocity (Figure 5-10). Figure 5-11 illustrates the particle trajectories for 100μm particles with a inlet velocity of 5m.s^{-1}. Due to the greater inertia of the 100μm particles, the particles are not sucked towards the centre of the boiler bank as much as the 10μm particles for the same conditions (Figure 5-10). It can therefore be concluded that the concentration of smaller particles is higher in the centre of the boiler bank than for larger particles.

These results prove that the CFD solution predicts erosion in the region of observed erosion patterns during boiler shutdown. This is the case, because, as already discussed, erosion is a linear function of particle concentration and a function of velocity to the power of two to four. As the velocity and particle concentration is high in the centre of the boiler, erosion will be more prevalent in this region.

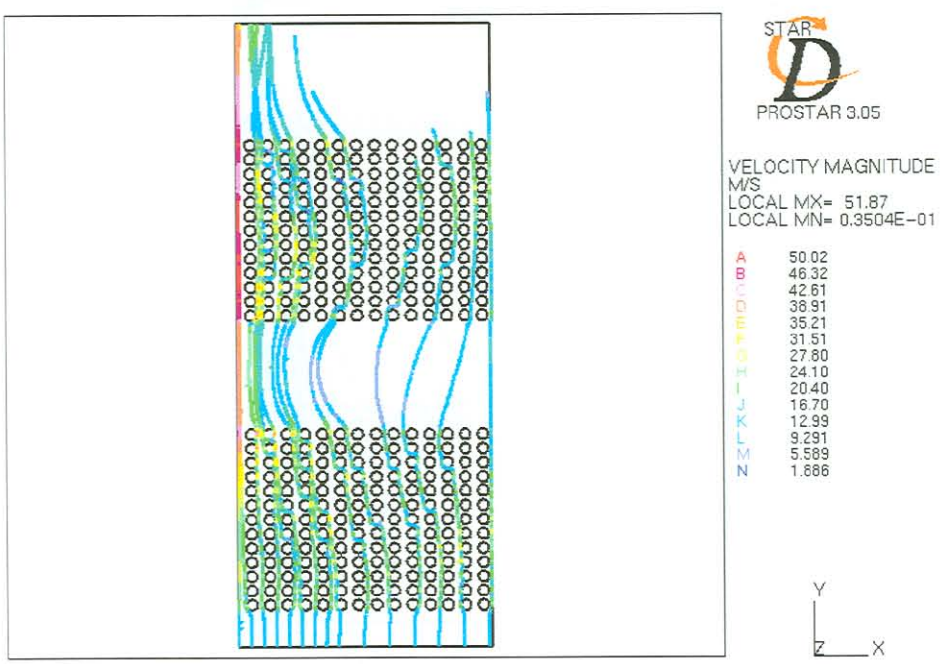

Figure 5-9 Particle Trajectories for 10μm Particles for 10m.s^{-1} Inlet Velocity

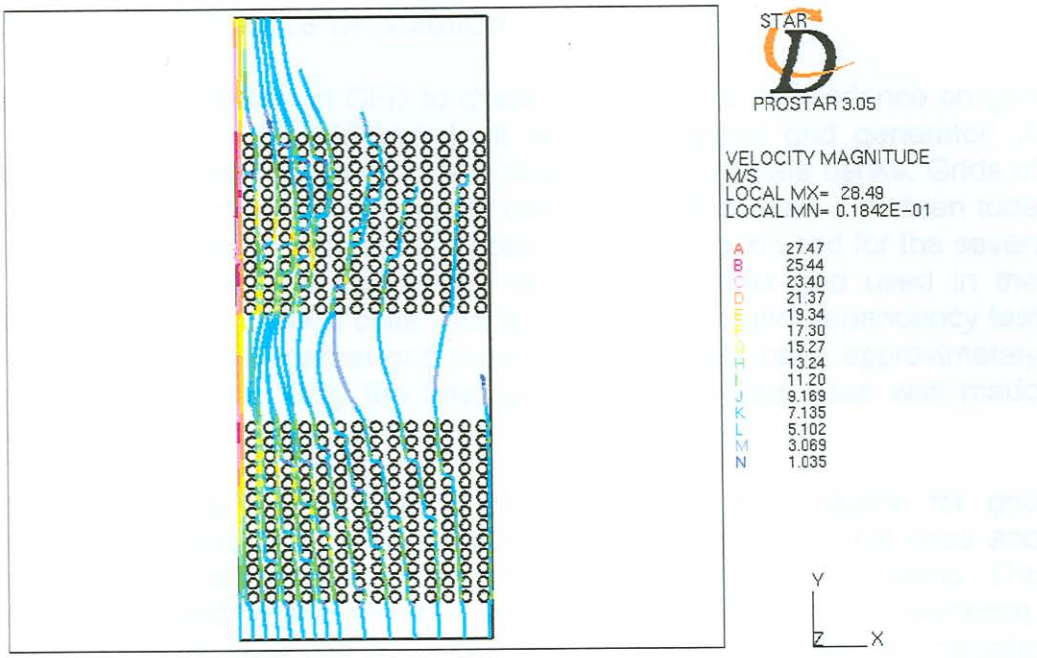

Figure 5-10 Particle Trajectories for 10μm Particles for 5m.s^{-1} Inlet Velocity

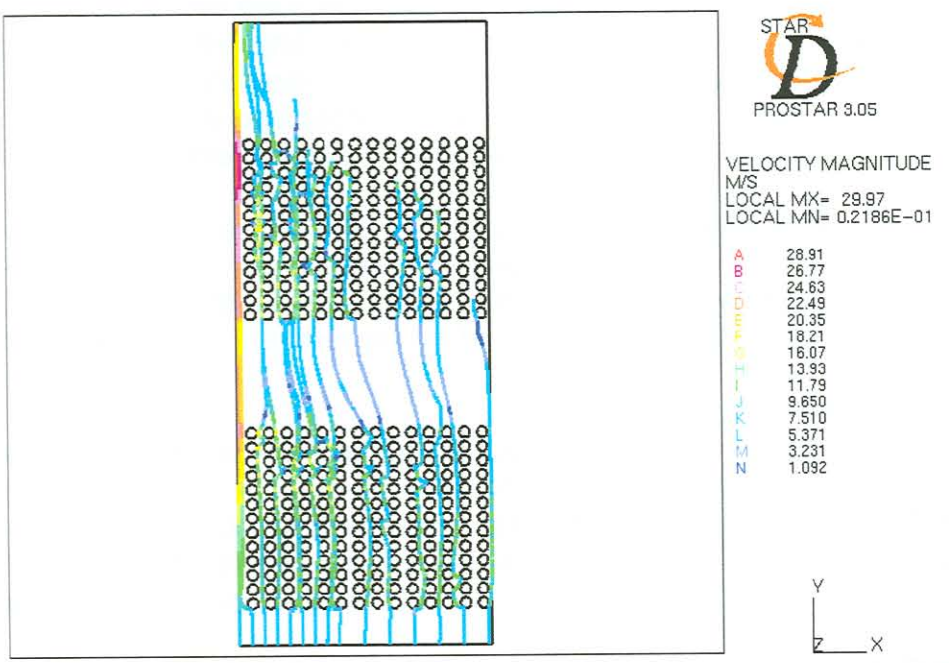

Figure 5-11 Particle Trajectories for 100μm Particles for 5m.s^{-1} Inlet Velocity

5.2.3 Grid Dependence of Solution

It is always good practice in CFD to check the solution's dependence on grid size and shape. A new grid was built with an elliptical grid generator. A elliptical grid generator are used to test its applicability to tube banks. Grids of two sizes were again used in the same computational domain. Fourteen tube rows are used for the grid dependency test with a finer grid used for the seven tube rows nearest to the centre gap of the boiler. The grid used in the previous section had 375000 cells. The grid used for the grid dependency test has 243000 cells. The coarser grid regions of both grids have approximately the same grid density. Only the finer grid of the previous case was made coarser.

The reason why a coarser grid is used to check the solution for grid dependence is because a relatively fine grid was used in the first case and further refinement is not possible due to computer memory limitations. The fineness of the grid in the previous section was chosen from experience. When the pressure drop characteristics was obtained in the hydraulic model of the tube bank to obtain porosity coefficients, it was concluded that a fine grid was necessary to obtain the correct separation point on each tube.

Figure 5-12 and Figure 5-13 show the piezometric and total pressure distributions respectively. If these results are compared to Figure 5-3 and Figure 5-5 it can be seen that the pressure distributions are very similar. The pressure drop across the tube bank for this grid is approximately 2% less than was the case for the grid used in Chapter 5.2.1. As a difference of 2% is acceptable for the purposes of this study it can be concluded that the finer grid used in the previous section is appropriate for this study and that further grid refinement to the fine grid will not increase solution accuracy significantly.

Figure 5-14 shows the velocity magnitude plot for the coarser elliptical grid used. If this figure is compared to Figure 5-7 it can be seen that there is an approximately 6% difference in the maximum velocity obtained where the maximum velocity of the finer grid is higher than the maximum velocity of the coarser grid.

Figure 5-15 illustrates the particle trajectories of 10μm particles for the case where a coarser grid was used. If this solution is compared to Figure 5-9 that shows the solution for the same case but with a finer grid it can be seen that the particles are sucked in more towards the centre of the boiler bank as was the case with the coarser grid.

It can be concluded that the finer grid is acceptable for accurate CFD results. The fine grid has 54% more cells than the coarser grid but the maximum pressures for the two cases differ by only 2% and the maximum velocities differ by only 6%. As grid refinement to the finer grid will increase solution time significantly, the results will not change much though. The fine grid used in Chapter 5.2.1 is thus acceptable and further grid refinement to the fine grid will not greatly influence the solution.

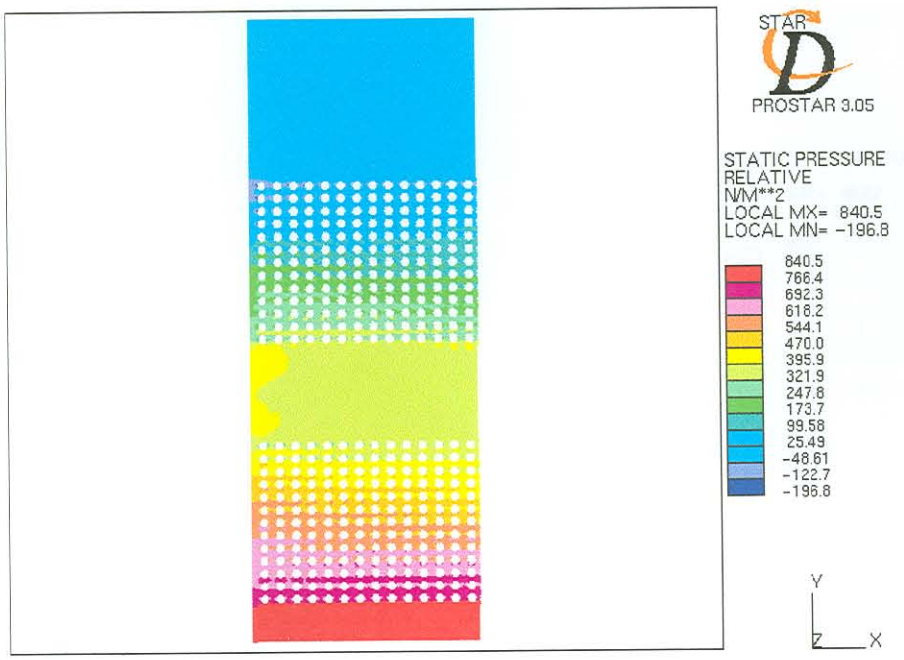

Figure 5-12 Piezometric Pressure Contours for Elliptical Grid for a 10ms^{-1} Inlet Velocity – Coarser Grid

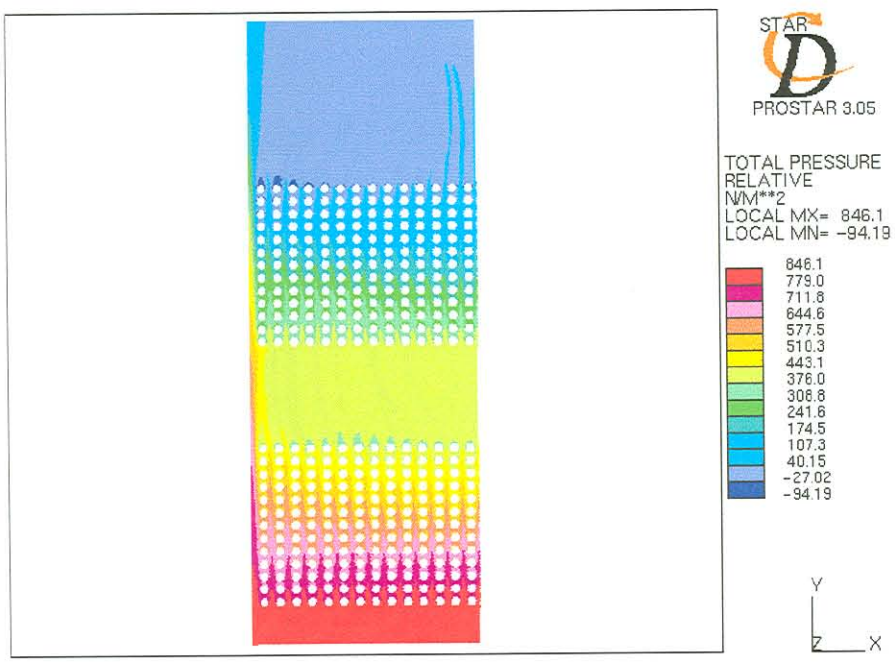

Figure 5-13 Total Pressure Contours for Elliptical Grid for a 10ms^{-1} Inlet Velocity – Coarser Grid

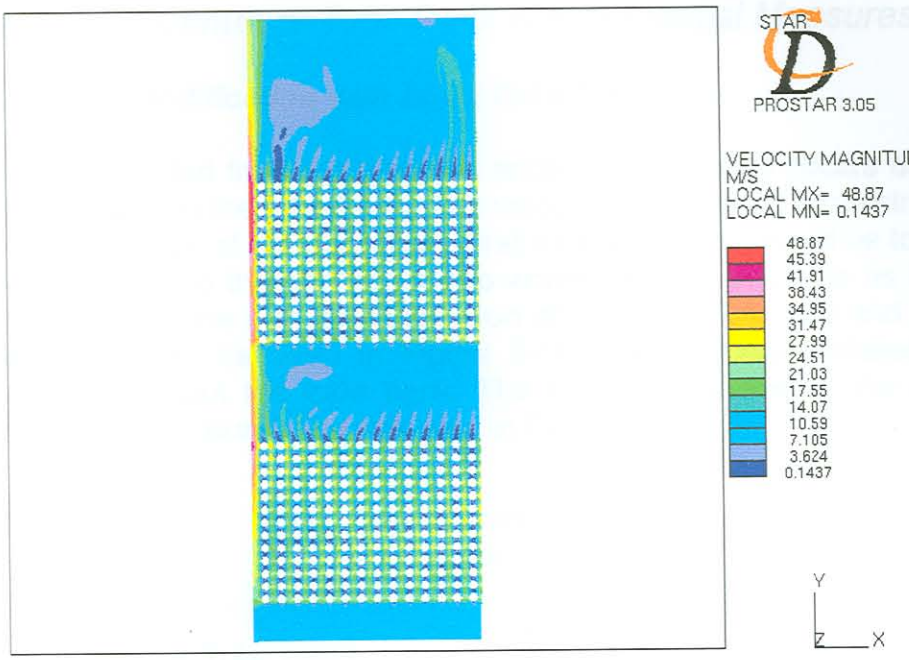

Figure 5-14 Velocity Magnitude Contours for Elliptical Grid for a 10ms^{-1} Inlet Velocity – Coarser Grid

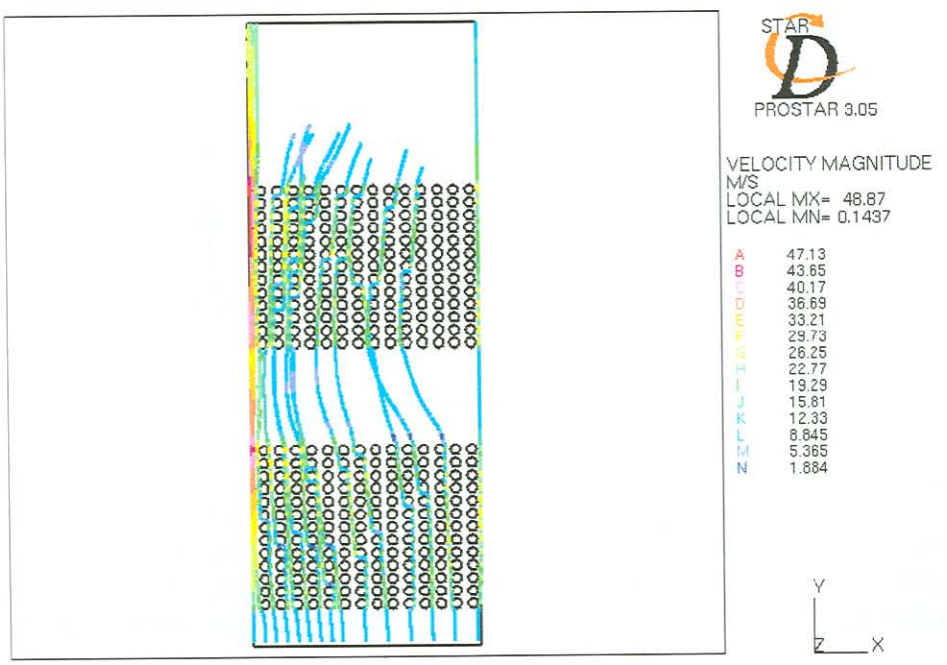

Figure 5-15 Partical Traces for 10μm Particles with a 10ms^{-1} Inlet Velocity - Coarser Grid

5.2.4 Flow in Centre of Tube Bank with Remedial Measures

5.2.4.1 Flow-Modification with Eight Tube Fins

It can be concluded from the previous section that erosion occurs due to the effect of the gap in the tube bank. The velocity and particle concentration are higher in the region of the gap. One's first intuitive feeling would be to suggest to cover the gap so that the larger gap would be the same size as the other gaps. This was done with the installation of tube fins. The size and shape of the fins used can be seen in Figure 5-16. The fins are installed at four locations throughout the tube bank. The fins are installed at the inlet and outlet of each tube bundle as indicated in Figure 5-17.

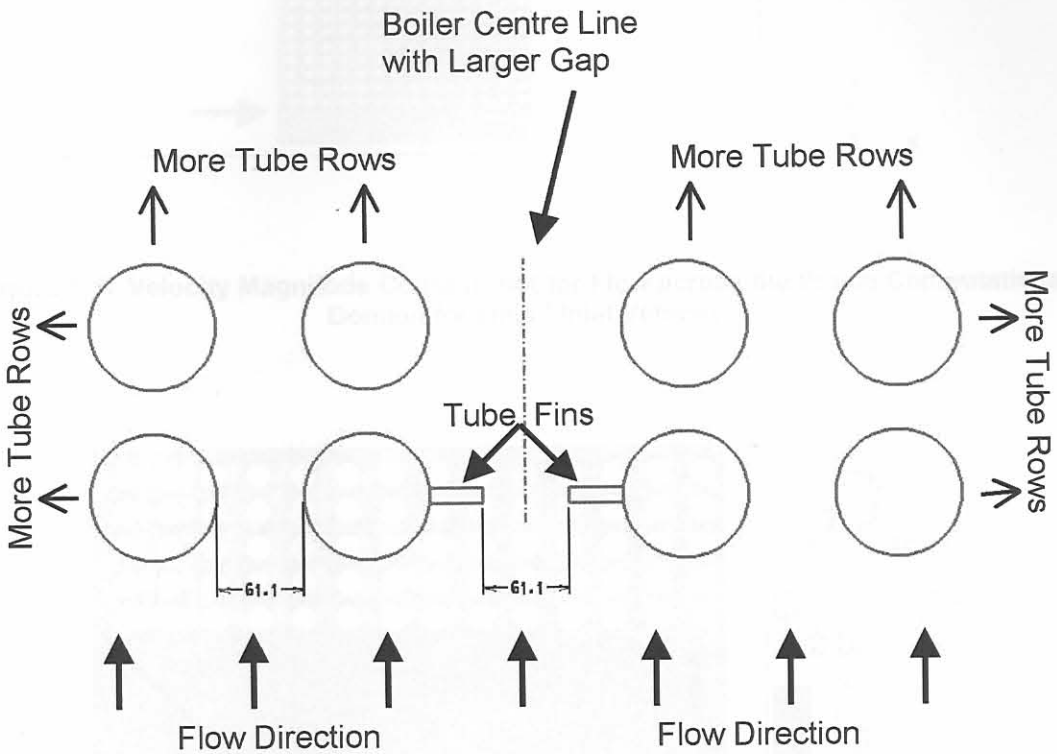

Figure 5-16 Position of Tube Fins

Figure 5-17 illustrates the velocity magnitude plot across the whole computational domain for an inlet velocity of 5m.s^{-1}. The maximum velocity in the domain is 24.13m.s^{-1}. The maximum velocity obtained in the case where no fins were used was 28.49m.s^{-1}. The maximum velocity is thus reduced by 15.3%.

Figure 5-18 is a close-up view of the flow in the centre of the tube bank. It can be seen that the fin at the outlet of the first tube bundle deflects the flow onto adjacent tubes, which can lead to degradation of those tubes. The same is happening at the outlet of the second tube bundle as shown in Figure 5-19.

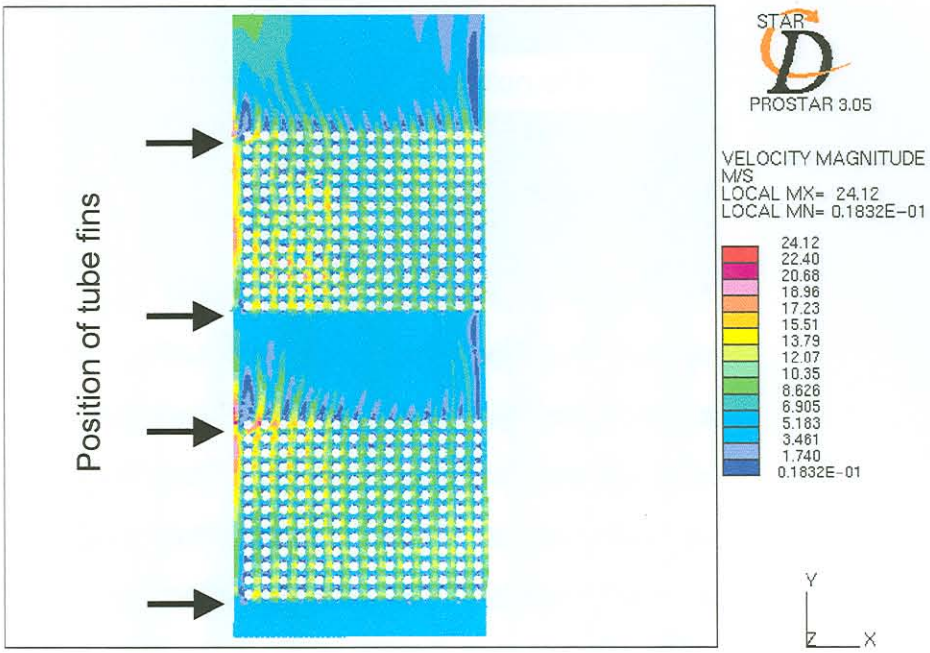

Figure 5-17 Velocity Magnitude Contour Plot for Flow across the Whole Computational Domain for 5m.s^{-1} Inlet Velocity

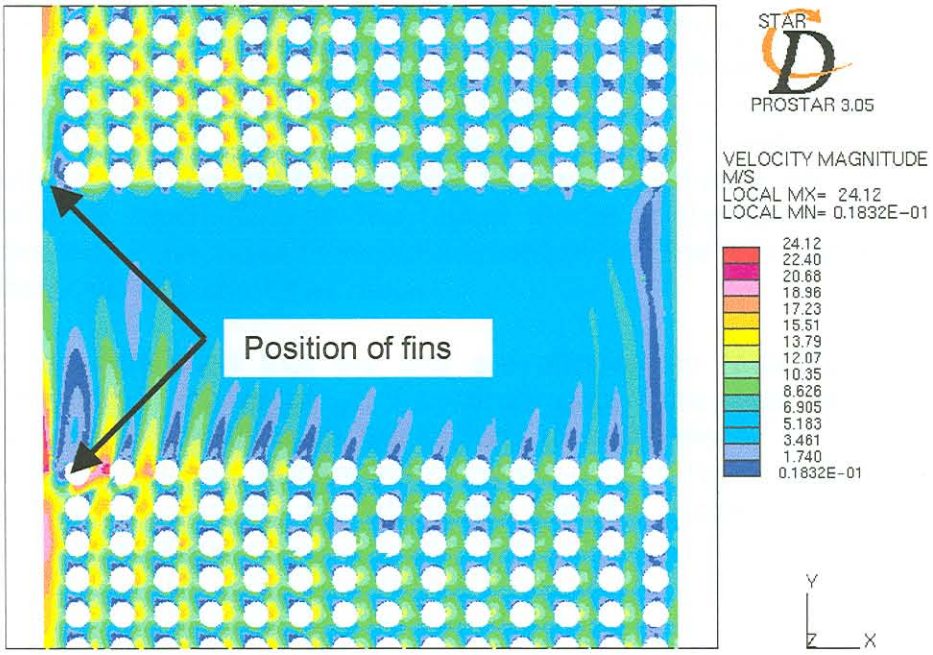

Figure 5-18 Velocity Magnitude Contour Plot for Flow in the Centre of the Tube Bank

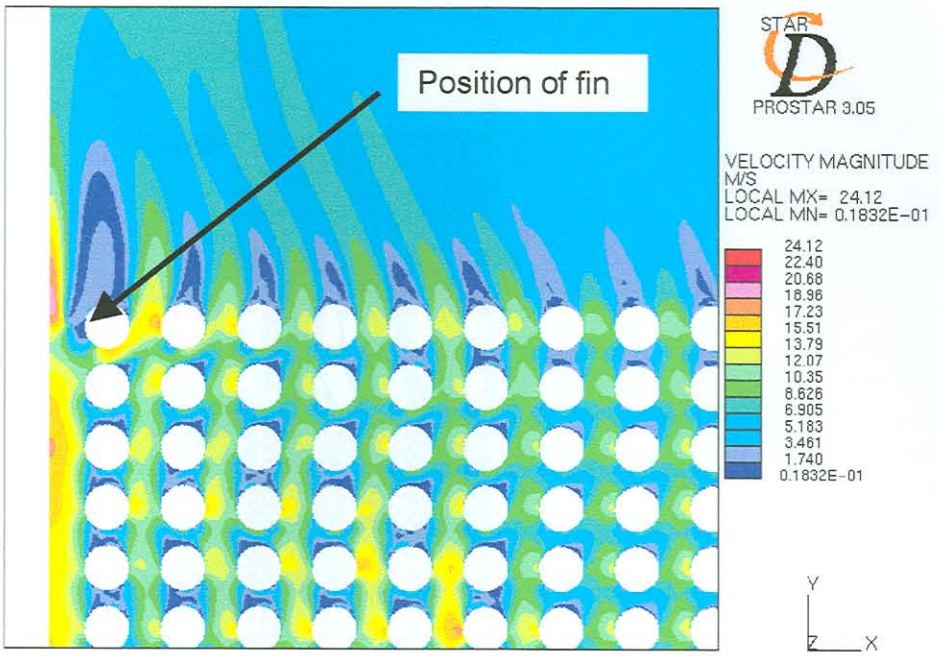

Figure 5-19 Velocity Magnitude Contour Plot for Flow at the Outlet of the Tube Bank

Figure 5-20 and Figure 5-21 show the particle traces for 100μm and 10μm particles respectively for the case where eight fins are used in the CFD model. If these results are compared to Figure 5-10 and Figure 5-11, which are the particle traces of 10μm and 100μm particles respectively for the case where no fins were used, it can be seen that the particle traces differ. The 10μm particles are not sucked towards the centre gap as much as was the case where no fins were used. The fins are thus effective in reducing the particle concentration for the smaller particles. For the 100μm particles, the results do not differ as much. Due to the higher inertia of the larger particles, the particles tend to keep their forward momentum and the effect of the gap does not effect their trajectories as much.

It can be concluded that the fins are effective in reducing the particle concentration in the region of the centre gap. Care must be taken when installing these fins because the regions of high velocity can be shifted to adjacent tubes as was evident from Figure 5-18 and Figure 5-19. Channelling of the flow in the centre gap still exists after the modelling of eight fins to prevent this problem.

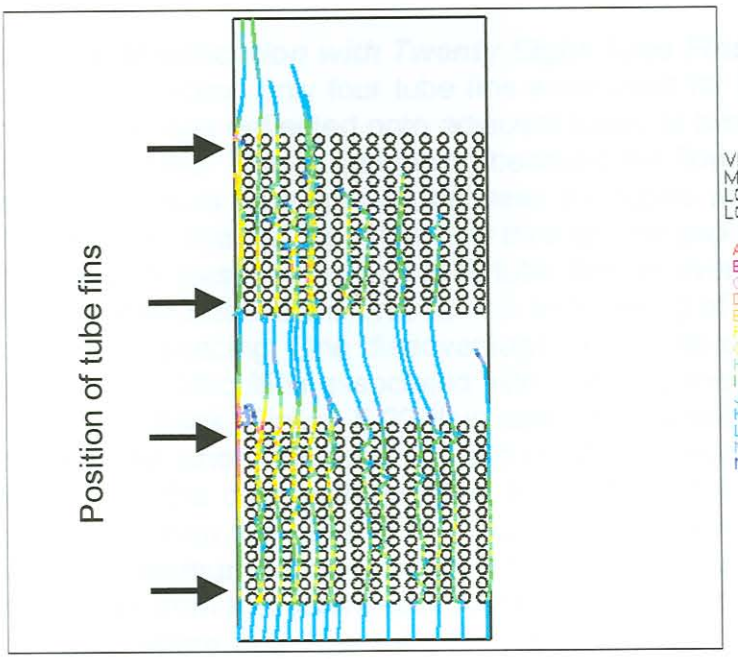

Figure 5-20 Particle Trajectories for 100μm Particles for 5m.s^{-1} Inlet Velocity

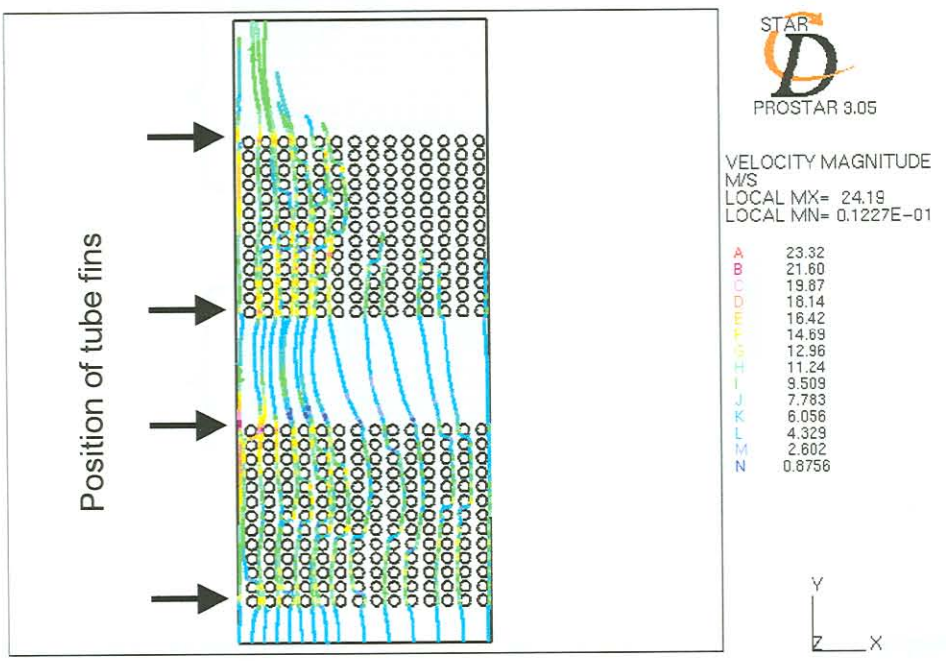

Figure 5-21 Particle Trajectories for 10μm Particles for 5m.s^{-1} Inlet Velocity

5.2.4.2 Flow-Modification with Twenty Eight Tube Fins

In the previous section only four tube fins were used for the symmetrical half shown. The flow was deflected onto adjacent tubes at two locations at the exit of each tube bundle. This is happening because the flow is still channelling in the larger than usual tube spacing between the tubes with the fins. One way of eliminating the channelling of the flow through the gap is through the use of more tube fins. It was decided to install tube fins on every second tube in the gap with the idea that this will prevent the channelling of the flow in the larger than usual tube spacing. One disadvantage of the use of fins throughout the tube bank is the difficulties associated with installing the tubes with fins deep within the tube bank. Figure 5-22 illustrates the velocity magnitude contour plot for the case where fourteen fins are used. The maximum velocity in the flow domain for the case with fourteen fins is 23.59m.s^{-1}. This represents a 2.2% decrease from the case where four tube fins were used, and a 17.2% decrease in maximum velocity where no fins were used. Again the flow is deflected away from the centre gap by the tube fins but to a lesser extent as was the case where only four tube fins were used. This can be seen in the close-up view in Figure 5-23.

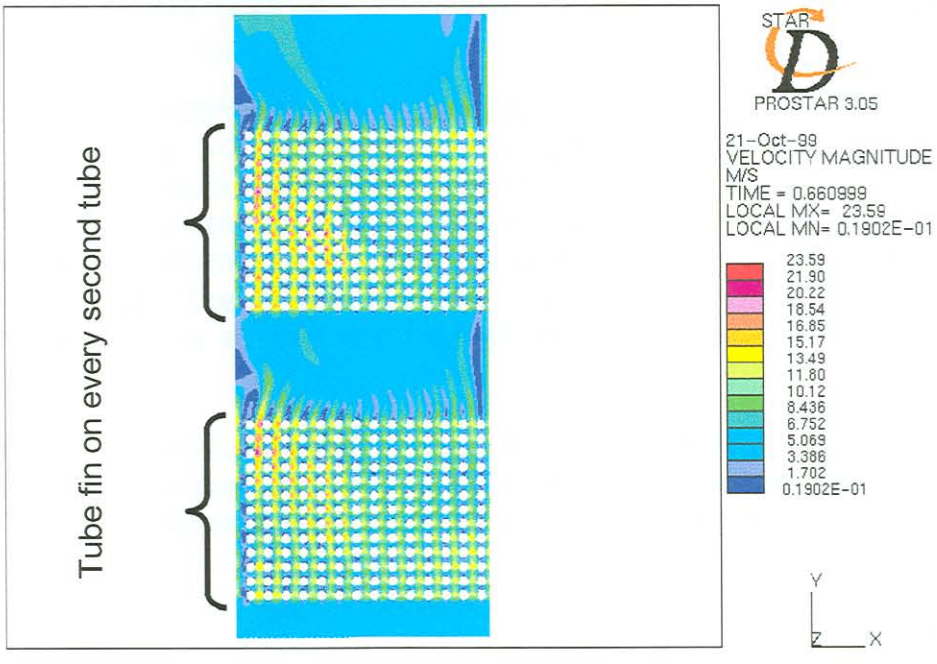

Figure 5-22 Velocity Magnitude Contour Plot for Flow across the Whole Computational Domain for 5m.s^{-1} Inlet Velocity

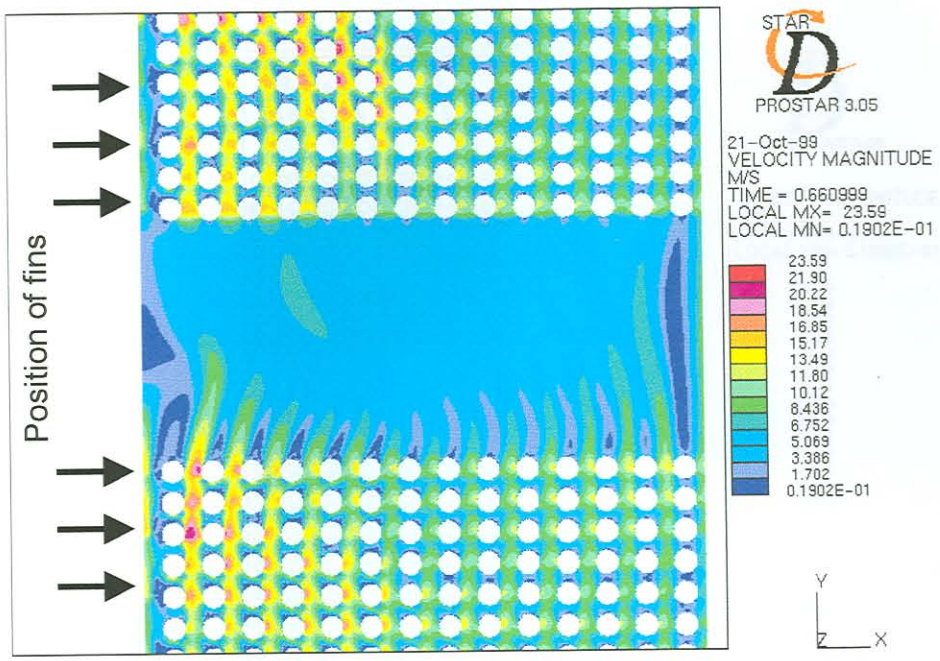

Figure 5-23 Velocity Magnitude Contour Plot for Flow in the Centre of the Tube Bank

The particle trajectories for 10μm and 100μm particles can be seen in Figure 5-24 and Figure 5-25 respectively. The particle trajectories of the 10μm particles are not sucked towards the centre gap as was the case with the four tube fins. The particle trajectories behave somewhat strange due to the fact that some particles move away from the centre gap and others move towards the centre gap. The 100μm particles, as with the previous cases, move approximately in a straight line through the tube bank due to their higher inertia.

This remedial measure where 14 tube fins are used, is a very viable option because the maximum velocity in the flow domain is reduced. The flow is not deflected onto adjacent tubes as much as the case where four tube fins were used.

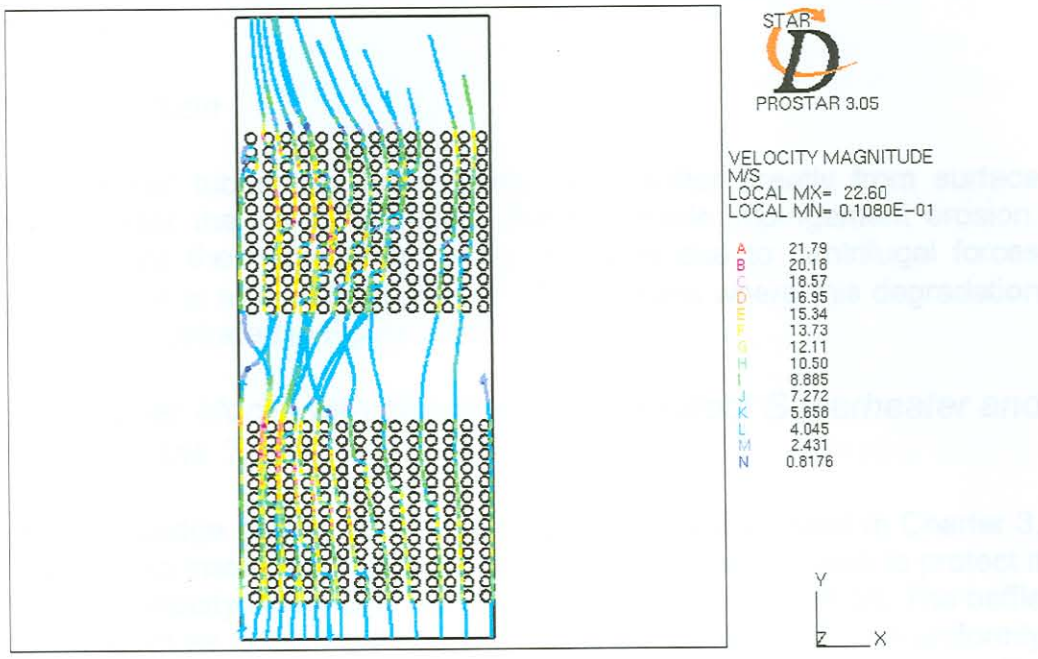

Figure 5-24 Particle Trajectories for 10μm Particles for 5m.s^{-1} Inlet Velocity

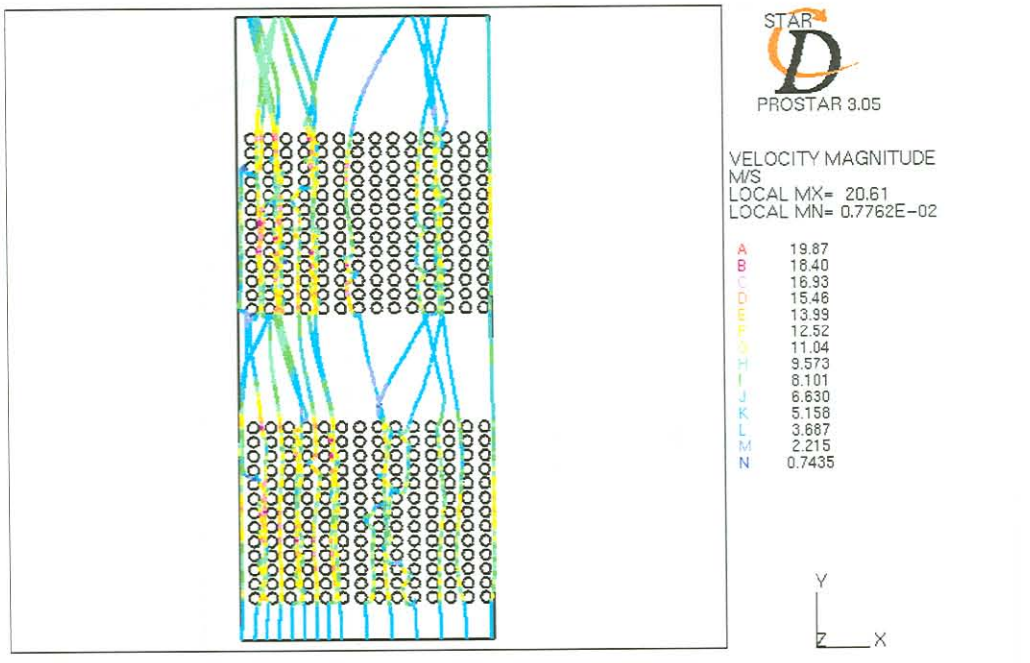

Figure 5-25 Particle Trajectories for 100μm Particles for 5m.s^{-1} Inlet Velocity

5.3 Remedial Measures for Superheater and Tube Bank Erosion

5.3.1 Introduction

The superheater tubes and boiler bank tubes suffer greatly from surface degradation near the top of the boiler due to particle impingement erosion. That is because the particles are flung outwards due to centrifugal forces because the flow is turning through 180°. The regions where this degradation take place are illustrated in Figure 5-26.

5.3.2 2D Boiler Model with Small Baffle to Protect Superheater and Tube Bank Tubes

From the knowledge gained from the literature survey discussed in Charter 3, it was decided to install a screen in front of the superheater tubes to protect it from the high velocity flow with a high fly-ash particle concentration. The baffle will hopefully act as a device that will redistribute the fly-ash more uniformly across the superheater and boiler bank tubes. Figure 5-26 illustrates the position of the baffle used for the protection of boiler tubes.

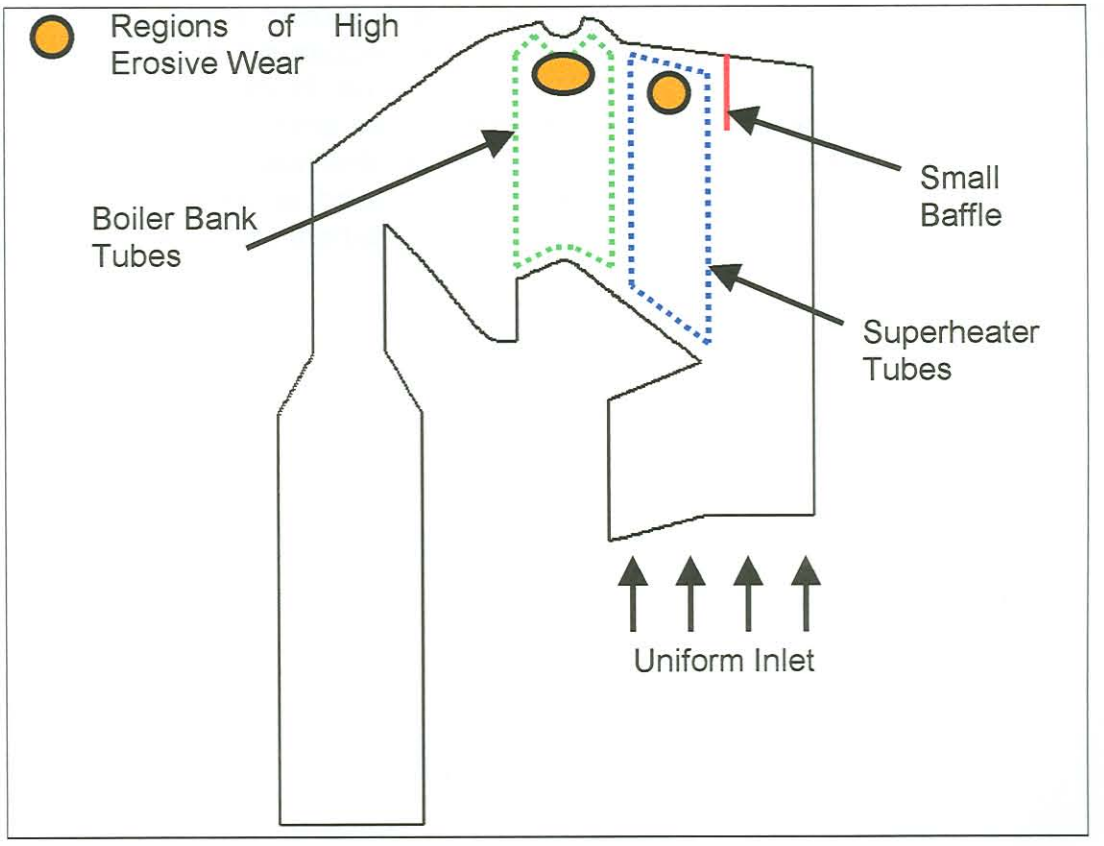

Figure 5-26 Schematic Diagram showing the Position of Tubes ,Small Baffle and Regions of High Erosive Wear in the Upper Boiler

5.3.2.1 Solid Baffle

Dooley and Westwood[**29**] warned that the use of solid baffles can cause movement of erosion to an adjacent area. Nevertheless, it is a useful first analysis to see if the baffle has the desired effect on the flow pattern through the boiler.

Figure 5-27 illustrates the velocity magnitude field for a 2D model of the boiler without any flow-modification devices. A large recirculation zone is evident above the bullnose. The region where high superheater tube wastage occurs is indicated with the circle in Figure 5-27. Figure 5-28 shows the plot of velocity magnitude with the installed solid baffle. The recirculation above the bullnose is much smaller but there is now essentially no flow in the top of the boiler leading to a loss in heat transfer to the wall tubes. There is also a large region of high velocity as indicated by the circle. This can possibly lead to tube wastage by erosion in those regions.

The particle traces for 100μm and 10μm particles for the boiler geometry with the solid baffle can be seen in Figure 5-29 and Figure 5-30 respectively. It is clear that the particle trajectories are essentially the same in the upper boiler for the different size particles. There are no particles in the recirculation zone above the bullnose or near the top of the boiler. It is now possible that erosion might be prevalent in this region because the particle and velocity distributions are not uniform across the superheater and boilerbank tubes but are concentrated in the middle section. A solid baffle is therefore not appropriate for the prevention of erosion. It can next be investigated what the flow patterns would be if the baffle were permeable or of a different size. The size of the baffle was arbitrarily chosen. Mathematical optimisation can be used to design the baffle to have the optimum size and permeability to obtain a uniform flow across the tube bank.

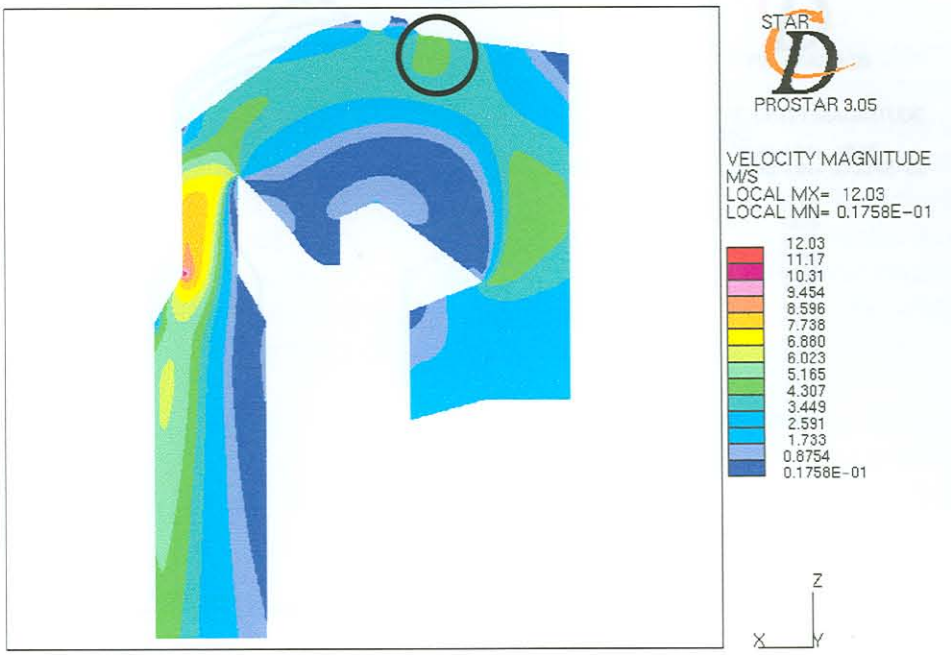

Figure 5-27 Velocity Magnitude Contour Plot without any Flow-Modification Devices ($2m.s^{-1}$ Inlet Velocity)

Figure 5-28 Velocity Magnitude Contour Plot with Solid Baffle ($2m.s^{-1}$ Inlet Velocity)

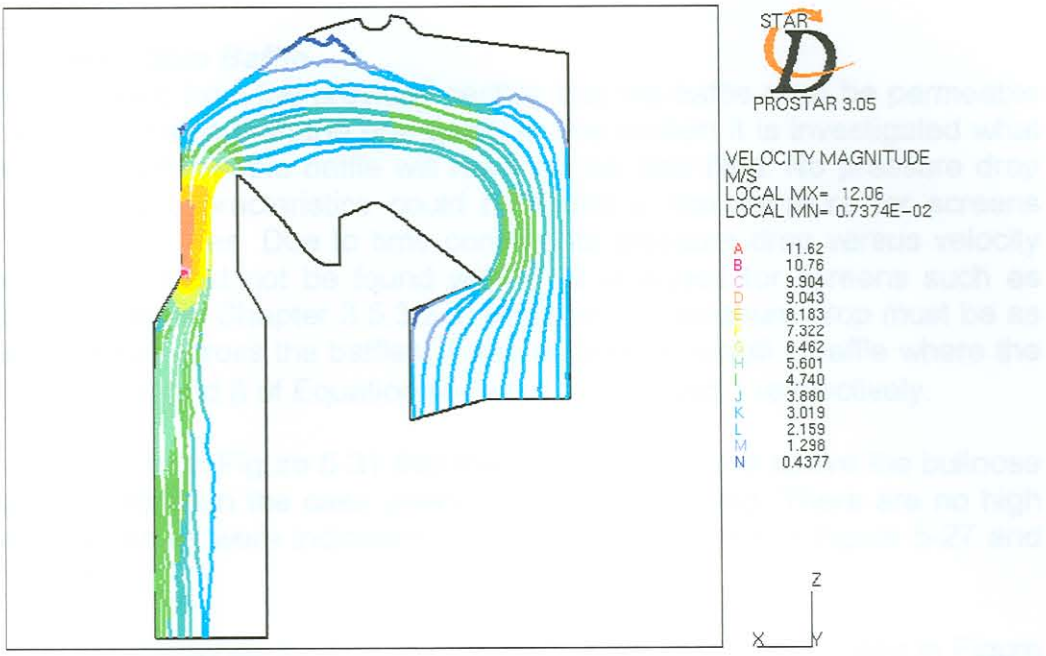

Figure 5-29 Particle Trajectories of 100μm Particles with Solid Baffle (2m.s^{-1} Inlet Velocity)

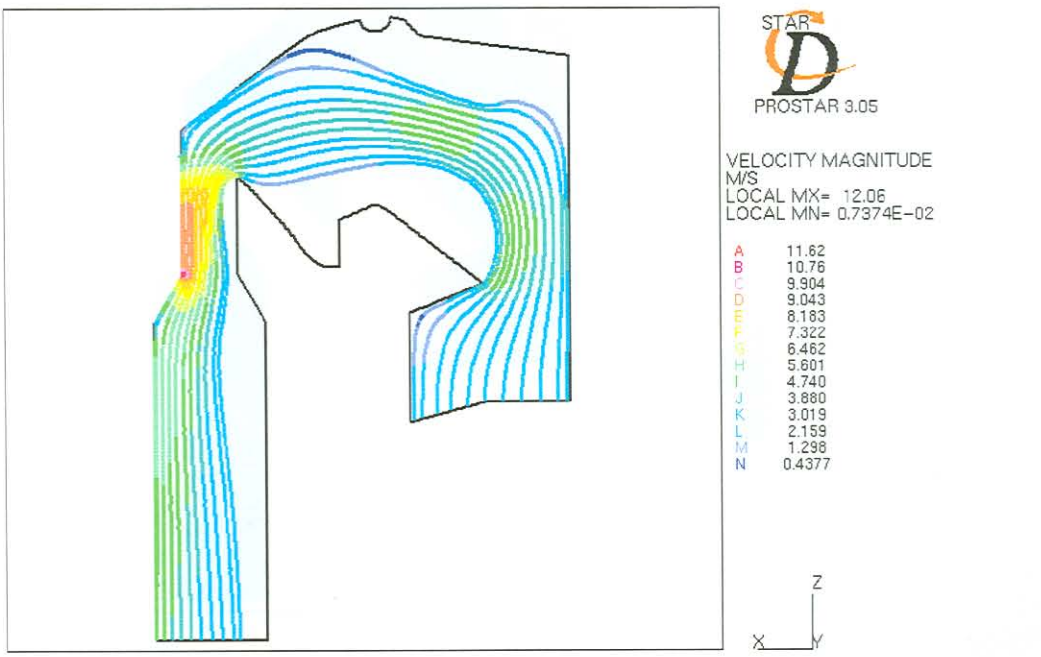

Figure 5-30 Particle Trajectories of 10μm Particles with Solid Baffle (2m.s^{-1} Inlet Velocity)

5.3.2.2 Permeable Baffle

It was concluded from the previous section that the baffle must be permeable or of a different size than the one used. In this section it is investigated what effect a small permeable baffle will have on the flow field. No pressure drop versus velocity characteristics could be found in the literature for screens used in boiler utilities. Due to time constraints pressure drop versus velocity characteristics could not be found with CFD analyses for screens such as those mentioned in Chapter 3.5.3.2.5. Because the pressure drop must be as little as possible across the baffles, it was decided to install a baffle where the coefficients of α and β of Equation (4-5) are 1.5555 and 1 respectively.

It can be seen from Figure 5-31 that the recirculation zone above the bullnose is much smaller than the case where no baffle was used. There are no high velocities areas as were indicated in the circles illustrated in Figure 5-27 and Figure 5-28.

The particle trajectories for 100μm and 10μm particles are illustrated in Figure 5-32 and Figure 5-33 respectively. The different sizes particles follow almost the same trajectories in the upper boiler, with the 100μm particles flung outwards just a bit more than the 10μm particles. If these results are compared to Figure 4-14 and Figure 4-15, the case where no baffles were used, it can be seen that the flow is more uniform across the tube bank.

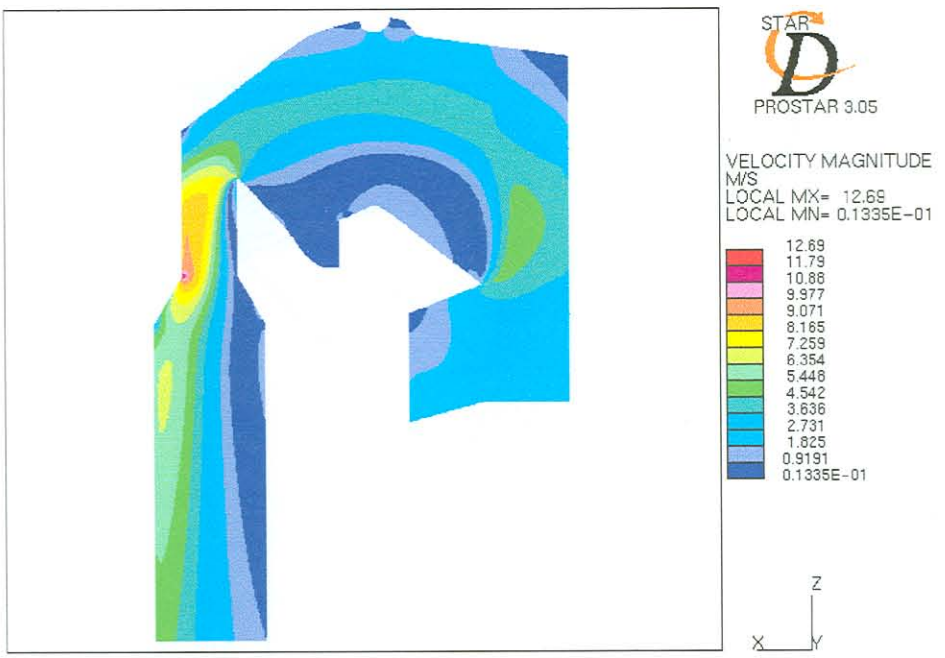

Figure 5-31 Velocity Magnitude Contour Plot with Permeable Baffle (2m.s^{-1} Inlet Velocity)

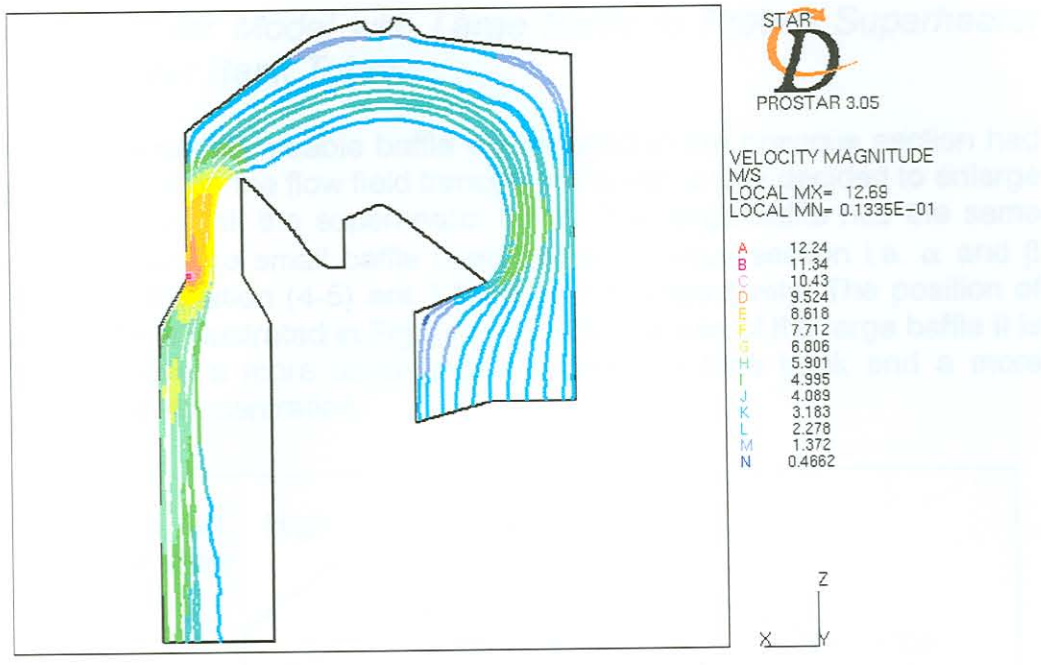

Figure 5-32 Particle Trajectories for 100μm Particles for Boiler Model with Permeable Baffle

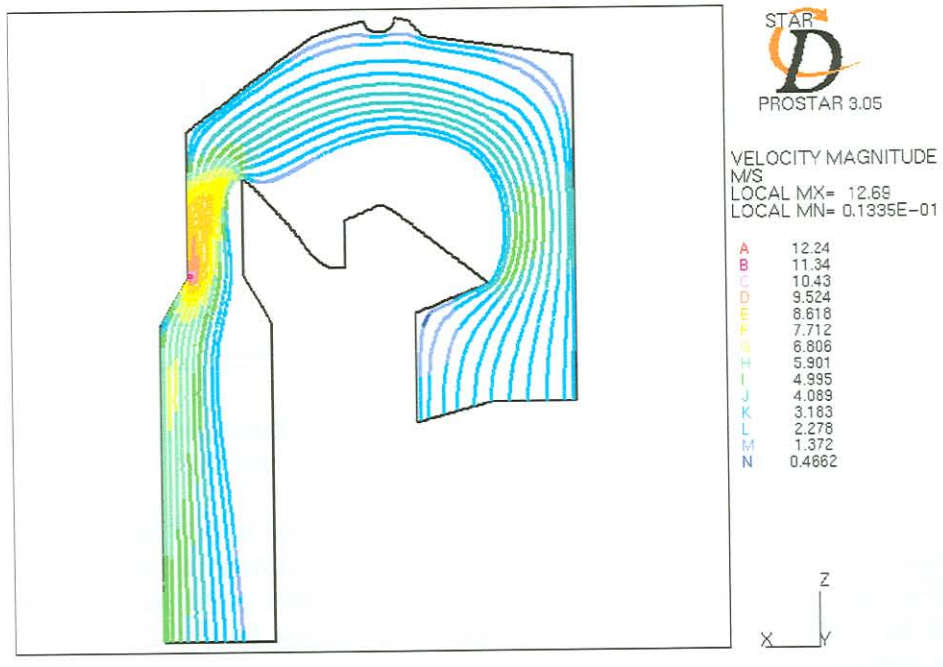

Figure 5-33 Particle Trajectories for 10μm Particles for Boiler Model with Permeable Baffle

5.3.3 2D Boiler Model with Large Baffle to Protect Superheater and Boiler Bank Tubes

Although the small permeable baffle investigated in the previous section had the desired effect on the flow field through the boiler, it was decided to enlarge the baffle to cover all the superheater tubes. The large baffle has the same permeability than the small baffle used in the previous section i.e. α and β coefficients of Equation (4-5) are 1.5555 and 1 respectively. The position of the large baffle is illustrated in Figure 5-34. With the use of the large baffle it is hoped to achieve a more uniform flow across the tube bank and a more uniform particle concentration.

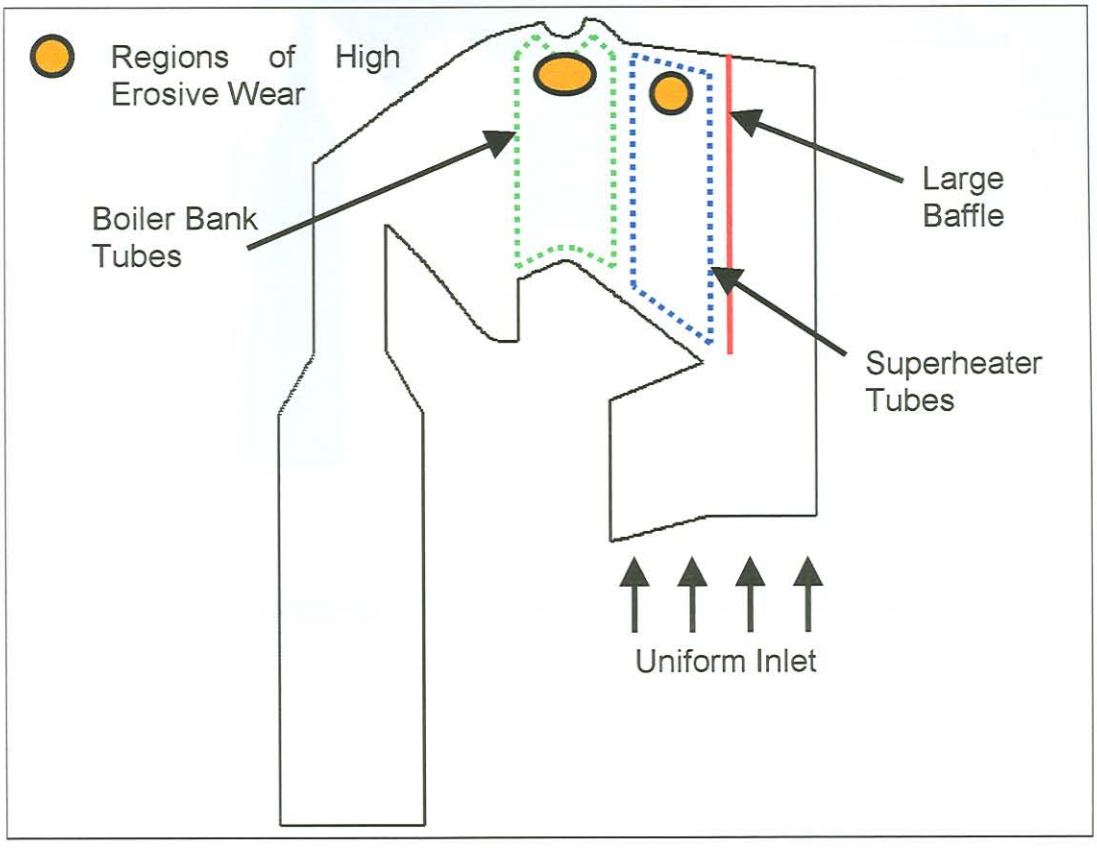

Figure 5-34 Schematic Diagram showing the Position of Tubes ,Large Baffle and Regions of High Erosive Wear in the Upper Boiler

The results that follow are the results where a large baffle is used in the CFD boiler model to combat boiler tube erosion. The results are also compared to the results where the effect of the tube bank is included in the CFD boiler model. The CFD analysis is then repeated with only the effect of the tube bank included in the CFD model. This is done to see whether the baffle is effective. Although it was concluded in Chapter 4 that the usage of porous cells, to model the effect of the tube bank, was not reliable at this stage, it was decided to see what effect the tube bank has on boiler flows. This is done because the screens as well as the tube bank are a resistance to flow in the tube bank, and both cause a pressure to drop across these devices.

Figure 5-35 shows the velocity magnitude contour plot where the large baffle is included in the CFD boiler model. If this velocity field is compared to Figure 5-31, the case where the small permeable baffle was used, it can be seen that there is not a large difference in the size of the recirculation zone above the bullnose. The recirculation zone for the case with the large permeable baffle is only a bit smaller than the case with the small permeable baffle.

Figure 5-35 Velocity Magnitude Contour Plot for Boiler Model with Large Baffle (2m.s^{-1} Inlet Velocity)

The following three figures show the particle traces for 100μm particles through the boiler for three different cases. Figure 5-36 illustrates the particle trajectories for the case where a large permeable baffle is included in the CFD model. Figure 5-37 illustrates the case where the large baffle is used, but this time the effect of the tube bank is included in the model through a porous section. To test the effectiveness of the baffle, Figure 5-38 illustrates the particle traces through the boiler with the effect of the tube bank included in the CFD model but with no baffle.

If the particle traces of Figure 5-36 are compared to Figure 5-32, it can be seen that the particles are similarly distributed across the tube bank. The small permeable baffle is far more effective than the large baffle because it has almost the same effect on particle trajectories but is much smaller and thus more cost effective to implement.

Figure 5-37 illustrates the particle traces where the effect of the tube bank is included in the CFD model together with the large baffle. It can be seen that the particles are distributed more uniformly across the tube bank than the CFD model where there is no tube bank in the model. To test the effectiveness of the large baffle, it was removed from the CFD model. Only the effect of the tube bank is included in the CFD model. The particle trajectories are shown in Figure 5-38 for this case. The particles are flung outwards towards the top of the boiler more than was the case where the large baffle was included in the model. It can thus be concluded that this baffle will distribute 100μm particles more uniformly across the tube bank whether the effect of the tube bank is included in the CFD model or not.

Figure 5-36 Particle Trajectories of 100μm Particles for Boiler Models with Large Baffle

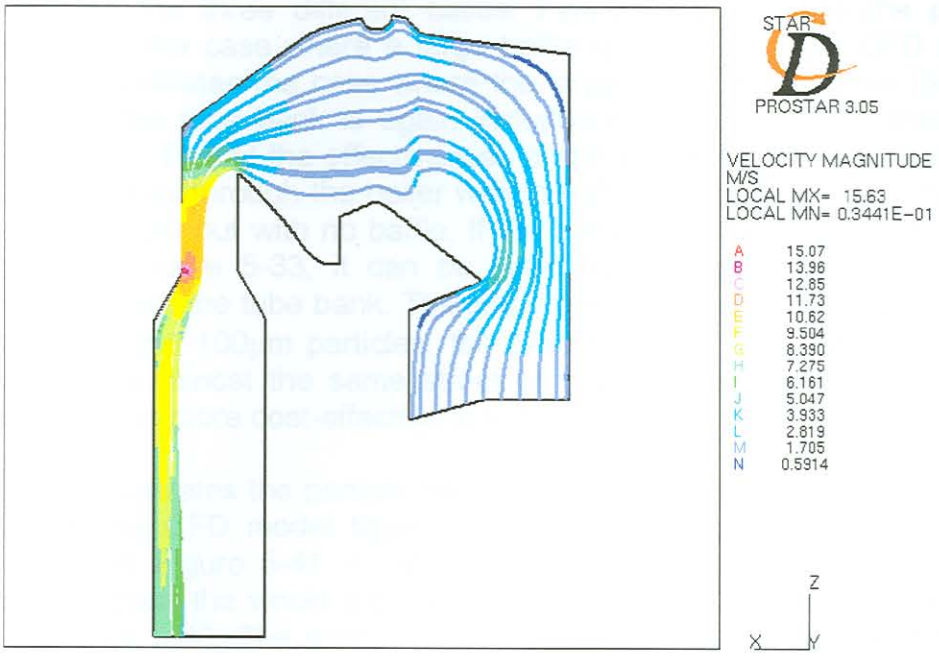

Figure 5-37 Particle Trajectories for 100μm Particles for Boiler Model with Large Particles – Effect of Boiler Bank Included in Model

Figure 5-38 Particle Trajectories of 100μm Particles with only the Effect of the Boiler Bank Included in the CFD Boiler Model

The following three figures show the particle traces for 10μm particles through the boiler for the three different cases. Figure 5-39 contains the particle trajectories for the case where a large baffle is included in the CFD model. Figure 5-40 illustrates the case where the large baffle is used, but this time the effect of the tube bank is again included in the CFD model through a porous section. To test the effectiveness of the baffle, Figure 5-41 illustrates the particle traces through the boiler with the effect of the tube bank included in the CFD model but with no baffle. If the particle traces of Figure 5-39 are compared to Figure 5-33, it can be seen that the particles are similarly distributed across the tube bank. The small permeable baffle is again, as was the case with the 100μm particles, far more effective than the large baffle, because it has almost the same effect on particle trajectories but is much smaller and thus more cost-effective to implement.

Figure 5-40 illustrates the particle traces where the effect of the tube bank is included in the CFD model together with the large baffle. If this result is compared with Figure 5-41, it can be seen that the particles are uniformly distributed across the whole tube bank in the crossflow direction as was the case in Figure 5-40. The major difference is in the size of the recirculation zone. When no large baffle is used, the recirculation zone is larger than the recirculation zone when a baffle is used. This will have an effect on superheater tube erosion because the superheater is just above the bullnose. It can thus be concluded that the large baffle will distribute 10μm particles more uniformly across the superheater tubes. The results are effective to obtain a uniform distribution across the superheater and tube bank whether the effect of the tube bank is either included or omitted in the CFD model.

Figure 5-39 Particle Trajectories of 10μm Particles for Boiler Model with Large Baffle

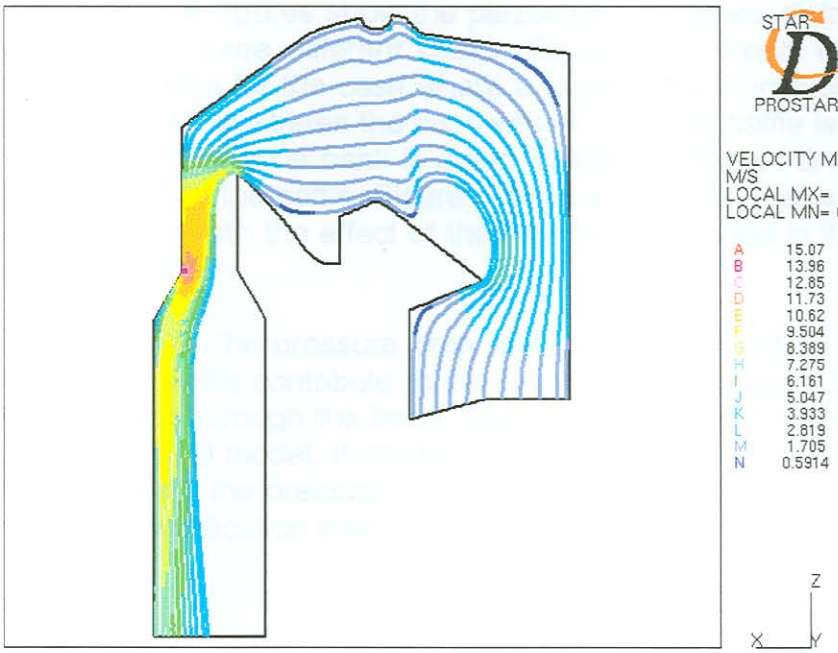

Figure 5-40 Particle Trajectories for 10μm Particles for Boiler Model with Large Particles – Effect of Boiler Bank Included in Model

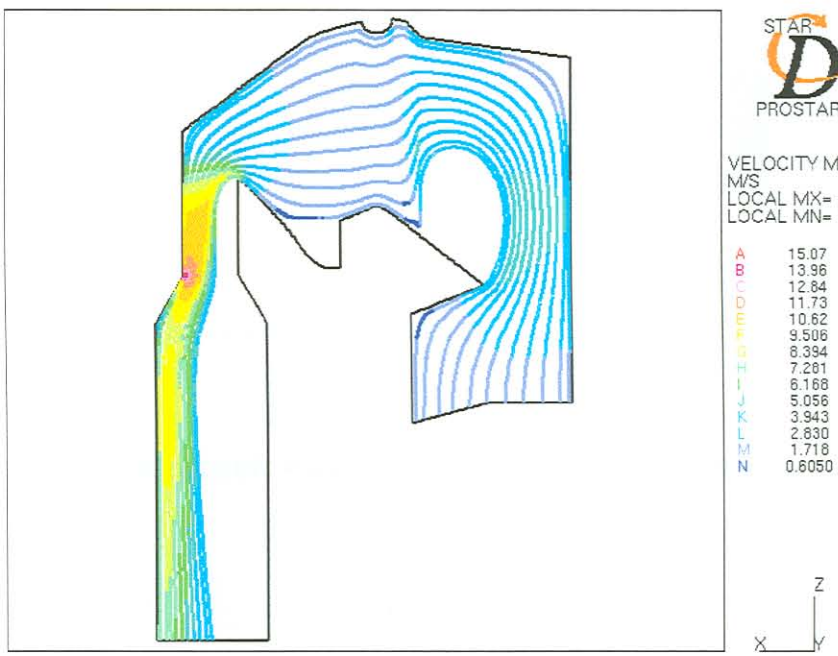

Figure 5-41 Particle Trajectories of 10μm Particles with only the Effect of the Boiler Bank Included in the CFD Boiler Model

The following three figures show the piezometric pressure distribution across the boiler for the three different cases. Figure 5-42 shows the piezometric pressure distribution for the case where a large baffle is included in the CFD model. Figure 5-43 illustrates the case where the large baffle is used, but this time the effect of the tube bank is again included in the CFD model. To test the effectiveness of the baffle, Figure 5-44 illustrates the pressure distribution through the boiler with the effect of the tube bank included in the CFD model but with no baffle.

Figure 5-43 shows the pressure drop across the boiler where both the tube bank and large baffle contribute to the pressure drop. Figure 5-44 illustrates the pressure drop through the boiler where only the effect of the tube bank is included in the CFD model. It can be seen from these results that the effect of the large baffle on the pressure drop is almost negligible even though it has desirable flow modification properties.

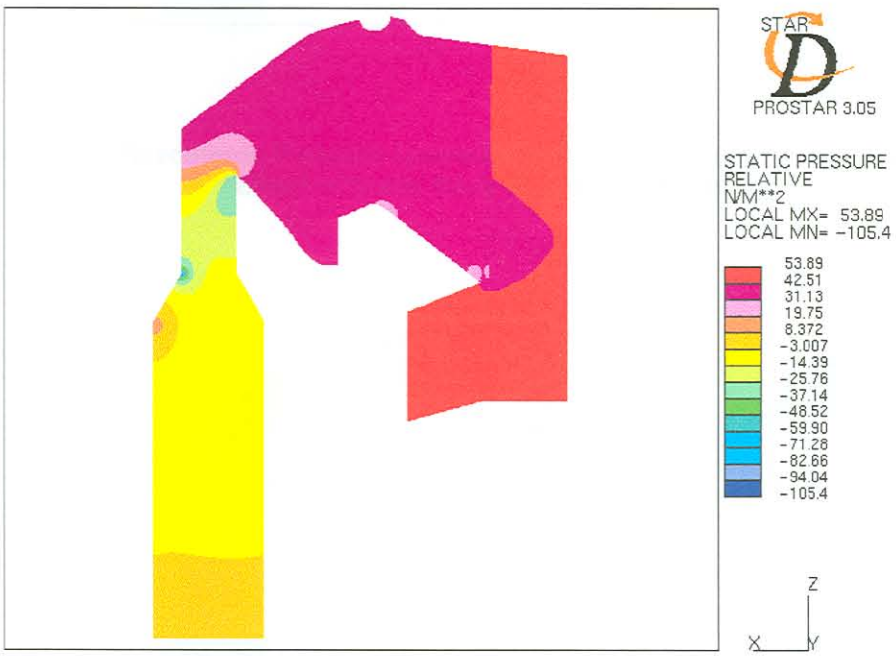

Figure 5-42 Piezometric Pressure Conrour Plot for Boiler Model with Large Baffle

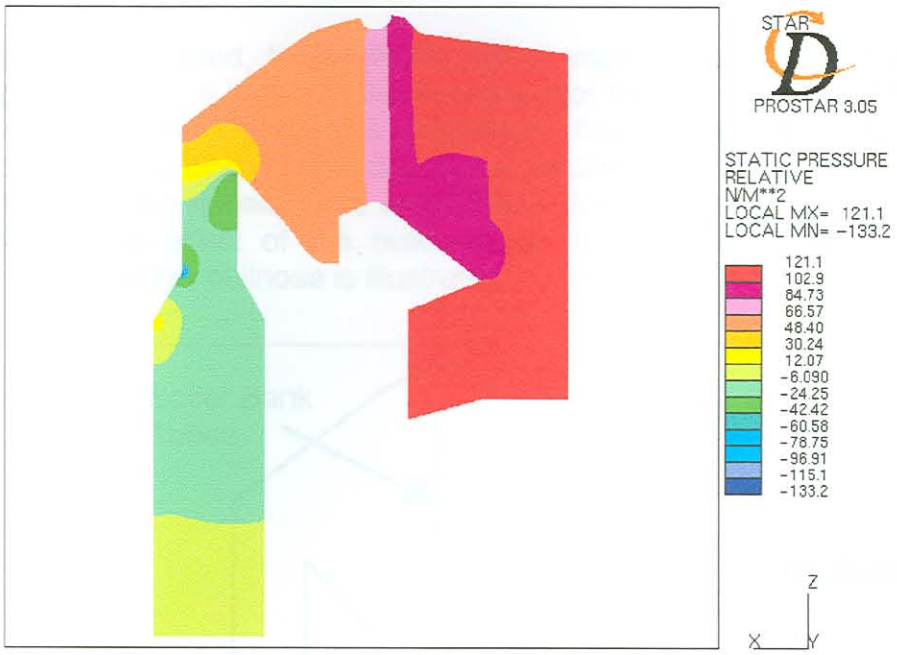

Figure 5-43 Piezometric Pressure Conrour Plot for Boiler Model with Large Baffle-Effect of Boiler Bank Included in Model

Figure 5-44 Piezometric Pressure Contour Plot with only the Effect of the Boiler Bank Included in the CFD Boiler Model

5.3.4 Removal of the Bullnose

As already discussed, the bullnose has a major effect on the flow pattern through the boiler. It is due to the bullnose that there is channelled flow in the top section of the boiler. This channelled flow is the main contributor to erosion in the top of the boiler due to the resulting high velocities and particle concentration. To remedy tube degradation due to erosion, it was decided to investigate the effect of the bullnose by removing it. The computational domain without the bullnose is illustrated in Figure 5-45.

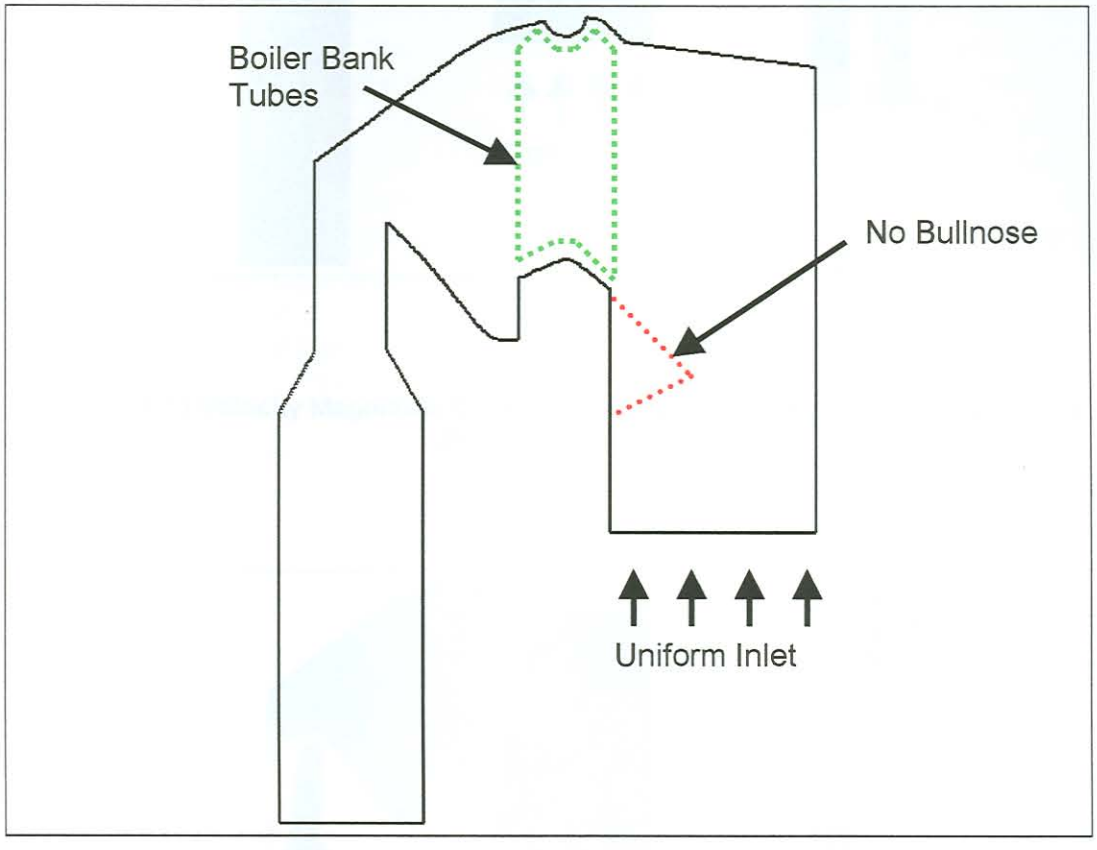

Figure 5-45 Computational Domain for Boiler Geometry without Bullnose

From the velocity magnitude plot in Figure 5-46, it can be seen that there exists no channelled flow in the top of the boiler. There is, however, a large dead volume section in the top right-hand corner of the boiler that was much smaller when the bullnose was included in the boiler CFD model.

Figure 5-47 shows the velocity magnitude contour plot where the effect of the tube bank is included in the CFD model. Although there are some concerns about the reliability of the porosity of the tube bank in the CFD model, as discussed in Chapter 4, it gives an indication of the effect of the tube bank on boiler flows. It can be seen that the dead volume section in the top right-hand corner of the boiler is almost the same as was the case in Figure 5-46 where the effect of the tube bank was not included in the model. The flow across the tube bank is much more uniform than the case where no tube bank was modelled.

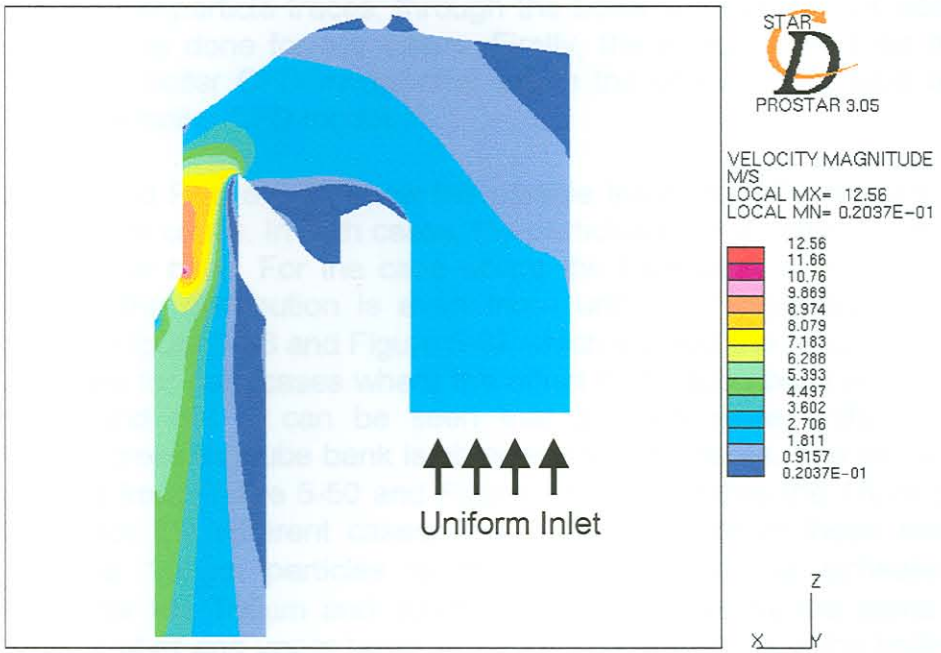

Figure 5-46 Velocity Magnitude Contour Plot of Boiler Geometry without Bullnose ($2m.s^{-1}$ Inlet Velocity)

Figure 5-47 Velocity Magnitude Contour Plot of Boiler Geometry without Bullnose. The Effect of the Boiler Bank Included in CFD Boiler Model ($2m.s^{-1}$ Inlet Velocity).

Again, when the particle traces, through the boiler without the bull nose, are investigated, it is done for two cases. Firstly, the effect of the tube bank is omitted in the boiler CFD model after which the effect of the tube bank is included in the boiler CFD model.

Figure 5-48 and Figure 5-49 show the particle traces for 100μm particles for the two different cases. In both cases, the particles have a uniform distribution across the tube bank. For the case where the tube bank is included in the CFD model, the distribution is even more uniform. These results can be compared to Figure 5-36 and Figure 5-37 which showed the results for 100μm particle traces for both cases where the effect of the tube bank is included in the model and not. It can be seen that a much more uniform particle distribution across the tube bank is obtained for both cases. The same trends are obtained from Figure 5-50 and Figure 5-51 that shows the 10μm particle trajectories for the different cases. The only difference in these results to those of the 100μm particles is the trajectories in the airheater. The trajectories for the 100μm and 10μm particles are exactly the same in the radiation chamber and upper boiler when there is a bullnose in the boiler.

With the removal of the bullnose in the boiler, channelled flow in the top of the boiler is eliminated. The distribution of all size particles is uniform across the tube bank. Erosion will be minimised considerably if the bullnose could be removed from the boiler because there are no regions of high velocity and high particle concentration in the upper boiler. The removal of the bullnose will have great cost implications but could prove viable in the long run. As screens can be used to minimise localised boiler tube erosion, at the fraction of the cost, the removal of the bullnose it is recommended as a remedial measure only if the other remedial measures fail to combat tube erosion effectively. The main reason for the existence of the bullnose, as mentioned in Chapter 3, namely the shielding of the tube bank and superheater from furnace radiation, should also be kept in mind when suggesting such major re-designs.

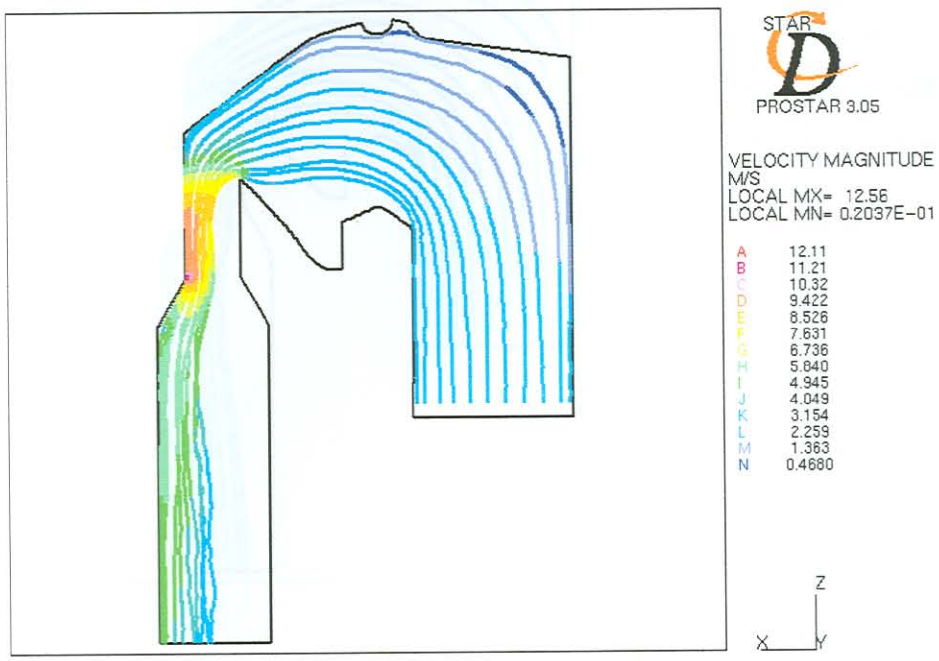

Figure 5-48 Particle Trajectories of 100μm Particles for Boiler Geometry without Bullnose

Figure 5-49 Particle Trajectories of 100μm Particles for Boiler Geometry without Bullnose. The Effect of the Boiler Bank Included in CFD Boiler Model.

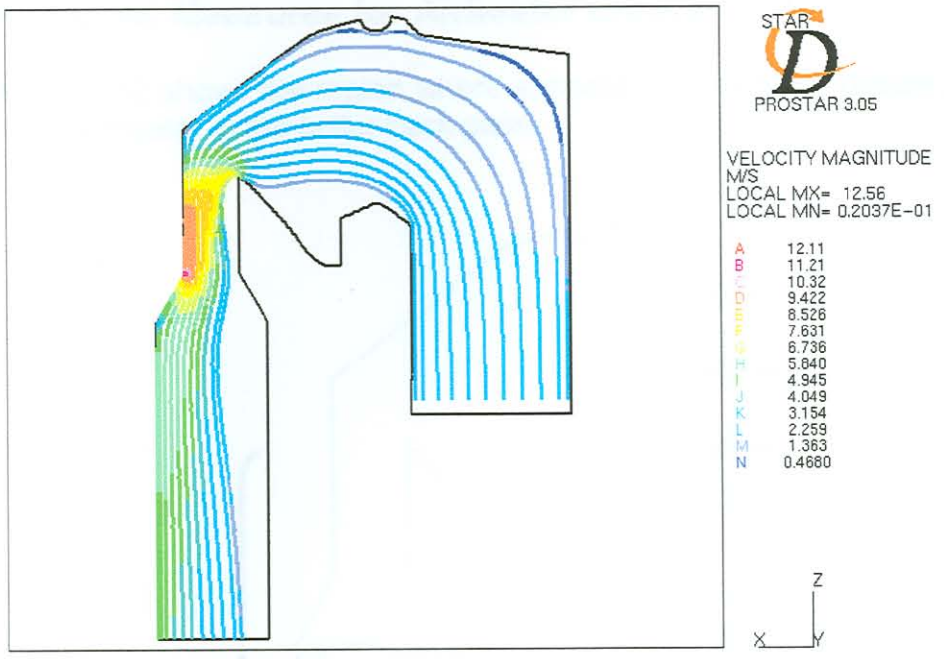

Figure 5-50 Particle Trajectories of 10μm Particles for Boiler Geometry without Bulnose

Figure 5-51 Particle Trajectories of 10μm Particles for Boiler Geometry without Bulnose. The Effect of the Boiler Bank Included in CFD Boiler Model

5.4 Remedial Measures for Airheater Erosion

The Figure 5-52 shows the region where airheater tube erosion occurs at the inlet of the airheater in the boiler back pass.

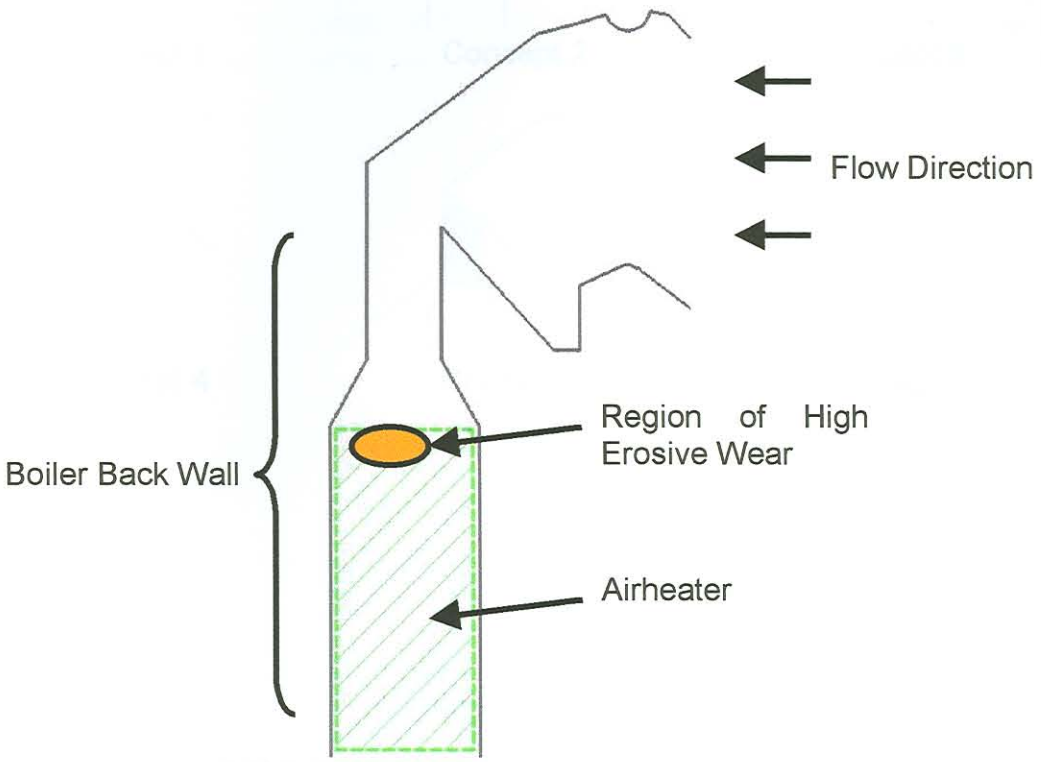

Figure 5-52 Diagram showing Regions of High Erosive Wear in the Airheater

Again it is believed that a skewed velocity field distribution and high particle concentration are the main contributors to erosion in the boiler back pass. The particles are flung against the boiler back wall due to centrifugal forces. The location of the boiler back wall can be seen in Figure 5-52. The rest of this section describes two concepts to successfully alleviate airheater tube erosion. Seven different concepts were investigated to reduce tube degradation due to particle erosion in the boiler back pass of which the two best concepts are discussed in the main text while the other less successful concepts are discussed in detail in Appendix C. All these concepts involve flow-modification approaches. Figure 5-53 illustrates the different flow modifying concepts of which Concepts 6 and 7 are the most successful ones to reduce airheater tube erosion. The effect of the tube bank is not modelled in this comparative investigation because the flow in the boiler back pass shows very similar tendencies due to the flow turning. This can be seen by comparing the particle trajectories in Figure 4-12 and Figure 4-13 for 10μm and 100μm particles respectively where no tube bank was modelled, to Figure 4-45 and Figure 4-46 respectively, where the effect of the tube bank is included in the CFD model.

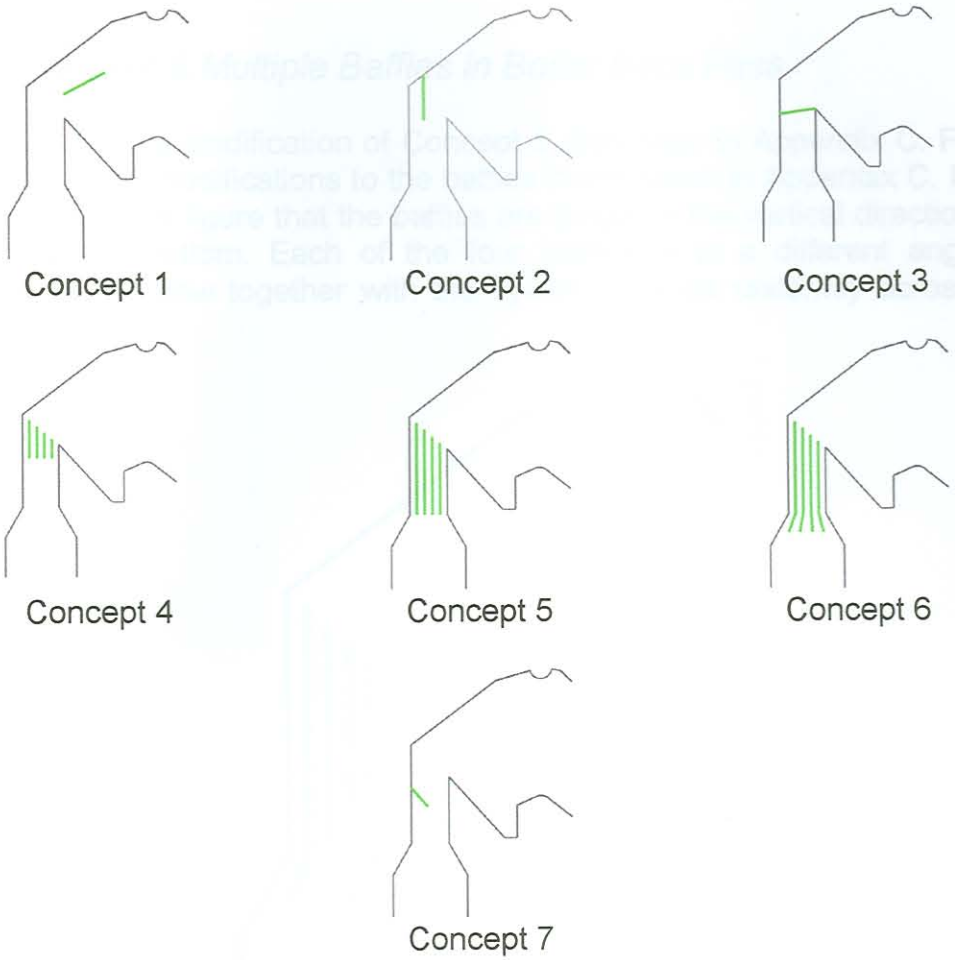

Figure 5-53 Different Concepts to Alleviate Airheater Erosion

The boiler can still be operational after an airheater tube failure because there is gas on both sides of the airheater tubes. The pressure difference between the gas phases is not so high that it can lead to other problems within the boiler. It is thus not critical if these tubes fail contrary to the case where there is water or steam under high pressure in the tubes, such as the superheater and tube bank tubes. If these tubes fail the boiler must be shut down. It is, nevertheless, still important to find remedial measures for these tube failures as continuous tube degradation can lead to major failures across the entire airheater in the long run which can severely affect boiler operational integrity.

5.4.1 Concept 6:Multiple Baffles in Boiler Back Pass

This concept is a modification of Concept 5 discussed in Appendix C. Figure 5-54 shows the modifications to the baffles investigated in Appendix C. It can be seen from this figure that the baffles are longer in the vertical direction but angled at the bottom. Each of the four baffles is at a different angle to redistribute the flow together with the fly-ash particles uniformly across the airheater.

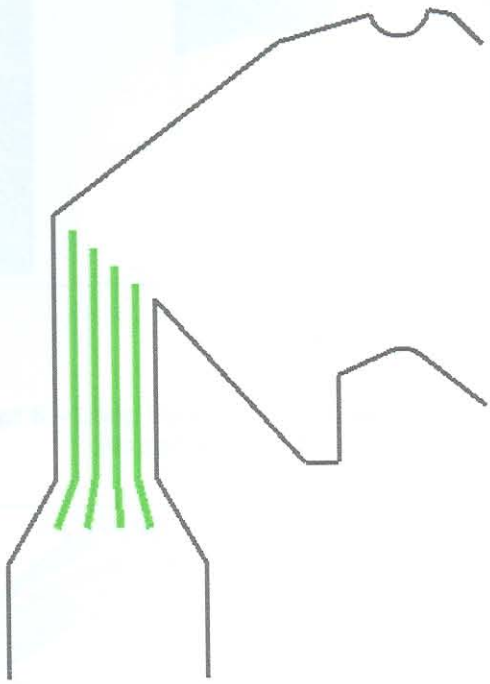

Figure 5-54 Concept 6: Location of Multiple Baffles in Boiler Back Pass – Modification to Concept 5

The velocity magnitude contour plot can be seen in Figure 5-55 for this concept. The maximum velocity in the flow domain increased by 3% from the results obtained in Concept 5 in Appendix C, but the particles are distributed more uniform across the airheater. Refer to Figure 5-56 and Figure 5-57 for the particle trajectories for this flow-modifying concept for 100μm and 10μm particles respectively.

Figure 5-55 Concept 6 – Long Vertical Baffles Angled at the Bottom: Velocity Magnitude Contour Plot

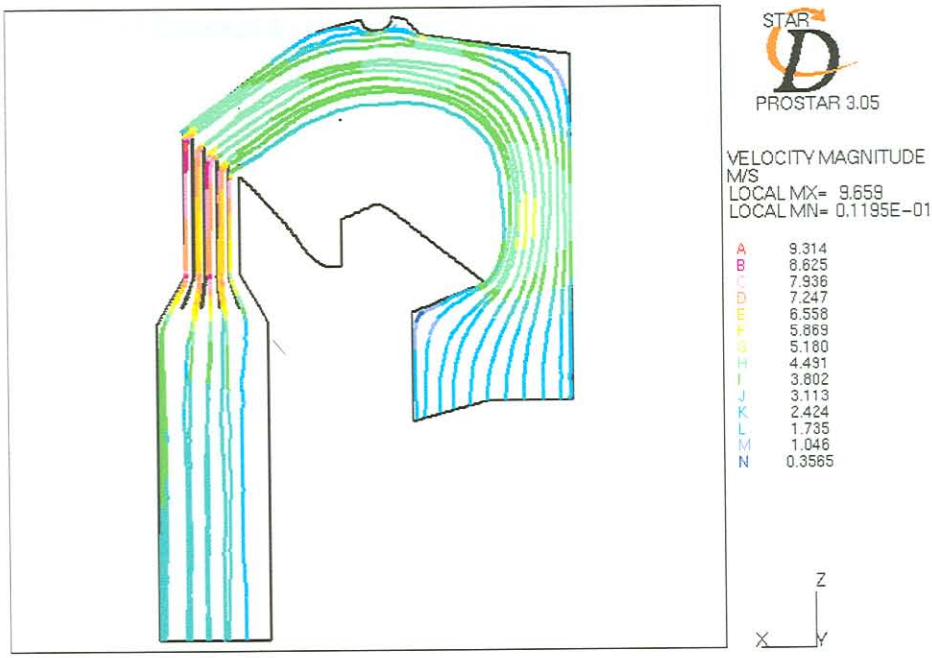

Figure 5-56 Concept 6 - Long Vertical Baffles Angled at the Bottom: Particle Trajectories of 100μm Particles

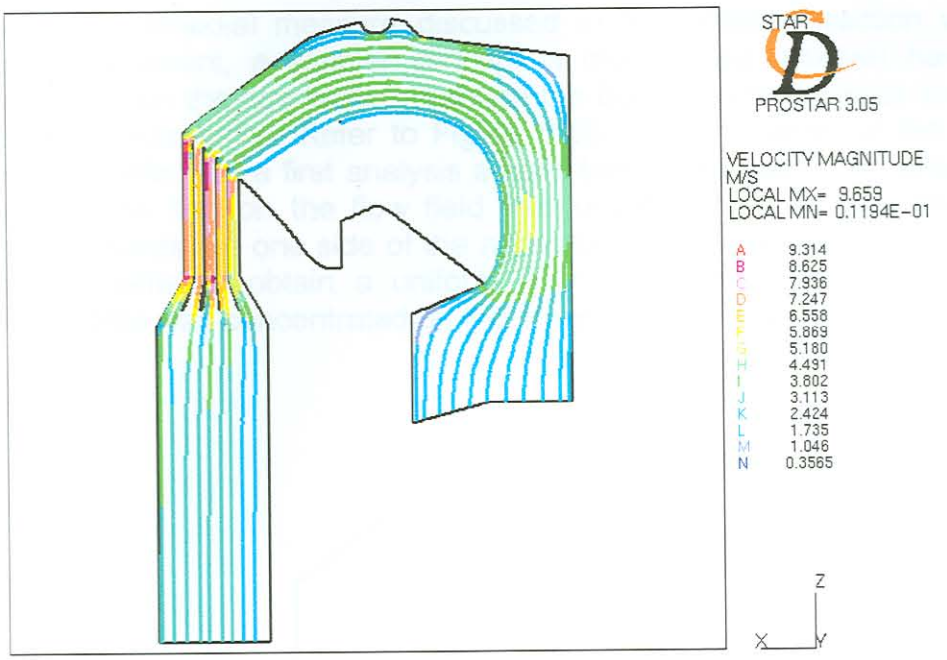

Figure 5-57 Concept 6 - Long Vertical Baffles Angled at the Bottom: Particle Trajectories of 10μm Particles

5.4.2 Concept 7: Permeable Baffle to Deflect the Flow

Because the remedial measure discussed in the previous section will be costly to implement, a simpler concept is investigated that will have the desired effect on the flow pattern through the boiler. It was decided to use a single permeable baffle. Refer to Figure 5-58 for the location of the single permeable baffle. For a first analysis a solid baffle was used. The effect that the solid baffle had on the flow field was unsatisfactory. All the flow was deflected towards the one side of the airheater. It was then decided to use a permeable baffle to obtain a uniform flow distribution, because the flow without a baffle was concentrated on the other side of the airheater.

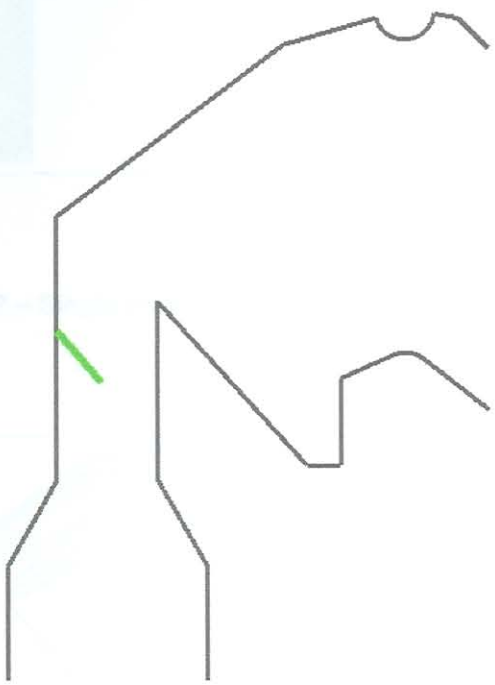

Figure 5-58 Concept 7: Solid Baffle to Deflect the Flow

It can be seen from Figure 5-59 that the maximum velocity in the flow domain is 8.127m.s^{-1}, which is a 32% decrease from the case where no flow-modifying approaches are used, which is illustrated in Figure 5-27. The region of high peak velocity is above the baffle but is dissipated before the flow interacts with the airheater tubes.

Figure 5-60 and Figure 5-61 illustrates the particle trajectories for 100μm and 10μm particles respectively. It is evident that the particles are distributed approximately uniformly across the airheater, especially in the 10μm case.

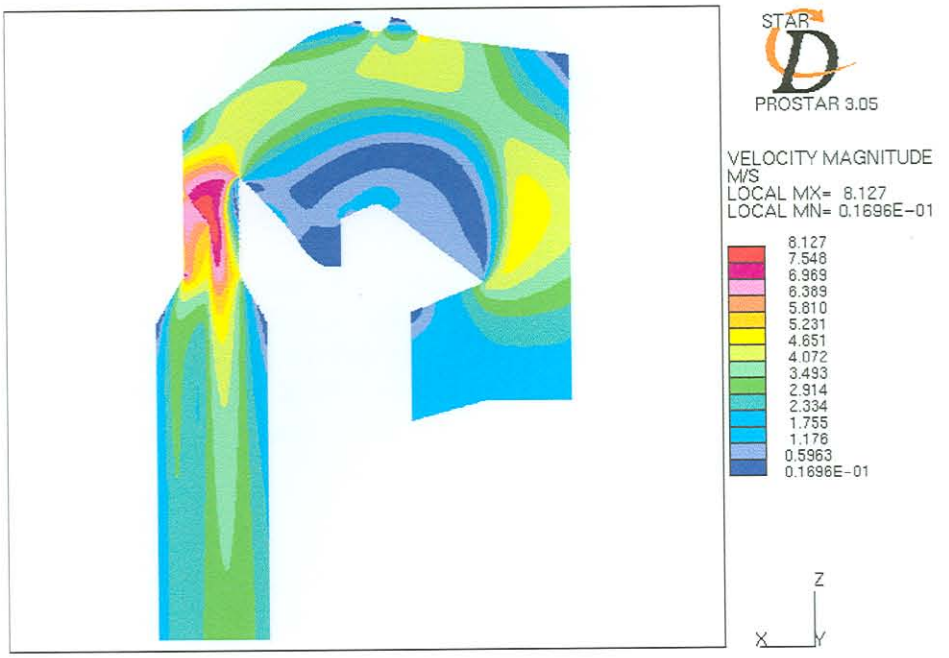

Figure 5-59 Concept 7 – Single Permeable Baffle: Velocity Magnitude Contour Plot

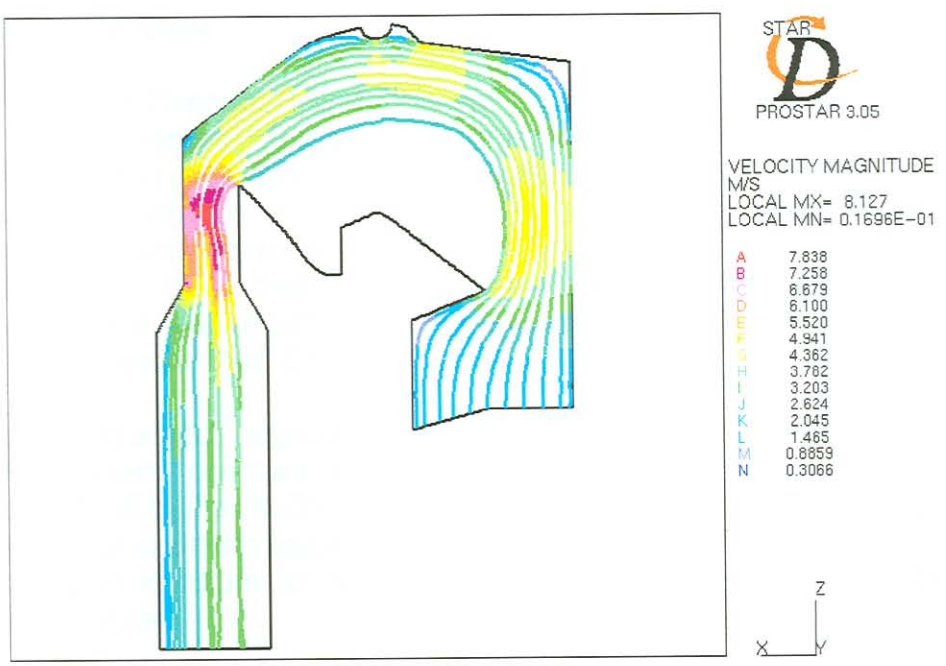

Figure 5-60 Concept 7 – Single Permeable Baffle: Particle Trajectories of 100μm Particles

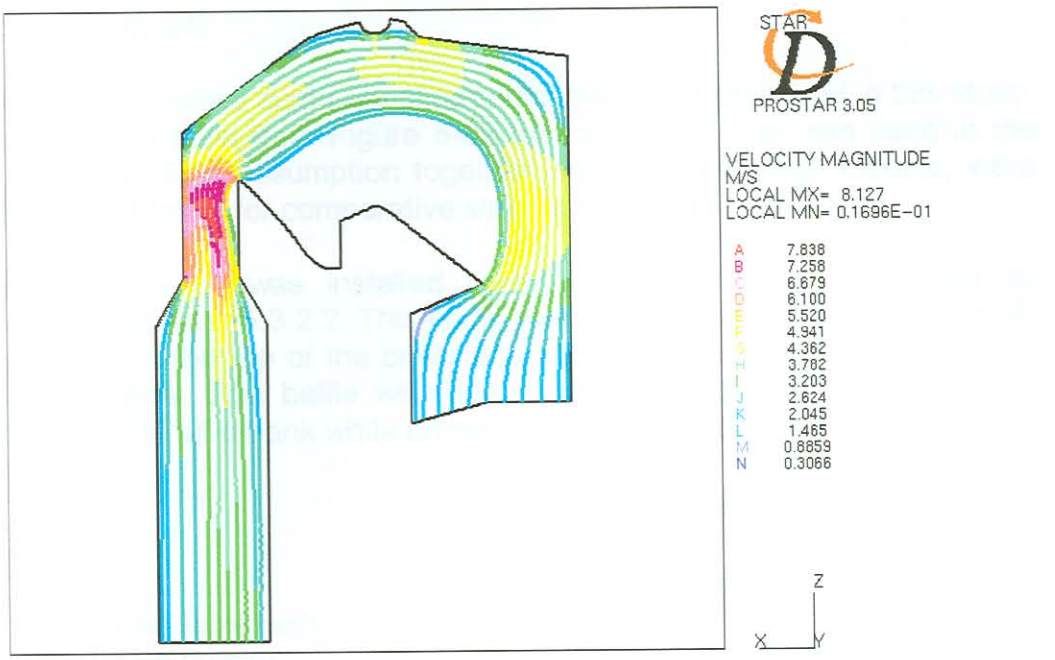

Figure 5-61 Concept 7 – Single Permeable Baffle: Particle Trajectories of 10μm Particles

5.4.3 Conclusion

The results of Concept 6 and Concept 7 investigated are both promising in obtaining permanent remedial measures for airheater tube erosion in the boiler back pass. Only one permeable baffle was used in Concept 7 whereas four large baffles with a more complex geometry were used in Concept 6. Both the concepts have essentially the same effect on the flow field through the airheater. It is therefore recommended that Concept 7 must be implemented to reduce airheater tube erosion because it is much simpler and more cost effective than Concept 6.

It must be stressed, however, that the concepts were arbitrarily chosen and do not present optimum solutions. As there are numerous parameters influencing the baffles such as permeability, size and location, it will be difficult to obtain real optimum solutions by trial-and-error. Mathematical optimisation can be used in future to optimise the baffle used in Concept 7 to obtain optimum results.

5.5 Conclusion

Figure 5-62 contains a summary of remedial measures proposed in this study. Firstly it can be seen from Figure 5-62 that a uniform inlet was used in the CFD analyses. This assumption together with the use of 2D models, were found to be sufficient for comparative studies of remedial measures.

A permeable baffle was installed in front of the superheater tubes as discussed in Chapter 5.3.2.2. This baffle reduces channelled flow and particle concentration in the top of the boiler and contributes to a more uniform flow across the tubes. This baffle will reduce particle erosion at the top of the superheater and tube bank while enhancing heat transfer across these tubes.

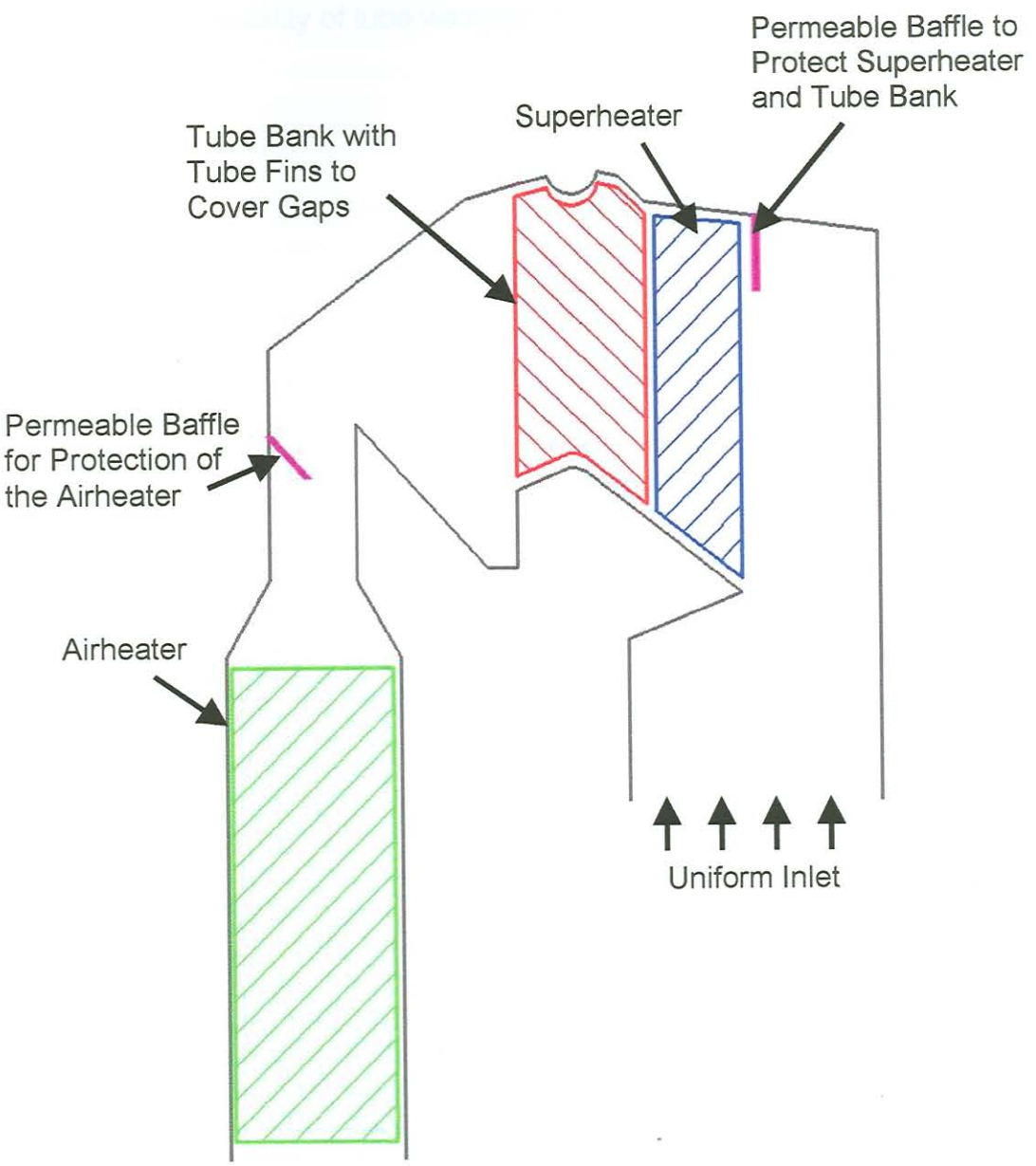

Figure 5-62 Summary of Remedial Measures for Boiler Tube Erosion

Because of the gaps in the tube bank the baffle could be ineffective to reduce erosion in those gaps. High erosion rates occur in regions adjacent to the larger than usual tube spacing because of channelling of the flow with a high particle concentration. As shown in Chaprter 5.2.4.2 tube fins must be installed, preferably on every second tube, to eliminate channelling of the flow that causes high peak velocities with high particle concentration of mainly small (in the region of 10μm) particles.

Airheater erosion, although not as critical as tube bank or superheater erosion, can be reduced by installing a permeable baffle, as indicated in the boiler back pass in Figure 5-62. This permeable baffle causes both the particle sizes considered to be more uniformly spaced across the airheater. If this baffle is not installed, the fly-ash concentration is high near the boiler back wall with a possibility of tube wastage in that region.

6 Conclusion

6.1 Boiler CFD Model Simplification

It is evident from Chapter 4 that great simplifications can be made to CFD boiler models. It was observed from CFD analyses that different inlet geometries did not significantly influence the flow patterns in the upper boiler and boiler back pass. Both a uniform inlet geometry below the bullnose and the inlet through the actual location of the burners were considered. The location of high peak velocities, recirculation zones, and particle concentration were approximately the same for the different cases. Because combustion in boiler environments is very complex and expensive to simulate in CFD, great simplifications can be made regarding inlet geometry and grid size because the flow pattern in the upper boiler is approximately the same for the different cases due to channelled flow forced by the bullnose when excluding the burner region and including it.

Another great simplification that can be made to CFD boiler models is the fact that 2D boiler models can be used to great effect to determine the flow field through the boiler. This is especially true for quantitative results to obtain regions of high peak velocity and particle concentration. The flow field will only differ near the boiler side walls as determined by other researchers. 2D models can therefore be used near the centre section of the boiler with symmetrical boundaries on both sides. Boiler CFD models can therefore be greatly simplified for erosion studies in the centre of the boiler through the use of 2D models.

Because of the fine-scale grid needed to model boiler internals such as the airheater and tube bank, it is necessary to 'replace' the boiler internals with porous cells with the same pressure drop versus velocity characteristics. After constructing a detailed hydraulic model of the tube bank, the pressure drop versus velocity characteristics of the tube bank were determined. These results did not exhibit good correlation with experimental results published by another author. The numerical results from this study under-predict the pressure drop with respect to the experimental correlations by a factor of five. The CFD model was also very unstable and the velocity field was not realistic at the inlet of the tube bank due to the directional properties of the porous cells. It was therefore decided to omit the effect of the tube bank in the overall CFD boiler models. However, the effect of the boiler bank was included in some CFD analyses for reasons of comparison. This was only done on a quantitative basis for the identification of global trends, such as the influence of the tube bank on particle trajectories through the boiler. The scope for future work in this field is the determination of more reliable porosity coefficients for boiler internals. As CFD gives only guidelines, experimental research is necessary for the validation of the results in actual boilers. This can be done through cold flow boiler studies to determine flow parameters at certain pre-selected locations throughout the boiler.

6.2 Remedial Measures for Boiler Tube Failures

6.2.1 Erosion in the Centre of the Tube Bank

Tube fins can be used to cover larger than usual tube spacing in tube banks in order to eliminate the channelling of the flow in these larger than usual gaps. It is important that the flow-modifying devices do not shift the erosion to other areas. It was therefore necessary to install multiple tube fins across the whole tube bank in the larger than usual gap to prevent the flow from being deflected by fins onto adjacent tubes. Multiple fins were used because if only a few fins are used, channelling of the flow still occurs in the larger gaps and the flow is then deflected onto adjacent tubes by the fins. With multiple fins installed in the tube bank, the particles are distributed more evenly across the tube bank with lower local peak velocities. As flow velocity and particle concentration are major factors influencing particle erosion, erosion in the tube bank will therefore be decreased. For future work, the optimum number and size of tube fins can be determined through mathematical optimisation. Experimental verification of this work should also be conducted to check the inherent assumptions of the CFD model.

6.2.2 Erosion of Superheaters and Tube Bank at the Top of the Boiler

Tube erosion of the superheater and tube bank occur at the top of the boiler. This is due to channelling of the flow in the top of the boiler because of the influence the bullnose has of the flow field. The channelling is exacerbated even further due to the 180° turn the flow must follow through the boiler. Larger particles are also flung outwards towards the top of the boiler due to centrifugal forces. One effective remedial measure that can be used is to remove the bullnose completely from the boiler. As this will alleviate tube erosion in the top of the boiler due to the uniform flow across the tube bank after the removal of the bullnose. However, this method will be very expensive to implement because extensive boiler modifications will be necessary. As the bullnose shields the superheaters from furnace radiation other materials should probably be used for the superheater tubes which has further cost implications. The savings due to the reduced erosion will probably not justify the cost of boiler modification.

A much more cost-effective remedial measure is to install baffles in the boiler that will have the desired effect on the flow pattern through the boiler, i.e. a uniform flow across the superheaters and tube bank. A baffle that achieves this goal is a permeable baffle located just upstream of the superheaters at the top of the boiler. If a solid baffle is used, the flow is shifted downwards towards the middle of the superheaters and the tube bank with high flow velocities and a high particle concentration. This can lead to severe erosion in that area. A large permeable baffle, that covers the entire flow area from above the bullnose to the top of the boiler, was implemented in the CFD model. There are no major differences in the flow field when the small permeable or large baffle is used. The small baffle therefore represents the

best solution because it would prove more cost effective. For future work, the optimum size, permeability, and location of the baffle can be determined through mathematical optimisation.

6.2.3 Airheater Erosion

As airheater tube failures do not influence boiler availability to a great extent, it is therefore not critical if such a tube fails. It was, nevertheless, decided to investigate different concepts to obtain remedial measures for airheater tube erosion. All the different concepts involve the usage of flow-modification devices such as solid or permeable baffles. The aim here is to again have uniform flow across the airheater. Some concepts proved to be ineffective, while others showed some promise, of which two stood out from the rest. The one successful concept entailed only the usage of one permeable baffle, which is installed at an angle of approximately 45° from the vertical datum. The other concept uses four large baffles with a relatively complex geometry. As both concepts of flow-modifying approaches have essentially the same effect on the flow field, the concept with only one baffle is more cost-effective due to its simplicity compared to the multiple baffle concept. For future work, the optimum location, size, permeability and, angle of the baffle can be obtained through mathematical optimisation, and verified by experimental comparison.

6.3 Future Work

- Some suggestions for future work were already made in this chapter. These suggestions include the determination of more reliable methods to determine porosity coefficients for hydraulic CFD models of tube banks and the implementation of these porosity coefficients in stable CFD models of boilers. Because reliable results could not be found during this research, future work is necessary. Other suggestions of the future work mentioned previously in this chapter concern remedial measures through the usage of baffles. Mathematical optimisation can be used to great effect in this regard to obtain optimum solutions, as the current method relied on trial-and–error CFD runs.

- A large relatively untouched field in this study is Lagrangian two-phase flow. As the presence of particles in fluids can alter the properties of the fluid, the vortices, for example, can behave differently in tube banks. As only quantitative results are appropriate in this study, it was not important to investigate the influence of particles on fluid behaviour, but there is definitely scope for further investigation into this field.

- Heat transfer was omitted in the CFD models in this study. As cold flow studies in actual boilers was used very successfully by other researchers to determine regions of high velocity in tube banks, it was deemed unnecessary to include heat transfer in the CFD model. As heat transfer is an integral part of boiler operation it can be included in future CFD models to investigate the effect of heat transfer in boiler flows.

References

1 J.F. Wendt (Ed.), Computational Fluid Dynamics, An Introduction, Springer-Verlag, Berlin,1992.

2 C.A.J. Fletcher, Computational Techniques for Fluid Dynamics, Volume 1, Second Edition, Springer-Verlag, Berlin, 1991.

3 STAR-CD, Version 3.05 manuals, Computational Dynamics Ltd., London, UK, 1998.

4 F.M. White, Viscous Fluid Flow, Second Edition, McGraw-Hill, New York, 1991.

5 T. Cebeci and A.M.O. Smith, Analysis of Turbulent Boundary Layers, Academic Press, New York, 1974.

6 E.R. Van Driest, On Turbulent Flow Near a Wall, *Journal of Aeronautical Sciences*, Vol. 23, 1956, pp. 1007-1011.

7 B. Baldwin and H. Lomax, Thin Layer Approximation and Algebraic Model for Separated Turbulent Flow, AIAA Paper 78-0257, AIAA 16th Aerospace Sciences Meeting, 1978.

8 M. Vinokur, On One-Dimensional Stretching Functions for Finite Difference Calculations, *Journal of Computational Physics*, Vol. 50, 1983.

9 C.A.J. Fletcher, Computational Techniques for Fluid Dynamics, Volume 2, Second Edition, Springer-Verlag, Berlin, 1991.

10 J.F. Thompson, Z.U.A. Warsi and C.W. Mastin, Numerical Grid Generation: Foundations and Applications, North-Holland, New York, 1985.

11 J.G. Singer, Combustion Fossil Power Systems, Third Edition, Combustion Engineering Inc., Windsor, 1981.

12 P.J. James, The Role of Non-Destructive Testing in the Control of Boiler Tube Failures, *Insight*, Vol. 37, No. 3, March 1995.

13 B. Dooley and W.P. McNaughton, Don't Let Those Boiler Tubes Fail Again, *Power Engineering*, June 1997, pp. 56-61.

14 J.P. Dimmer and R.B. Dooley, Maintaining Availability of Fossil Plants Through a Formalized Approach to Boiler Tube Failure Prevention, *Materials Evaluation*, Vol. 48, January 1990, pp.17-25.

15 P. Mayer, Boiler Tube Failure Mechanism Recognition – An Expert System, *CIM Bulletin*, Vol. 83, No. 939, July 1990, pp. 92-95.

16 C. Jones, Tube Maintenance Extends Boiler Service Life and Reduces Outages, *Pulp & Paper*, July 1988, pp. 150-152.

17 B. Dooley, A Vision for Reducing Boiler Tube Failures, *Power Engineering*, March 1992, pp.33-37.

18 J. Colannino, Prevent Boiler Tube Failures. Part 1: Fire-Side Mechanisms, *Chemical Engineering Progress*, October 1993, pp. 33-36.

19 I.M. Hutchings, The Erosion of Materials by Liquid Flow, The Materials Technology Institute of the Chemical Process Industries, Inc., Columbus, 1986.

20 D.M. Rishel, F.S. Pettit, and N. Birks, Some Principal Mechanisms in the Simultaneous Erosion and Corrosion Attack of Metals at High Temperatures, *Materials Science and Engineering*, Vol. A143, 1991, pp. 197-211.

21 D.M. Rishel, F.S. Pettit, and N. Birks, Spalling Types and Mechanisms in the Erosion-Corrosion of Metals at High Temperature, *Corrosion Science*, Vol. 35, Nos 5-8 , 1993, pp. 1007-1013.

22 A.V. Levy, The Erosion-Corrosion of Tubing Steels in Combustion Boiler Environments, *Corrosion Science*, Vol. 35, Nos 5-8, 1993, pp. 1035-1043.

23 M. Suckling and C. Allen, Critical Variables in High Temperature Erosive Wear, *Wear,* Vol. 203-204, 1997, pp. 528-536.

24 Y. Shida and H. Fujikawa, Particle Erosion Behaviour of Boiler Tube Materials at Elevated Temperature, *Wear*, Vol. 103, 1985, pp. 281-296.

25 M. Suckling, High Temperature Erosive Wear of a Boiler Tube Steel, PhD Thesis, Department of Materials Engineering, University of Cape Town, November 1996.

26 E. Raask, Erosion Wear in Coal Utilization, Hemisphere Publishing Corporation, Washington, 1988.

27 Anon, Fireside Corrosion and Fly Ash Erosion in Boilers, Electric Power Research Institute, Final Report EPRI CS-5071, Project 2711-1, February 1987.

28 M. Suckling and C. Allen, The Design of an Apparatus to Test Wear of Boiler Tubes, *Wear*, Vol. 186-187, 1995, pp. 266-272.

29 R.B. Dooley and H.J. Westwood, Analysis and Prevention of Boiler Tube Failures, Canadian Electrical Association Research Report, 83/237G-31, November 1983.

30 E. Raask, Mineral Impurities in Coal Combustion, Hemisphere Publishing Corporation, Washington, 1985.

31 V. Scepanovic and R. Burelle, Boiler Tube Erosion Evaluation – Part 1, Canadian Electrical Association Research Report, CEA No. 218-G-408, March 1986.

32 P. Kratina, D. Speirs and J. McMillan, Hidden Factors in Boiler Gas-Side Erosion, Proceedings of the Symposium on Thermal Utilities Boiler Reliability, McMaster University, May 1983.

33 K. Anand, S.K. Hovis and H. Conrad, Flux Effects in Solid Particle Erosion, *Wear*, Vol. 118, 1987, pp. 243-257.

34 G. Grant and W. Tabakoff, Erosion Prediction in Turbomachinery Resulting from Environmental Solid Particles, *Journal of Aircraft*, Vol. 12, No. 5, May 1975, pp. 471-478.

35 J.Q. Sun, J.Q. Wang and S.B. Wan, Experimental Research on the Impact Erosion of Ash-Stream, *Two-Phase Flow and Heat Transfer: China-U.S. Progress*, May 1994, pp. 577-858.

36 W. Tabakoff and C. Balan, A Study of the Surface Deterioration due to Erosion, Transactions of the ASME: *Journal of Engineering for Power*, Vol. 105, October 1983, pp. 834-838.

37 A. Ninham, The Effect of Mechanical Properties on Erosion, *Wear*, Vol. 121, 1988, pp. 307-324.

38 G.P. Tilly and W. Sage, The Interaction of Particle and Material Behaviour in Erosion Processes, *Wear*, Vol. 16, 1970, pp. 447-465.

39 J. Fan, D. Zhou and K. Chen, An Investigation of Tube Erosion by Coal Ash Impaction in CFB Combustors, Third International Symposium of Gas-Solid Flows, San Diego, CA, July 1989.

40 W. Tabakoff, R. Kotwal and A. Hamed, Erosion Study of Different Materials Affected by Coal Ash Particles, *Wear*, Vol. 52, 1979, pp. 161-173.

41 S. Bahadur and R. Badruddin, Erodent Particle Characterization and the Effect of Particle Size and Shape on Erosion, *Wear*, Vol. 138, 1990, pp. 189-208.

42 D. Chen, M. Sarumi and S.T.S. Al-Hassani, Computational Mean Particle Erosion Model, *Wear*, Vol. 214, 1998, pp. 64-73.

43 L. Ambrosini and S. Bahadur, Erosion of AISI 4140 Steel, *Wear*, Vol. 117, 1987, pp. 37-48.

44 I.G. Wright, V.K. Sethi and A.J. Markworth, A Generalized Description of the Simultaneous Processes of Scale Growth by High-Temperature Oxidation and Removal by Erosive Impact, *Wear*, Vol. 186-187, 1995, pp. 230-237.

45 I.G. Wright, V.K. Sethi and V. Nagarajan, An Approach to Describing the Simultaneous Erosion and High Temperature Oxidation of Alloys, Transactions of the ASME: *Journal of Engineering for Gas Turbines and Power*, Vol. 113, October 1991, pp. 616-620.

46 J.J. Xie and P.M. Walsh, Erosion-Oxidation of Carbon Steel in the Convection Section of an Industrial Boiler Cofiring Coal-Water Fuel and Natural Gas, Transactions of the ASME*: Journal of Engineering for Gas Turbines and Power*, Vol. 119, July 1997, pp. 717-722.

47 E.J. Morgan-Warren, Thermal Spraying for Boiler Tube Protection, *Welding & Metal Fabrication*, Jan/Feb 1992, pp. 25-31.

48 J.Y. Tu, C.A.J. Fletcher and M. Behnia, Prediction of Flow and Erosion in Power Utility Boilers and Comparison with Measurement, Transactions of the ASME*: Journal of Engineering for Gas Turbines and Power*, Vol. 119, July 1997, pp. 709-717.

49 P. Kratina and J.F. Drennen, Convective Pass Erosion Control and Prevention in Utility and Industrial Boilers, International Conference on Boiler Tube Failures, EPRI, 1991.

50 Anon., Duplex Stainless Steel Alloy Proves to be Ally in Boiler Tube Maintenance, *Welding Journal*, November 1988, pp. 53-54.

51 V.H. Hidalgo, F.J.B. Varela and E.F. Rico, Erosion Wear and Mechanical Properties of Plasma-Sprayed Nickel- and Iron-Based Coatings Subjected to Service Conditions in Boilers*, Tribology International*, Vol. 30, 1997, pp. 641-649.

52 T. Nguyen, Heat Transfer Characteristics of SA-178 Boiler Tubes Covered with Erosion Resistance Coatings, *International Communications in Heat and Mass Transfer*, Vol. 19, 1992, pp. 817-825.

53 A.V. Levy and B. Wang, Erosion of Hard Material Coating Systems, *Wear*, Vol. 121, 1988, pp. 325-346.

54 H. Naoi, S. Araki and H. Yasuda, Development of High-Strength Ferritic Steel NF616 for Boiler Tubes, *Nippon Steel Technical Report*, No. 50, July 1991.

55 T. Takahashi, M. Kikuchi and H. Sakurai, Development of High-Strength 20Cr-25Ni (NF 709) Steel for USC Boiler Tubes, *Nippon Steel Technical Report*, No. 50, July 1991.

56 L. Oshinowo, D.C.S. Kuhn and M.E. Charles, Flow Modifying Screens Applied to Pulverized Coal-Fired Utility Boilers, EC-Vol. 3/FACT-Vol. 20, *Joint Power Generation Conference*, Vol. 1, ASME, 1995, pp. 121-129.

57 D.N. Robinette and D.P. Piccirillo, Soot Blower Control System Upgrade Provides Win/Win Opportunities, Proceedings of the 57th Annual American Power Conference, Part 2, Chicago, IL, 1995.

58 J.F. Unsworth, D.J. Barrat, D. Park and K.J. Titcher, Ash Formation During Pulverized Coal Combustion: 2. The Significance of Crystalline Anorthite in Boiler Deposits, *Fuel*, Vol. 67, May 1988, pp. 632-641.

59 B. Dooley, A Vision for Reducing Boiler Tube Failures: Part II, *Power Engineering*, May 1992, pp. 41-42.

60 B. Gallman, A.C. Henderson and R.D. Huffman, Application of FPL's Quality Improvement Program to Reduce Tube Failures in a 400 MW Fossil Plant Boiler, Proceedings of the 53rd Annual Meeting of the American Power Conference, Chicago, IL, USA, April 1991, pp. 1363-1378.

61 H. Gonzalez and P.S. Chang, Boiler Tube Root Cause Analysis Advisory System, Proceedings of the 29th Southeastern Symposium on System Theory, Cookeville, Tennessee, March 1997.

62 R. Kumar, Boiler Tubes – Types of Failures – Reasons and Remedial Measures, *Electrical India*, December 1987.

63 M. Prager and S. Ibarra, Approaches to Long Term Life Prediction of Furnace and Boiler Tubes, PVP-Vol. 359, Fitness for Adverse Environments in Petroleum and Power Equipment, ASME, 1997.

64 K. Zarrabi, A Comparison of Several Boiler Tube Life Prediction Methods, *International Journal of Pressure Vessels. & Piping*, Vol. 58, 1994, pp. 167-201.

65 J.F. Drennen, P. Kratina and R.B. Dooley, Control and Prevention of Flyash Erosion, Power Generation Conference, Orlando, Florida, December 1988.

66 D.L. Black and M.Q. McQuay, Particle Size and Velocity Measurements in the Radiant Section of an Industrial-Scale, Coal-Fired Boiler: The Effect of Coal Type, HTD-Vol.328*, National Heat Transfer Conference*, Vol. 6, ASME, 1996, pp.19-27.

67 W.R. MacDonald, Boiler Tube Erosion Evaluation – Phase II, Canadian Electrical Association, CEA Project No. 218 G 408, March 1993.

68 J.F. Drennen, J.D. Bianca and P. Kratina, Outline of a Program to Control and Prevent Boiler Tube Failures from Fly Ash Erosion, International Conference on Boiler Tube Failures, EPRI, 1991.

69 B.V.R. Vittal and W. Tabakoff, Two-Phase Flow Around a Two Dimensional Cylinder, *AIAA Journal*, Vol. 25, No. 5, 1986, pp. 648-654.

70 S.A. Morsi and A.J. Alexander, An Investigation of Particle Trajectories in Two-Phase Flow Systems, *Journal of Fluid Mechanics*, Vol. 55, part 2, 1972, pp. 193-208.

71 F. Jianren, C.Lihua, Z. Xinyu and C. Kefa, Numerical Simulation of the Tube Erosion Resulted from Particles Impacts, *Chinese Journal of Chemical Engineering*, Vol. 5, No. 4, 1997, pp. 337-346.

72 F. Jianren, D. Zhou, Q. Hua and K. Cen, Numerical Computation of Particle-Laden Gas Flows Past Staggered Tube Banks Undergoing Erosion, *Powder Technology*, Vol. 80, 1994, pp. 1-10.

73 Y. Jun and W. Tabakoff, Numerical Simulation of a Dilute Particulate Flow (Laminar) Over Tube Banks, Transactions of the ASME: *Journal of Fluids Engineering*, Vol. 116, December 1994, pp. 770-777.

74 M. Fujii and T. Fujii, A Numerical Analysis of Laminar Flow and Heat Transfer of Air in an In-Line Tube Bank, *Numerical Heat Transfer*, Vol. 7, 1984, pp. 89-102.

75 D.S. Weaver and A. Abd-Rabbo, A Flow Visualization Study of a Square Array of Tubes in Water Crossflow, Transactions of the ASME: *Journal of Fluids Engineering*, Vol. 107, September 1985, pp.354-363.

76 M.J. Schuh, C.A. Schuler and J.A.C. Humphrey, Numerical Calculation of Particle-Laden Gas Flows Past Tubes, *AiChE Journal*, Vol. 35, No. 3, March 1989, pp. 466-480.

77 O. Prakash, S.N. Gupta and P. Misra, Newtonian and Inelastic Non-Newtonian Flow Across Tube Banks, *Industrial & Engineering. Chemistry. Research,* Vol. 26, 1987, pp. 1365-1372.

78 T. Nishimura, K. Itoh, K. Ohya and H. Miyashita, Experimental Validation of Numerical Analysis of Flow Across Tube Banks for Laminar Flow, *Journal of Chemical Engineering of Japan*, Vol. 24, No. 5, 1991, pp. 666-669.

79 T. Nishimura, H. Itoh and H. Miyashita, The Influence of Tube Layout on Flow and Mass Transfer Characteristics in Tube Banks in the Transitional Flow Regime, *International Journal of Heat and Mass Transfer*, Vol. 36, No. 3, 1993, pp. 553-563.

80 J.W. Baughn, M.J. Elderkin and A.A. McKillop, Heat Transfer from a Single Cylinder, Cylinder in Tandem, and Cylinders in the Entrance Region of a Tube Bank with Uniform Heat Flux, Transactions of the ASME: *Journal of Heat Transfer*, Vol. 108, May 1986, pp. 386-391.

81 S. Mereu and E. Sciubba, Parametric Study of Particle Distribution in Gas-Solid Flow over Multiple Tubes, Proceedings of the 1993 ASME Winter Meeting, New Orleans, LA, USA, 1993.

82 J. Fan , D. Zhou and K. Cen, An Investigation of Tube Erosion by Coal Ash Impaction, Third International Symposium of Gas-Solid Flows – 1989, San Diego, CA, USA, 1989.

83 S. Hsieh and D. Huang, Comparisons of Thermal Performance and Pressure Drop of Counterflow and Parallel-Flow Heat-Pipe Heat Exchangers with Aligned/Staggered Tube Rows, *Energy Conversion Management*, Vol. 30, No. 4, 1990, pp. 357-368.

84 D. Traub, Turbulent Heat Transfer and Pressure Drop in Plain Tube Bundles, *Chemical Engineering and Processing*, Vol. 28, 1990, pp. 173-181.

85 A. Zukauskas, Heat Transfer from Tubes in Crossflow, *Advances in Heat Transfer*, Vol. 8, 1972, pp.93-160.

86 T. Grace, A. Walsh and A. Jones, A Three-Dimensional Mathematical Model of the Kraft Recovery Furnace, 1989 International Chemical Recovery Conference: April 3-6 1989, The Skyline Ottawa, Ottawa, Ontario.

87 Y. Zhang and Z. Chen, The Effect of a Gap Between Layers on the Heat Transfer Performance of Aligned Tube banks, *Heat Transfer Engineering*, Vol. 13, No. 2, 1992, pp. 33-41.

88 J.Y. Tu and C.A.J. Fletcher, Numerical Modelling of Three-Dimensional Fly-Ash Flow in Power Utility Boilers, *International Journal for Numerical Methods in Fluids*, Vol. 24, 1997, pp. 787-807.

89 X.H. Shen, D.C.S. Kuhn and H.N. Tran, Simulation of Flue Gas Flow in the Upper Furnace of a Recovery Boiler, 80th Annual Meeting, Technical Section, CPPA, pp. B165-B168.

90 E.K. Vakkilainen, S. Nikkanen and J. Hautamaa, Flows in the Upper Region of Recovery Boilers, Advances in Chemical Recovery – AIChE Meeting, November 17-22, 1991.

91 E.K. Vakkilainen, T.N. Adams and R.R. Horton, The Effect of Recovery Furnace Bullnose Designs on Upper Furnace Flow and Temperature Profiles, 1992 International Chemical Recovery Conference, 1992, pp. 101-112.

92 Anon., Further Validation of STAR-CD for Coal Combustion, STAR-CD News, Issue 9, Spring 1999.

93 A.K. Gupta, Burner Geometry Effects on Flow and Combustion Characteristics in a Power Plant Boiler, Proceedings of the 1989 ASME International Computers in Engineering Conference and Exposition, New York, 1989.

94 F.P. Incropera and D.P. DeWitt, Fundamentals of Heat and Mass Transfer, 4th Edition, John Wiley & Sons, New York, 1996.

Appendices

Appendix A - Fly-Ash Particle Sizes

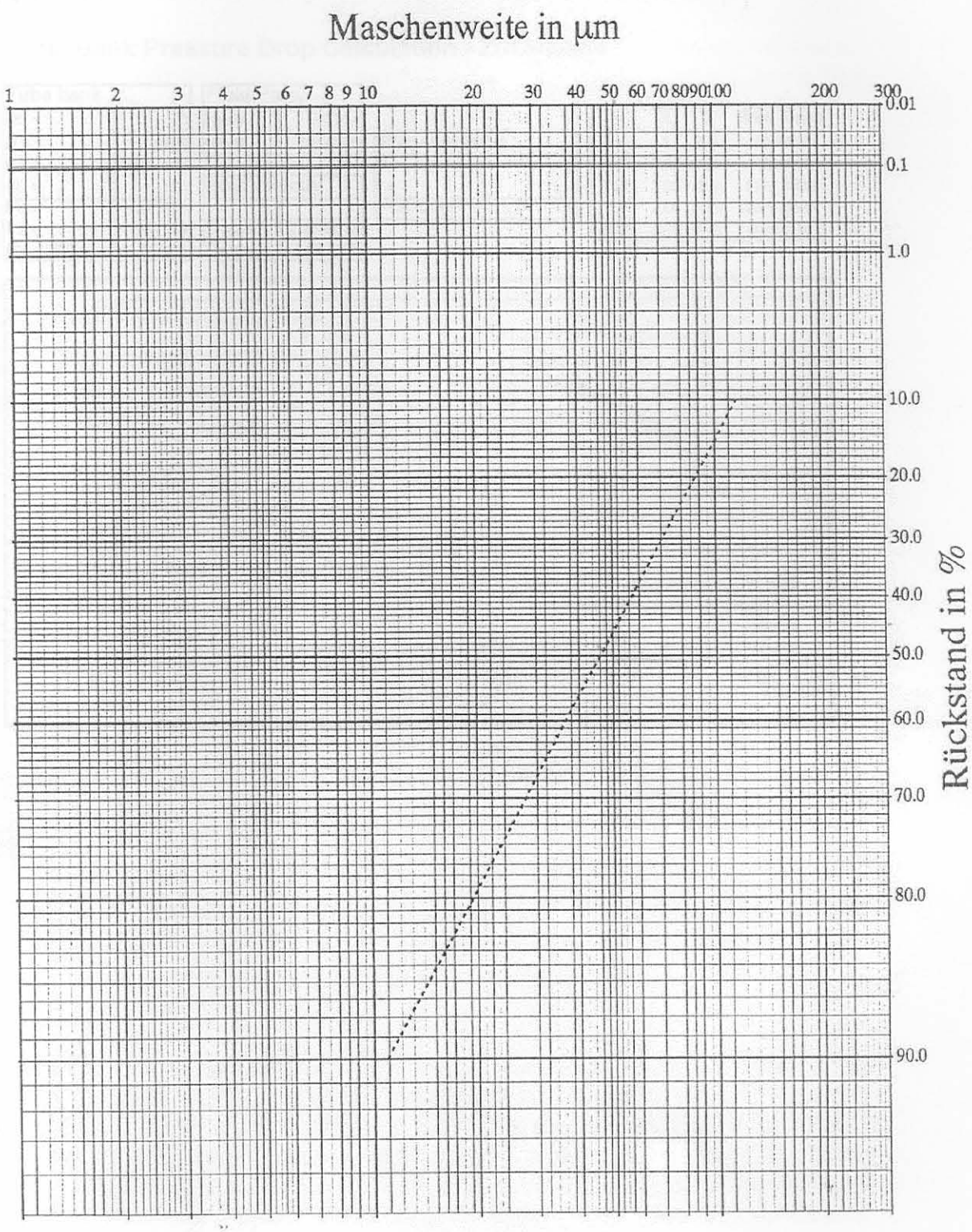

Appendix B - Tube Bank Pressure Drop Calculation

Tube Bank Pressure Drop Calculation - Zukauskas

Tube bank	
NL =	13
D =	88.9
ST =	150
SL =	120
PL =	1.349831
PT =	1.687289
(PL-1)(PT-1) =	0.240435

Fluid Prop.	
rho =	0.354
mu =	4.15E-05

Inlet Velocity	
v =	1
vmax=	2.4549918
Re =	1.86E+03

Pressure Drop	
X =	3
f =	0.4
Pres. Drop =	16.6417105

V	X	f	Pres Drop
1	3	0.4	16.6417
4	2.05	0.35	159.2057
10	2.05	0.4	1137.1836
17	2.05	0.35	2875.6529
25	2.05	0.32	5685.918

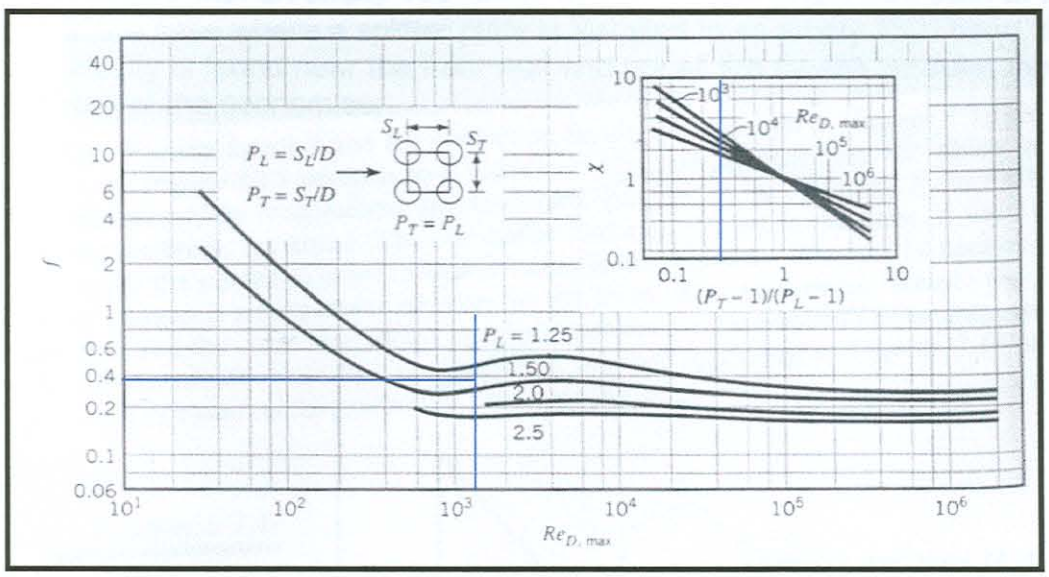

Appendix C - Concepts to Alleviate Airheater Erosion

This appendix discusses different flow-modification remedial measure concepts for airheater tube erosion. The two most successful approaches were discussed in Chapter 5.4.

Concept 1: Splitter Plate

As discussed in Chapter 3.5, Tu et al.[**48**] proposed the installation of a splitter plate in boilers with an empty 180° bend by providing a longer flow path at the bend. In the case where a splitter plate is installed in an empty 180° bend, the peak velocity is found near the front wall and not all the fly-ash particles move to the rear of the economiser.

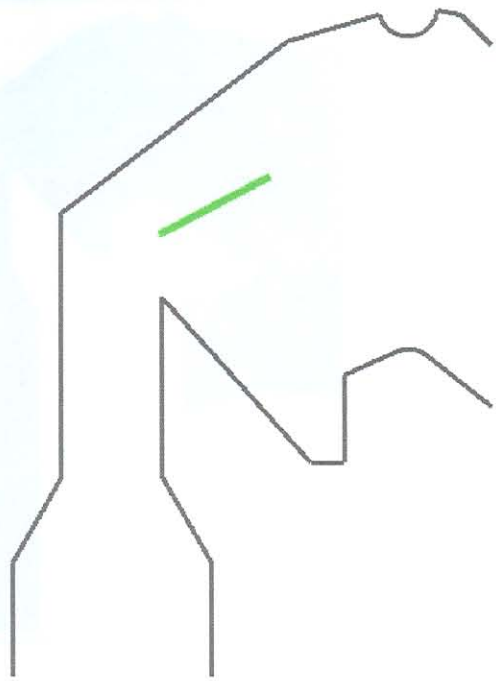

Figure C-1 Concept 1: Location of Splitter Plate

The location of the splitter plate used in this study is illustrated in Figure C-1. Through the use of this flow-modifying device it is hoped to obtain a uniform particle distribution in the airheater with low peak velocities. Figure C-2 illustrates the velocity magnitude contour plot for the case where the splitter plate is included in the CFD model. It can be seen from Figure C-2 that the maximum velocity in the flow domain for the chosen inlet boundary conditions is 13.22m.s^{-1}. If this velocity is compared to Figure 5-27, the case without any flow-modifying devices, it can be seen that the maximum velocity increased by almost 10% from 12.03m.s^{-1}. The location of the maximum velocity is in the same position for both cases. Therefore, the splitter plate is ineffective in reducing the maximum velocity.

The other parameter of erosion that can be altered by flow-modifying approaches is the particle concentration. Figure C-3 and Figure C-4 illustrate the particle trajectories for 100μm and 10μm particles respectively. If this results are compared to Figure 4-15 and Figure 4-14, the case where no flow-modifying were used, it can be seen that there are no major differences in the particle trajectories for the different cases.

It can thus be concluded that the splitter plate is ineffective in redistributing the flow in such a manner that the particle concentration is uniform across the airheater. The maximum velocity in the flow domain also increased as a result of the splitter plate. As splitter plate parameters such as the size, shape and location of the splitter plate was arbitrarily chosen, other parameters can result in better results. Mathematical optimisation can be used in achieving this.

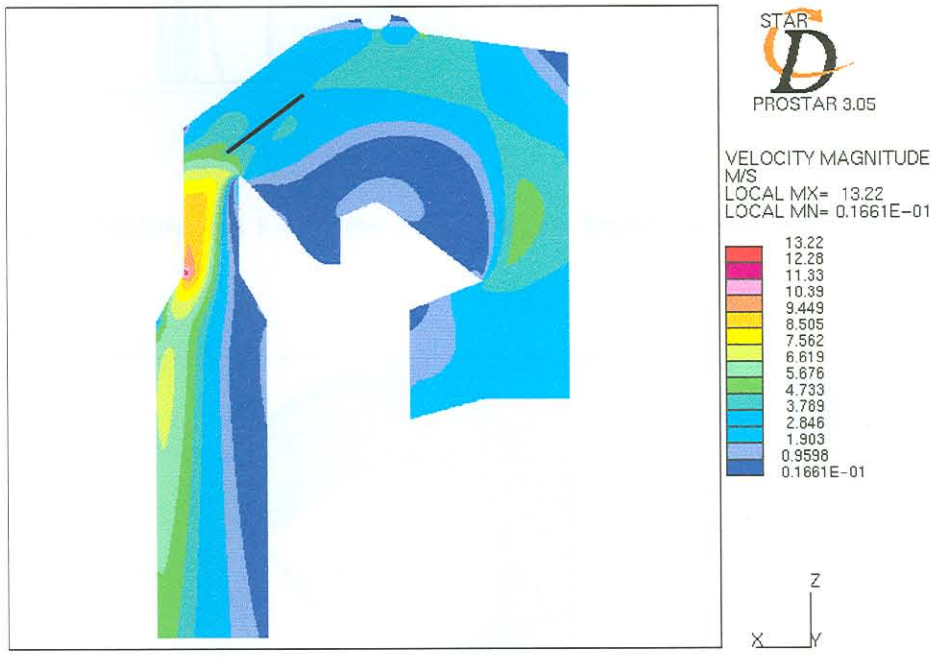

Figure C-2 Concept 1 – Splitter Plate: Velocity Magnitude Plot (2m.s^{-1} Inlet Velocity)

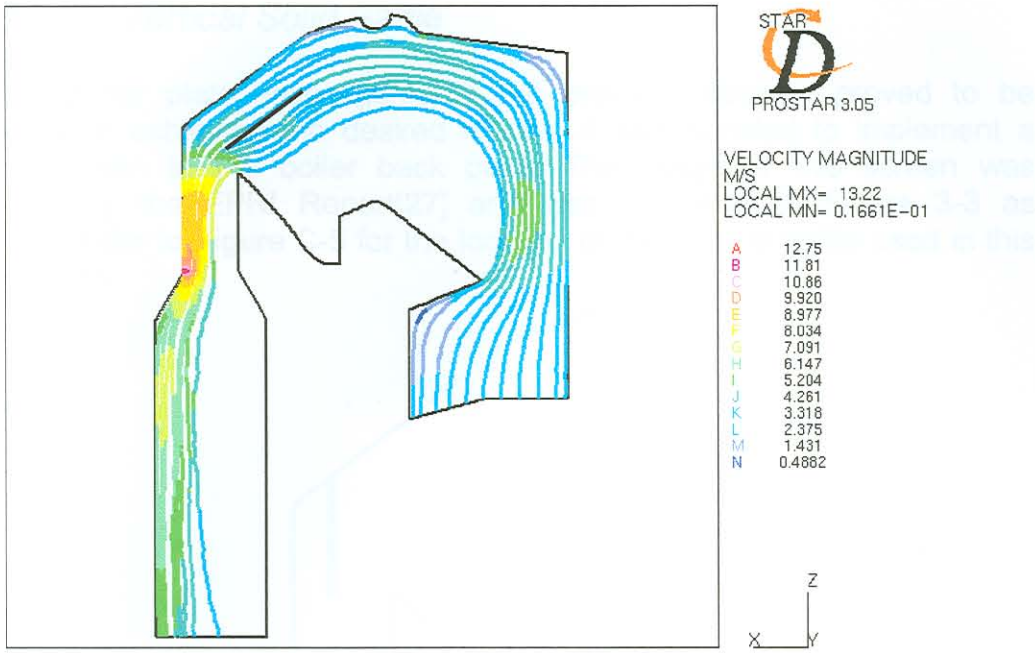

Figure C-3 Concept 1 – Splitter Plate: Particle Trajectories of 100μm Particles

Figure C-4 Concept 1 – Splitter Plate: Particle Trajectories of 10μm Particles

Concept 2: Vertical Solid Baffle

As the splitter plate, investigated in the previous section, proved to be ineffective in achieving the desired results, it was decided to implement a vertical screen in the boiler back pass. The usage of this screen was proposed by the EPRI Report[**27**] and was illustrated in Figure 3-3 as Screen I. Refer to Figure C-5 for the location of the vertical baffle used in this investigation.

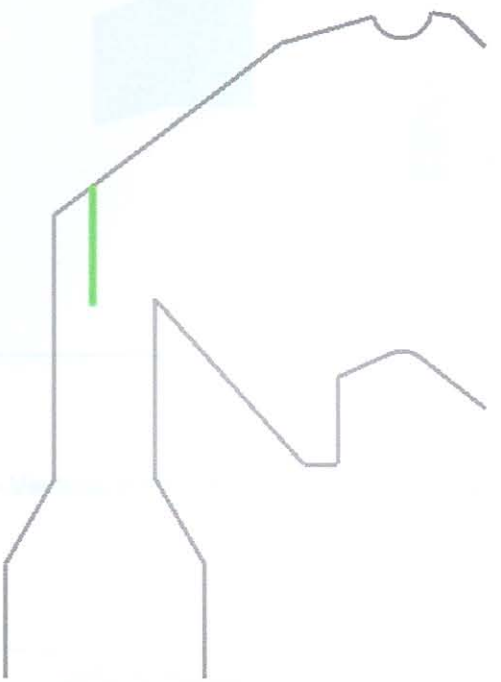

Figure C-5 Concept 2: Location of Verticle Baffle

The velocity magnitude contour plot is illustrated in Figure C-6 for this case. The maximum velocity in the flow domain for the chosen inlet boundary conditions is 13.98m.s^{-1}. This is a 16% increase in the maximum velocity from when no flow-modifying devices are used. The location of the high peak velocity is not near the back wall anymore. However, it is now located at the lower top of the vertical baffle. Boiler wall and baffle erosion can therefore occur in that region.

Particle trajectories for 100μm and 10μm particles can be seen in Figure C-7 and Figure C-8 respectively. The results obtained from this analysis are even worse than those obtained when no flow-modifying devices were used. The particle concentration is high only on the one side of the airheater, with a possible concentration of tube failures there.

In conclusion, the vertical solid baffle is not suited as a remedial measure for airheater tube erosion. This baffle will rather exacerbate tube erosion in the airheater.

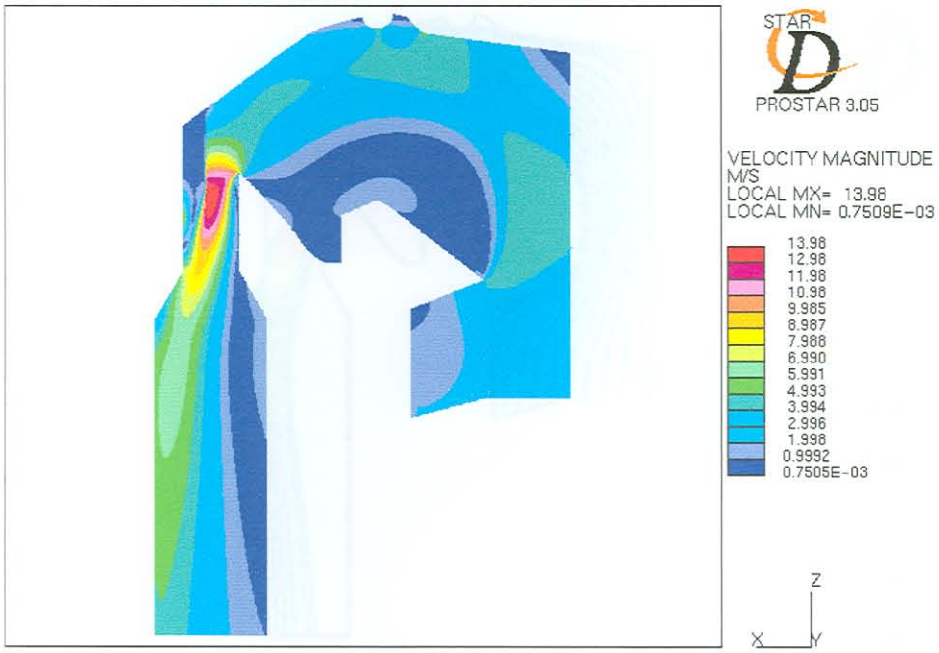

Figure C-6 Concept 2 – Vertical Solid Baffle: Velocity Magnitude Contour Plot (2m.s^{-1} Inlet Velocity)

Figure C-7 Concept 2 – Vertical Solid Baffle: Particle Trajectories of 100μm Particles

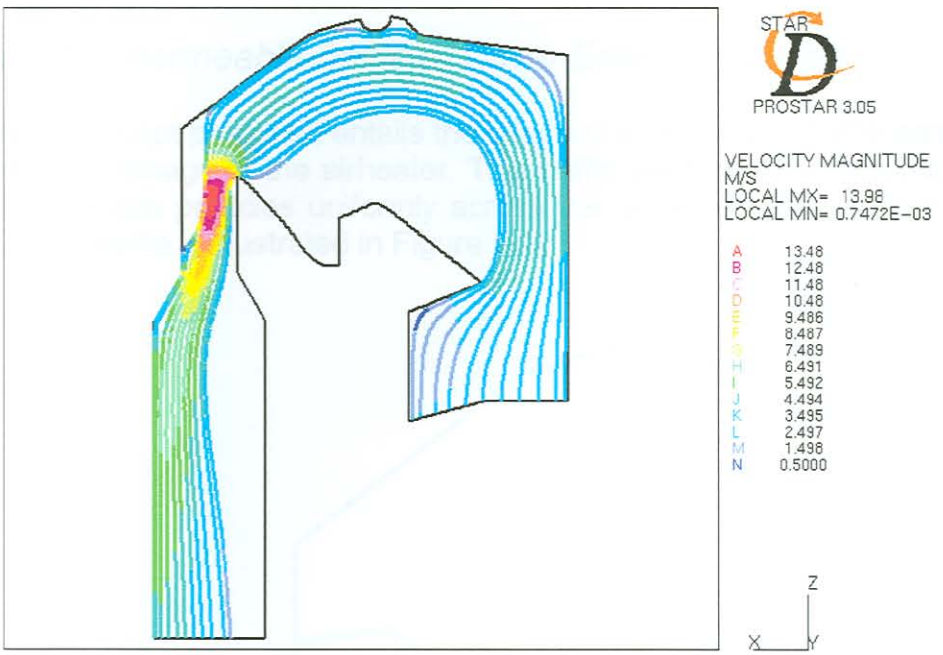

Figure C-8 Concept 2 – Vertical Solid Baffle: Particle Trajectories of 10μm Particles

Concept 3: Permeable Baffle to Cover Entire Flow Area

The third concept proposed entails the usage of a permeable baffle across the entire inlet passage of the airheater. This baffle will hopefully redistribute the flow and fly-ash particles uniformly across the airheater. The location of the permeable baffle is illustrated in Figure C-9.

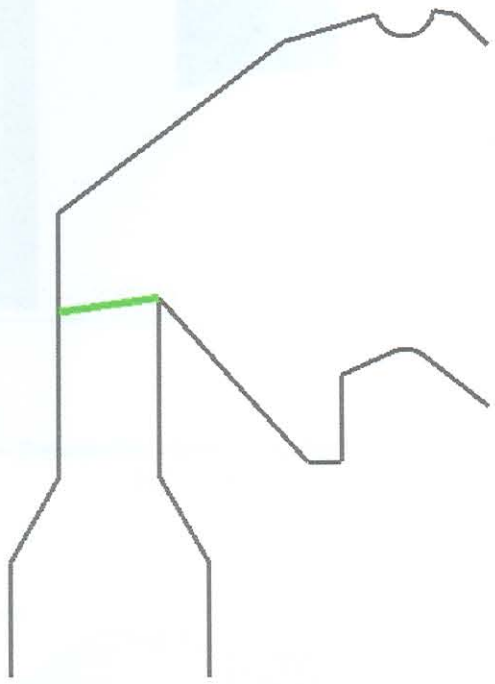

Figure C-9 Concept 3: Location of Baffle to Cover Entire Flow Area

It can be seen from Figure C-10 that the baffle has no major effect on the flow pattern through the airheater. There still exists a large recirculation zone in one side of the airheater. The maximum velocity in the flow is 10.09m.s^{-1}, which is a 16% drop from the case where no flow-modifying devices were used. This is encouraging but with an expense of pressure drop across the baffle.

From Figure C-11 and Figure C-12, which illustrate the particle trajectories for 100μm and 10μm respectively, it can be seen that the baffle is still ineffective to provide a uniform particle distribution across the airheater.

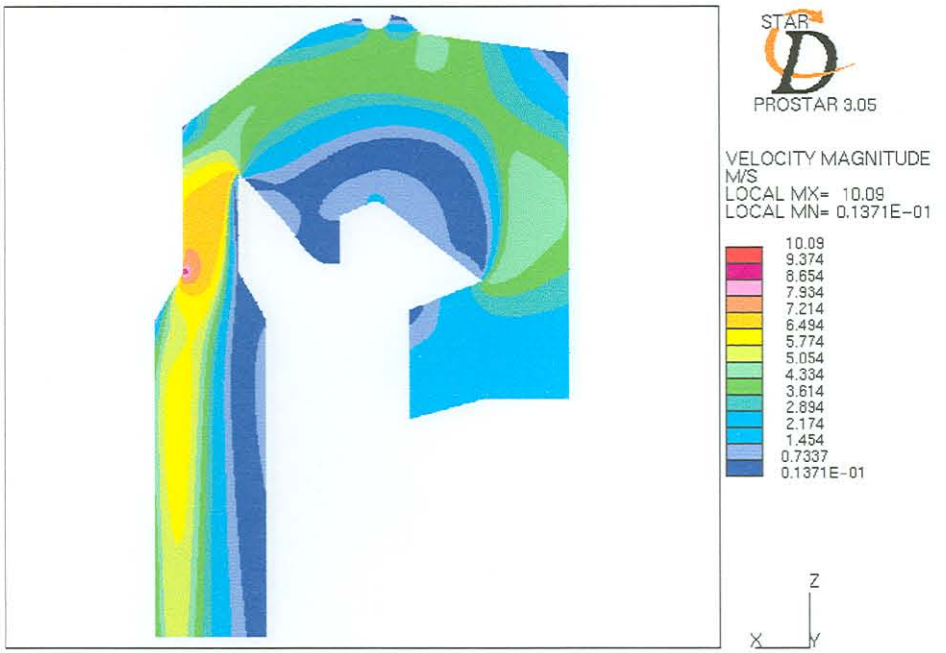

Figure C-10 Concept 3 – Permeable Horizontal Baffle: Velocity Magnitude Contour Plot ($2m.s^{-1}$ Inlet Velocity)

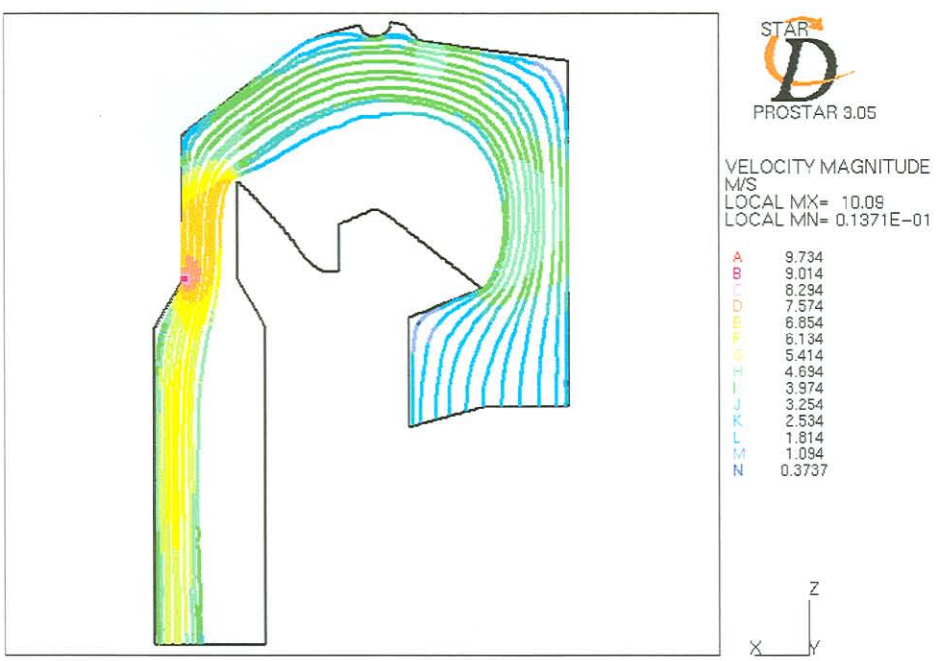

Figure C-11 Concept 3 – Permeable Horizontal Baffle: Particle Trajectories of 100μm Particles

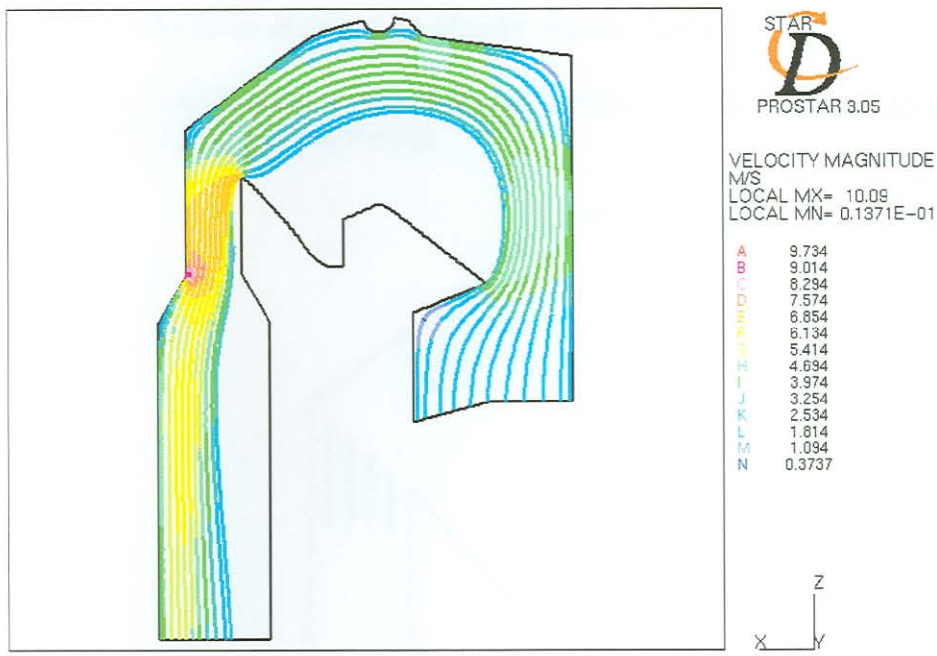

Figure C-12 Concept 3 – Permeable Horizontal Baffle: Particle Trajectories of 10μm Particles

Concept 4:Multiple Baffles in Boiler Back Pass

Figure C-13 illustrates the location of four baffles of different sizes to direct the flow uniformly across the airheater.

Figure C-13 Concept 4: Location of Multiple Baffles in Boiler Back Pass

Figure C-14 illustrates the velocity magnitude contour plot for this flow-modifying concept. The maximum velocity in the flow domain is 9.27m.s^{-1} for the given inlet boundary conditions. This translates into a 23% decrease in the maximum velocity for the case without flow-modifying devices and a 14% increase from the concept of the permeable baffle investigated in the previous section. However, the region of high peak velocity is at the top of the boiler between the baffle plates and is far from the airheater tubes.

The particle trajectories are shown in Figure C-15 and Figure C-16 for 100μm and 10μm particles respectively. The uniformity of the particles across the airheater is not as uniform as the particles from the previous section but is better that all the other concepts investigated thus far in this appendix.

Figure C-14 Concept 4 – Vertical Baffles: Velocity Magnitude Contour Plot (2m.s^{-1} Inlet Velocity)

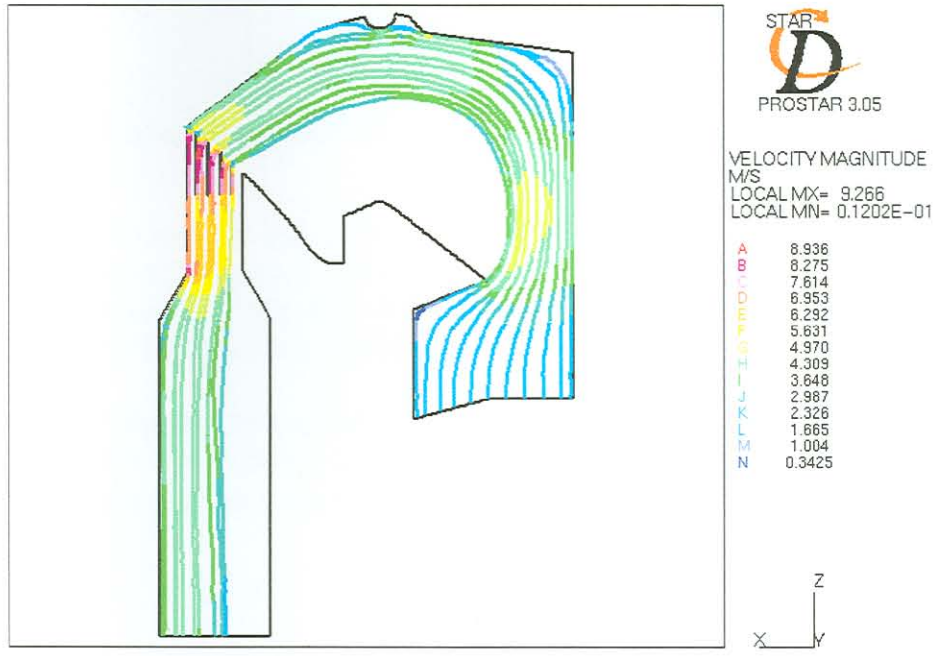

Figure C-15 Concept 4 – Vertical Baffles: Particle Trajectories of 100μm Particles

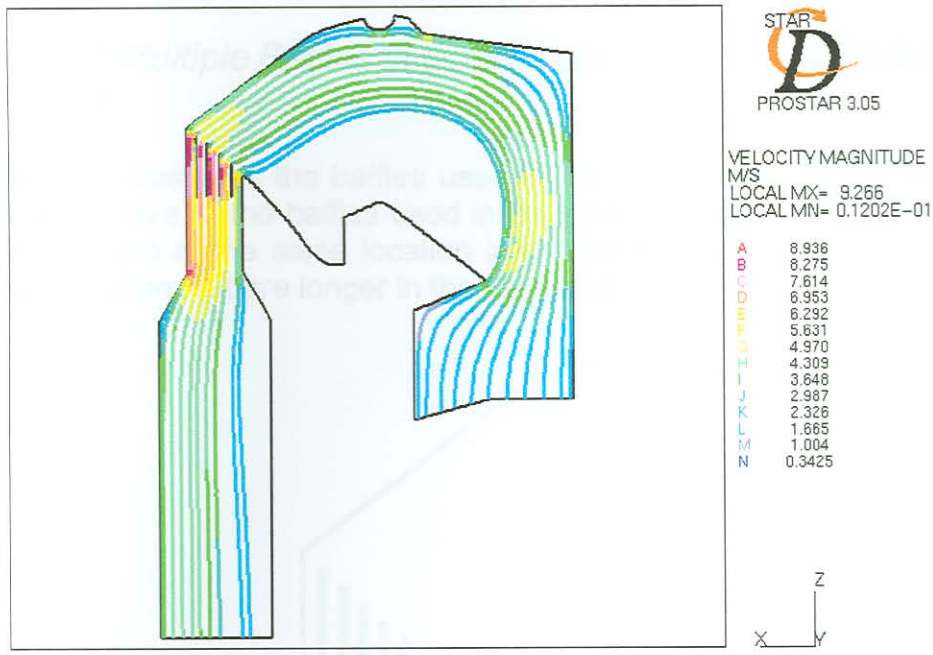

Figure C-16 Concept 4 – Vertical Baffles: Particle Trajectories of 10μm Particles

Concept 5:Multiple Baffles in Boiler Back Pass – Modification to Concept 4

Figure C-17 illustrates the baffles used in the CFD model to investigate the effect of the size of the baffles used in the previous section on the flow field. The baffles are at the same location in the boiler than the ones used in the previous section, but are longer in the vertical direction.

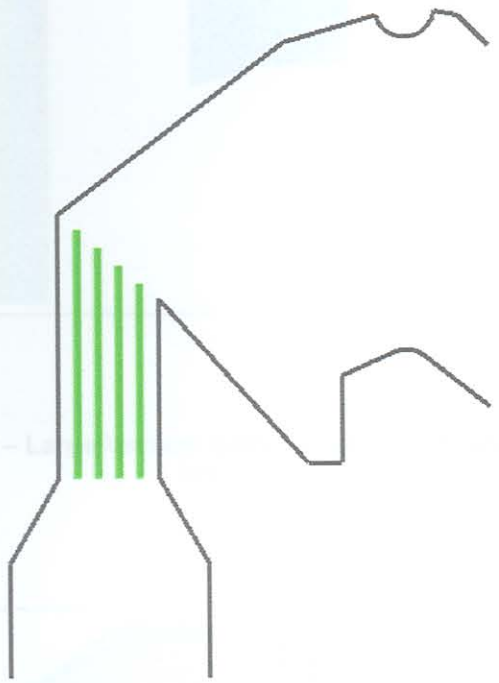

Figure C-17 Concept 5: Multiple Baffles in Boiler Back Pass – Modification to Concept 6

Figure C-18 illustrates the velocity magnitude contour plot for the CFD model with the baffles illustrated in Figure C-17. The maximum velocity in the flow domain increased by 5% from the maximum velocity in the previous concept, where smaller baffles were used.

The effect of the larger baffles on particle trajectories is minor as compared to the case with the smaller baffles. The particle trajectories for 100μm and 10μm particles can be seen in Figure C-19 and Figure C-20 respectively.

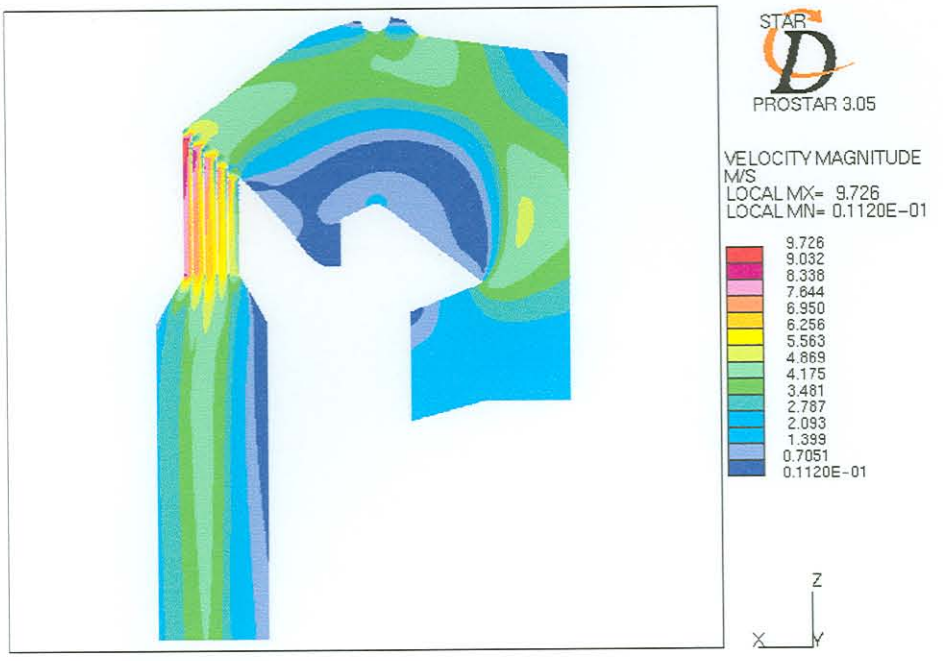

Figure C-18 Concept 5 – Large Vertical Baffles: Velocity Magnitude Contour Plot (2m.s^{-1} Inlet Velocity)

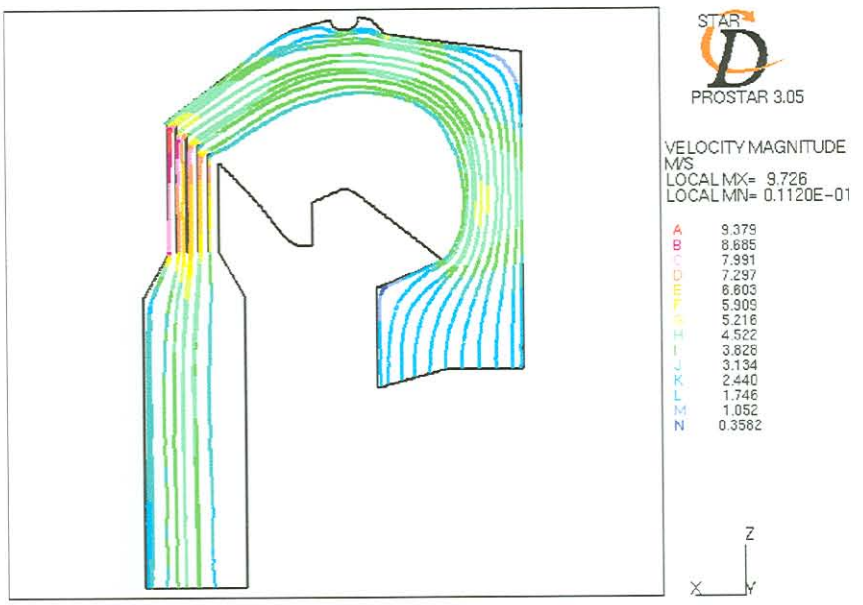

Figure C-19 Concept 5 – Large Vertical Baffles: Particle Trajectories of 100μm Particles

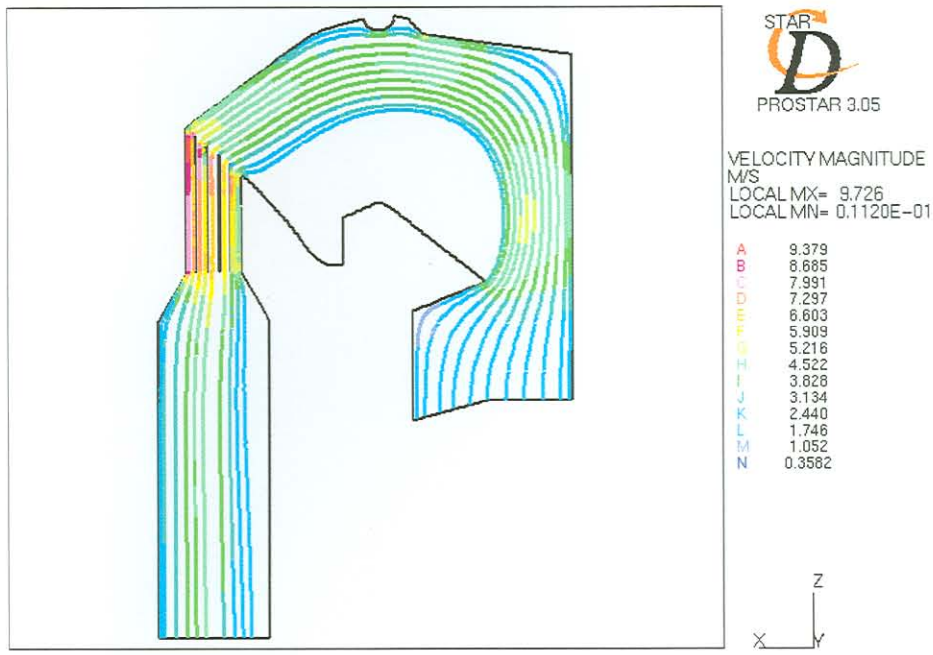

Figure C-20 Concept 5- Large Vertical Baffles: Particle Trajectories of 10μm Particles